UNDERSTANDING SEWER INFILTRATION AND INFLOW USING IMPULSE RESPONSE FUNCTIONS DERIVED FROM PHYSICS-BASED MODELS

BY

NAM JEONG CHOI

DISSERTATION

Submitted in partial fulfillment of the requirements
for the degree of Doctor of Philosophy in Civil Engineering
in the Graduate College of the
University of Illinois at Urbana-Champaign, 2016

Urbana, Illinois

Doctoral Committee:

Professor Albert J Valocchi, Chair
Research Assistant Professor Arthur R Schmidt, Director of Research
Professor Marcelo H Garcia
Associate Professor Richard A Cooke
Doctor Joshua Cantone (Wallbridge & Gilbert, University of Adelaide)

Abstract

Infiltration and inflow (I&I) are extraneous flow in a sanitary sewer system that originate from surface water and ground water. I&I can overload the sewer system and wastewater treatment plants, and cause sanitary sewer overflows (SSOs) or basement flooding. This flow can account for as much as ten times dry weather flow (DWF) but the estimation of the volume and peak of I&I involves a great deal of uncertainty.

Temporal and spatial variability of the I&I processes make it difficult to understand the phenomena. Depending on the time scale of different I&I processes, some watershed properties may only affect specific I&I sources. For example, the configuration of sewer network and the geology of the watershed may affect fast and slow I&I processes differently.

In this study, the physical process of three major I&I sources: roof downspout, sump pump, and leaky lateral, are investigated at the residential lot scale using physics-based models. The typical flow response of each I&I source is calculated and these flow responses, called Impulse Response Functions (IRFs), are evaluated. I&I estimation using the three IRFs, calibrated using a genetic algorithm (GA), was performed on a catchment in the Chicago area at the sewershed scale. Results are compared with one of the most widely used I&I estimation methods, the RTK method. The IRF method shows more stable solutions as the model is based on physical processes. The RTK method better predicts the monitoring data, however it is suspected that this is mainly because the RTK method is an empirical curve fitting method.

Uncertainty related to rainfall induced infiltration (RII) is further investigated on six different input parameters: Antecedent moisture condition (AMC), pedotransfer functions (PTFs), soil hydraulic conductivities, initial conditions (IC), sewer pipe depths, and rainfall characteristics.

The uncertainty analysis indicates that the model result is most sensitive to the soil hydraulic conductivity, which defines the maximum infiltration rate. Rainfall characteristics, including duration and hyetograph shape turn out to be the least influential factors affecting the infiltration response.

Results from this study help understand the sewer I&I process in a complex urban system. In particular, using a small scale, detailed distributed model enables examination of the sensitivity of the I&I process to the different factors contributing to uncertainty. While the modeling results are site specific to Hickory Hills, IL, this study can provide insights to researchers and engineers about characteristic behaviors of different I&I sources and the uncertainty factors that affect sewer infiltration response including AMC.

Table of Contents

List of Figures

List of Tables

1. Introduction

1.1. Research Background and Motivation

Capital investment needs for fixing and expanding sewer pipes in the US are estimated to exceed $200 billion over the next twenty years, which is three quarters of entire investment requirement in wastewater system (USEPA 2013). Between 700,000 and 800,000 miles of public sewer mains in the states are reaching the end of their useful life and 900 billion gallons of sanitary sewer overflows and combined sewer overflows are estimated each year (ASCE 2013). One of the biggest problems related to sewer system maintenance is infiltration and inflow (I&I) that causes sewer overflows and basement flooding. Thus, continuous maintenance of the system along with understanding the characteristics of the factors causing sewer problems is necessary.

I&I is recognized as one of the major problems affecting sewer systems and results in associated problems such as (Field & Struzeski 1972, NSFC 1999, Lai 2008):

- Flow overloading in sewer systems and water treatment plants and associated problems e.g. street flooding, basement flooding (Gottstein 1976)
- Increase in pumping costs (Backmeyer 1960)
- Sewer overflows and associated adverse effects of pollution and public health
- Decrease in treatment efficiency in water treatment plants caused by dilution

The excessive I&I flow can cause flow overloading in sewer systems and may result in basement flooding during periods of intensive rainfall (Gottstein 1976). In sewer systems with a large

number of pumping stations (e.g. Florida) pumping costs could be also substantial as the wastewater volume increases (Backmeyer 1960). Sewer overflow is strongly regulated by the EPA and failure to remove overflows or to correct I&I problems could prevent a city from receiving federal construction grant funds (Sliter 1974). Overflows and bypasses of sewage degrade receiving water quality and may cost the community a violation fee that is forced by state and federal laws. Bypassed raw sewage may also cause odor problems and adverse impacts on public health. In coastal areas, infiltration of salt water can deteriorate sewer pipes and water treatment plant facilities by providing an extra source of sulfur (Backmeyer 1960). Wastewater treatment and collection systems account for 10 to 15 percent of the total infrastructure values in the US (NCPWI 1988) and I&I problems need to be addressed with a great emphasis.

Based on Petroff (1996)'s estimation, around 50% of the treated wastewater in the US is from rainfall-derived I&I (RDII) and dry weather infiltration. Franz (2007) also highlighted that 20% of the waste water treated in Germany is extraneous water. The amount of I&I varies in different sewer systems depending on the age of the system, pipe material, construction practices, soil type, etc. Ratios of I&I to dry weather flow (DWF) compiled from a review of literature on this topic are summarized in Table 1.1. The range of the ratio varies from 0.4 to 10. For example, I&I for Baltimore City was ten times greater than the DWF, which means 90 percent of the wastewater flow is I&I. This indicates that I&I volume can affect the capacity of a sanitary sewer system significantly.

Table 1.1 Amount of I&I relative to DWF from different sources of literature

	Ratio of I&I to DWF	Reference
1	3.4	Bishop et al. (1987)
2	1.4 ~ 3.8	NSFC (1999)
3	0.4	Ertl et al. (2002)
4	1.2	Weiss et al. (2002)
5	1.2	Lucas (2003)
6	1.5	Pecher (2003)
7	1.4	Jardin (2004)
8	0.4	Kretschmer et al. (2008)
9	9	Bhaskar & Welty (2012)

Various I&I estimation modeling methods have been developed since the 1980s to quantify the impact of I&I (De Bénédittis & Bertrand-Krajewski 2005). Bishop et al. (1987) developed a simple synthetic hydrograph method for 300 study basins to estimate I&I and to evaluate flow data. Gustafsson (2000) presented a leakage model that takes account of the two way interaction between pipes and the aquifer using MOUSE (Lindberg et al., 1989) and MIKE SHE (DHI Software, 2007a, 2007b). Karpf & Krebs (2004) also used the same leakage approach. The model was calibrated using a leakage factor that is a function of groundwater infiltration rate, groundwater level, water level in sewer pipe, and the pipe surface to which the groundwater is exposed. Schulz et al. (2005) used the same modeling approach to estimate potential benefits of sewer pipe rehabilitation with different hypothetical infiltration rates. Qiao et al. (2007) presented a groundwater infiltration model using a two-reservoir approach: one reservoir for soil storage in unsaturated zone and another for groundwater storage in saturated zone. The elevations of the reservoir openings determine the trigger points that initiate infiltration into sewer pipes.

One of the most widely used I&I estimation methods is the "RTK method" that was developed by Camp Dresser & McKee (CDM) Inc. et al. (1985). According to Lai (2008) "the RTK method is probably the most popular synthetic unit hydrograph (SUH) method" in the stormwater management field. This method uses three triangular hydrographs to estimate the response times associated with the effect of fast, moderate, and slow I&I. By linear convolution of the three hydrographs, the model produces a total response hydrograph calibrated based on comparison to an observed hydrograph. The RTK model is calibrated using three parameters: R, T, and K for each hydrograph. Figure 1.1 illustrates the parameters using one of three hydrographs. R is the fraction of rainfall volume that is accounted for in this hydrograph as entering the sewer system as rainfall-derived infiltration and inflow (RDII). When three hydrographs are used in the RTK approach the total fraction of rainfall volume that enters the sewer system as RDII is allocated to three R components: R1, R2, and R3. R1 is for the fast inflow element while R2 and R3 represent the slower infiltration elements. T is the time to peak in each hydrograph (typically expressed in hours), and K is the ratio of time of recession to the time to peak. This method is embedded in EPA SWMM5 (Rossman 2010) and EPA SSOAP toolbox (Vallabhaneni et al. 2008). Despite its popularity, the model does not reflect the underlying physics of each I&I response so there can be a vast number of possible combinations of the nine RTK parameters. Also there is a little guidance for calibrating these models and for I&I modeling in general (Allitt, 2002).

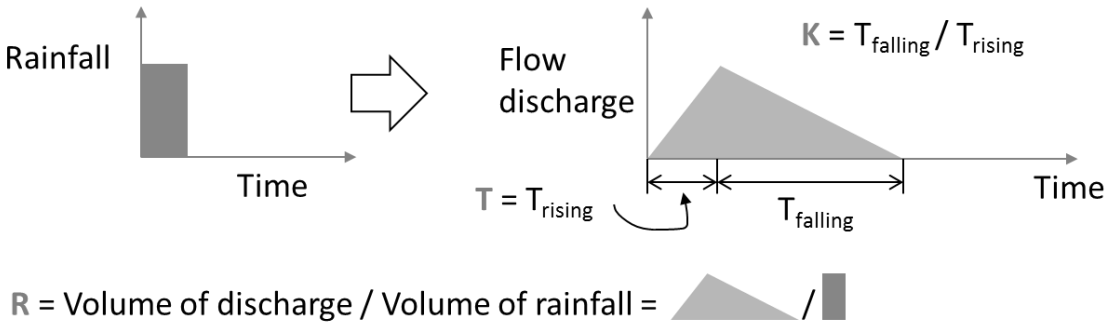

Figure 1.1 Three parameters: R, T, and K of the RTK method illustrated with one of three RTK hydrographs

InfoWorks CS (Innovyze 2011) is another popular stormwater modeling tool that has an option for I&I simulation. InfoWorks simulates I&I using two components: rainfall-induced infiltration, and groundwater infiltration. This is different from SWMM because the RTK method only takes into account rainfall induced I&I but not groundwater infiltration. In the InfoWorks CS infiltration module depicted in Figure 1.2, the percolation flow from the surface depression storage is assigned to the soil storage reservoir after a runoff occurs. When the soil reaches the percolation threshold, a proportion of this percolation flow goes to the sewer network. This represents RDII. The remainder of the percolation flow goes down to the groundwater storage reservoir. When the groundwater level reaches the sewer system invert level, groundwater infiltration occurs. The method enables engineers to model groundwater infiltration into a sewer system but the full physical process is not taken into account. For example, according to the model assumption, groundwater infiltration occurs when the groundwater level is higher than the pipe invert elevation not the water level in the sewer pipe. InfoWorks CS is widely used because it provides easy to use representation of RDII and it is useful for operational design. However,

the empirical approximations in this approach to model RDII and infiltration limit the ability to use this model to provide understanding of process behind I&I for a given system.

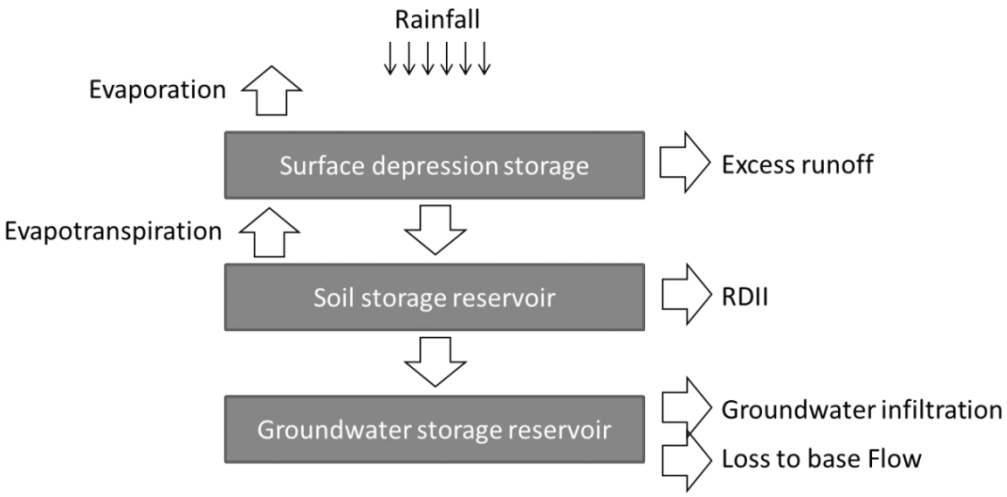

Figure 1.2 InfoWorks CS infiltration module

Both SWMM and InfoWorks take simple I&I estimation approaches that represent I&I with triangular hydrographs or constant rates. Simplified modeling methods are labor and cost effective and easy to apply but such approaches do not provide understanding of processes that actually occur and need much more calibration data for parameter estimation.

Various I&I prediction methods, including the above methods, are well documented by Crawford et al. (1999), Wright et al. (2001), Vallabhaneni et al. (2007), and Lai (2008) and summarized in Table 1.2. Crawford et al. (1999) summarized I&I estimation methods including constant unit rate, percentage of rainfall volume (R-value), and predictive equations based on rainfall and flow regression along with two case studies. Wright et al. (2001) provided an overview of different I&I estimation methods and evaluated a modified EPA SWMM RUNOFF model. Vallabhaneni et al. (2007) presented various computer tools for sanitary sewer system capacity analysis

including EPA SSOAP tool box. Lai (2008) also presented I&I prediction methods with sewer design practices. Even though there are many different methods available, none of these methods were developed based on physical process of I&I. These methods are event specific and the accuracy of prediction for different rainfall events is not reliable.

Table 1.2 Various I&I estimation methods presented in literature

Method	Literature	Explanation	Shortcomings
Constant unit rate	Crawford et al. (1999) Lai (2008)	• In flowrate per acre • Used for design manuals • Dependent on sewershed area, land use, population, and pipe length for large areas	Difficult to develop reasonable estimate since it may vary temporarily for all storms (Lai 2008)
Percentage of rainfall volume (R-value, R factor, or rational method)	Crawford et al. (1999) Wright et al. (2001) Vallabhaneni et al. (2007) Lai (2008)	• R = volume of wet weather RDII/rainfall volumex100 • Typically triangular hydrograph shape is used.	Too simple for design or permitting estimates as only volume is considered (Wright et al. 2001)
Percentage of streamflow	Crawford et al. (1999) Lai (2008)	• Relationship between sewer flow monitoring data and streamflow data	The sewer system condition and the sewershed area condition need to be consistent
Unit hydrograph	Crawford et al. (1999) Wright et al. (2001) Vallabhaneni et al. (2007) Lai (2008)	• RDII responds to rainfall volume and duration • Shape of the hydrograph depends on basin characteristics • Several unit hydrographs to represent the separate components contributing to RDII • Linear model based on the assumption that rainfall is constant in time and uniformly distributed in space • UH methods 1) Synthetic unit hydrographs (SUH): RTK method 2) Data-derived UH: the regression method 3) UH derivation using least square regression 4) UH derivation using a linear program 5) Conceptually derived UH	UH is often empirically fit to measurement and has no physical meaning
Probabilistic	Crawford et al. (1999) Lai (2008)	• Frequency analysis of peak RDII flows (rate or volume) • Relationship of sewer flow to recurrence interval	Rainfall effects are not reflected and the frequency analysis is more adequate for extreme events

Besides the I&I estimation modeling in urban hydrology, models of interactions between porous media flow and buried pipes have been developed and described in the agricultural tile drainage literature. Some of the agricultural drainage literature related to inflow into buried pipes is summarized in Table 1.3.

Table 1.3 Summary of the agricultural drainage literature related to modeling

	Authors	Year	Summary of key findings
1	Fipps & Skaggs	1986	Comparison of four different finite element methods for tile drain systems
2	Fipps & Skaggs	1992	Application of numerical solutions to various subsurface drain conditions and development of an approximate method
3	Kim & Delleur	1997	Comparison of physically based storage approach and a new approach using a transfer function, extended TOPMODEL, for tile drain flows
4	Tarboton & Wallender	2000	Comparison of different finite element grid configurations for steady and transient flow to a single drain
5	Cooke & Badiger	2001	Applicability of subsurface drainage theory for single tile system to irregular or random drainage system using unsaturated-flow finite element model
6	Buyuktas & Wallender	2002	Evaluation of a single equivalent soil hydraulic parameter to study water and solute transport to tile drains using three-dimensional deterministic model
7	Carluer & Marsily	2004	Man-made drainage network modeling using distributed watershed model (ANTHROPOG)
8	Purkey et al.	2004	Enhanced deforming finite element model to examine the interactions between tile drainage and a local groundwater table
9	Carlier et al.	2007	Equivalent representation of tile drains using a homogeneous anisotropic porous medium

At small scales, applying a detailed physics-based model improves the prediction, yet some simplification improves practicality. Carlier et al. (2007) presented an equivalent-medium approach for drains buried in a soil profile, which takes the entire soil column as a uniform layer with averaged soil properties. Although the water table showed slightly faster response with the simplified approach, the results provided were still considered reasonable. Despite the advantages that using a detailed model can provide to understand the infiltration process, this approach has not been widely used in urban hydrology. Thus, in this study, several I&I processes are investigated using physics-based models. In particular, the equivalent-medium approach from Carlier et al. (2007) is adopted to model a leaky sewer lateral, as described in chapter 3.

1.2. Research Objectives

The objective of this study is to understand the hydrologic behavior induced by the I&I process using physics-based models for three major I&I sources: roof downspout, sump pump connection, and leaky sewer lateral. In particular, the uncertainty in the rainfall induced infiltration (RII) and how this impacts hydrological response at sewershed scale are investigated.

In chapter 2, I&I and RII are defined and different I&I sources are summarized. Chapter 2 also discusses the relative contribution and behavior of different I&I sources and why roof downspout, sump pump, and leaky lateral are selected as the three representative sources. The methodology for the I&I modeling and the model calibration using genetic algorithm (GA) is presented in chapter 3. In chapter 4, physics-based modeling of three I&I sources: roof downspout, sump pump connection, and leaky sewer lateral, is introduced to better understand the I&I processes. Unique flow response for each I&I source is derived and the characteristics

are compared. The models are applied to Palos Hills, IL and are calibrated using sewer monitoring data. A GA technique is utilized for the calibration and the widely used RTK method is also tested for comparison. In addition to the model development, uncertainty associated with six different model parameters related to the RII process (antecedent moisture condition (AMC), soil characteristics, pedotransfer functions (PTFs), sewer pipe depth, initial condition, and rainfall characteristics) is investigated and presented in chapter 5.

References

Allitt, R. (2002) Rainfall, runoff and infiltration re-visited. *WaPUG Spring Meeting 2002* (pp. 1–9).

ASCE (2013) *Report Card for America's Infrastructure*.

Backmeyer, D. P. (1960) Effects of infiltration. *Water Pollution Control Federation* **32**(5), 539–540.

Bhaskar, A. S., & Welty, C. (2012) Water balances along an urban-to-rural gradient of metropolitan Baltimore , 2001 – 2009. *Environmental & Engineering Geoscience*, *XVIII*(1), 37–50.

Bishop, W. J., Diemer, D. M. & Wallis, M. J. (1987) Regional infiltration/inflow study solves wet weather sewer problems. *Journal of Water Pollution Control Federation* **59**(5), 289–293. Retrieved from http://www.jstor.org/stable/25043247?origin=JSTOR-pdf

Buyuktas, D. & Wallender, W. W. (2002) Numerical simulation of water flow and solute transport to tile drains. *Journal of Irrigation and Drainage Engineering* **128**(1), 49–56.

Camp Dresser & McKee (CDM) Inc., F.E. Jordan Associates Inc. & James M. Montgomery Consulting Engineers. (1985) East Bay infiltration/inflow study manual for cost-effectiveness analysis. Oakland, CA.

Carlier, J. P., Kao, C. & Ginzburg, I. (2007) Field-scale modeling of subsurface tile-drained soils using an equivalent-medium approach. *Journal of Hydrology* **341**(1-2), 105–115. doi:10.1016/j.jhydrol.2007.05.006

Carluer, N. & Marsily, G. De. (2004) Assessment and modelling of the influence of man-made networks on the hydrology of a small watershed: implications for fast flow components, water quality and landscape management. *Journal of Hydrology* **285**(1-4), 76–95. doi:10.1016/j.jhydrol.2003.08.008

Cooke, R. A. & Badiger, S. (2001) Drainage equations for random and irregular tile drainage systems. *Agricultural Water Management* **48**, 207–224.

Crawford, D., Eckley, P. & Pier, E. (1999) Methods for estimating inflow and infiltration into sanitary sewers. *New applications in modeling urban water systems, Volume 7, Conference on Stormwater and Related Water Systems Modeling; Management and Impacts*, 299–315. Toronto: CHI.

De Bénédittis, J. & Bertrand-Krajewski, J. L. (2005) Infiltration in sewer systems: comparison of measurement methods. *Water Science and Technology: a Journal of the International Association on Water Pollution Research* **52**(3), 219–27. Retrieved from http://www.ncbi.nlm.nih.gov/pubmed/16206862

DHI Software. (2007) *MIKE SHE user manual volume 1: user guide* (Vol. 1).

DHI Software. (2007) *MIKE SHE user manual volume 2: reference guide* (Vol. 2).

Ertl, T. W., Dlauhy, F. & Haberl, R. (2002) Investigations of the amount of infiltration / inflow into a sewage system. *Proceedings of the 3rd "Sewer Processes and Networks" International Conference*. Paris, France.

Field, R., & Struzeski, E. J. (1972) Management and control of combined sewer overflows. *Water Pollution Control Federation*, *44*(7), 1393–1415.

Fipps, G., & Skaggs, R. W. (1992) Simple methods for predicting flow to drains. *Journal of Irrigation and Drainage Engineering*, *117*(6), 881–896.

Fipps, G., Skaggs, R. W., & Nieber, J. L. (1986) Drains as a boundary condition in finite elements. *Water Resources Research*, *22*(11), 1613–1621.

Franz, T. (2007) *Spatial classification methods for efficient infiltration measurements and transfer of measuring results*. Dresden University of Technology, Dresden, Germany.

Gottstein, L. E. (1976) *Sewer system evaluation for infiltration/inflow*. Minneapolis, Minnesota.

Gustafsson, L. (2000) Alternative drainage schemes for reduction of inflow/infiltration - prediction and follow-up of effects with the aid of an integrated sewer/aquifer model. *1st International Conference on Urban Drainage via Internet* (pp. 21–37).

Innovyze. (2011) InfoWorks CS technical review.

Jardin, N. (2004) Fremdwasser – eine grundsätzliche Problembeschreibung (Extraneous water – a basic description). *Proceedings of 3rd Forum Ruhrverband*. Essen, Germany.

Karpf, C., & Krebs, P. (2004) Sewers as drainage systems – quantification of groundwater infiltration. In *Novatech 2004, 6th International conference on sustainable techniques and strategies in urban water managementWater Management* (pp. 969–975). Lyon.

Kim, S., & Delleur, J. W. (1997) Sensitivity analysis of extended TOPMODEL for agricultural watersheds equipped with tile drains. *Hydrological Processes, 11*, 1243–1261.

Kretschmer, F., Ertl, T., & Koch, F. (2008) Discharge monitoring and determination of infiltration water in sewer systems. In *11th International Conference on Urban Drainage* (pp. 1–7). Edinburgh, Scotland, UK.

Lai, F. D. (2008) Review of sewer design criteria and RDII prediction methods. Washington, DC.

Lindberg, S., Nielsen, J. B., & Carr, R. (1989) An integrated PC-modelling system for hydraulic analysis of drainage systems. *Watercomp '89: The First Australasian Conference on Technical Computing in the Water Industry*. Melbourne, Australia.

Lucas, S. (2003) *Auftreten, Ursachen und Auswirkungen hoher Fremdwasserabflüsse – eine zeitliche und räumliche nalyse (Occurence, causes and effects of high extraneous water flows)*. Universität Karlsruhe.

NCPWI (National Council on Public Works Improvement). (1988) Fragile foundations: a report on America's Public Works, Final report to the president and congress.

NSFC (National Small Flows Clearinghouse). (1999) Infiltration and inflow can be costly for communities. *Pipeline: Small Community Wastewater Issues Explained to the Public*, Vol.10, No.2.

Pecher, K. H. (2003) Fremdwasseranfall, Schwankungen und Konsequenzen für die Abwasserbehandlung (Amount of I/I, variations and consequences). *Proceedings of 36th Essener Tagung, Gewässerschutz-Wasser-Abwasser*. Aachen, Germany.

Petroff, R. G. (1996) An analysis of the root cause of sanitary sewer overflows. In: *Seminar Publication National Conference on Sanitary Sewer Overflows (SSOs): april 24-26, 1995, Washington D.C.*, 8–15. Cincinnati, OH: EPA.

Purkey, D. R., Wallender, W. W., Fogg, G. E. & Sivakumar, B. (2004) Describing near surface, transient flow processes in unconfined aquifers below irrigated lands: Model application in the Western San Joaquin Valley, California. *Journal of Irrigation and Drainage Engineering* **130**(6), 451–459. doi:10.1061/(ASCE)0733-9437(2004)130

Qiao, F., Lu, H., Derr, H. K., Wang, M., & Chen, M. (2007) A new method of predicting rainfall dependent inflow and infiltration. *Water Environment Federation* (pp. 1883–1890). doi:10.2175/193864707788116040

Rossman, L. A. (2010) Storm water management model user's manual version 5.0. Cincinnati, OH.

Schulz, N., Baur, R., & Krebs, P. (2005) Integrated modelling for the evaluation of infiltration effects. *Water science and technology: a journal of the International Association on Water*

Pollution Research, *52*(5), 215–23. Retrieved from http://www.ncbi.nlm.nih.gov/pubmed/16248198

Sliter, J. T. (1974). Infiltration/inflow guidelines spark controversy. *Journal of Water Pollution Control Federation*, *46*(1), 6–8.

Tarboton, K. C. & Wallender, W. W. (2000) Finite-element grid configurations for drains. *Journal of Irrigation and Drainage Engineering* **126**(4), 243–249.

USEPA (2008) *Clean Watershed Needs Survey 2008 Report to Congress* (EPA-832-R-10-002).

Vallabhaneni, S., Chan, C. C., & Burgess, E. H. (2007) *Computer tools for sanitary sewer system capacity analysis and planning*. Cincinnati, OH.

Vallabhaneni, S., Lai, F., Chan, C., Burgess, E. H. & Field, R. (2008) SSOAP − A USEPA toolbox for sanitary sewer overflow analysis and control planning. *EWRI 2008 World Environmental & Water Resources Congress, May 13-16, 2008*. Honolulu, HI: American Society of Civil Engineers (ASCE).

Weiss, G., Brombach, H. & Haller, B. (2002) Infiltration and inflow in combined sewer systems: long-term analysis. *Water science and technology : a journal of the International Association on Water Pollution Research* **45**(7), 11–9. Retrieved from http://www.ncbi.nlm.nih.gov/pubmed/11989885

Wright, L., Dent, S., Mosley, C., Kadota, P. & Djebbar, Y. (2001) Comparing rainfall dependent inflow and infiltration simulation method. In: *Models and Applications to Urban Water Systems. Monograph 9*, 235–258. Toronto, Ontario, Canada: CHI.

2. Literature Review

In this chapter, definitions of I&I that have appeared in the literature are presented. Various I&I sources are discussed and three common methods to estimate the I&I flow in a sewer system are introduced. In addition, spatial and temporal variability of I&I sources in a sewershed are investigated.

2.1. Definition and Sources of I&I

Infiltration and inflow (I&I) are extraneous water that enters into both sanitary and combined sewer systems unintentionally. Since sanitary sewer systems are designed only for wastewater I&I is also called 'parasite water.' The urban hydrologic literature contains a variety of definitions of I&I. One from the EPA is as follows (EPA 1995):

> "Inflow means that water enters the sewer system from the land's surface in an uncontrolled way. Usually, this happens when surface water runs in through unsealed manhole covers. It may also happen when people illegally connect their foundation drains, roof leaders, cellar drains, yard drains, or catch basins to the sewer system."
>
> "Infiltration happens when non-wastewater seeps into the sewer system from the ground. Ground water usually leaks into the sewer system through defective pipes, pipe joints, connections, or manholes."

Since inflow is originated from direct connections, the flow response is nearly immediate and flow peaks are large. Contrarily, infiltration shows slow and persistent responses in time. Belhadj et al. (1995) described the differences between infiltration and inflow in terms of behaviors. Inflow displays high peak flows that are directly related to rainfall events. In contrast, infiltration

creates slow change in flow. These flow characteristics have been also well recognized in the field of sewer management and rehabilitation (Peters & Troemper 1969).

According to the definition of I&I, there are various I&I sources (Table 2.1). Any direct connection in a sanitary sewer system to the surface water is an inflow source. These include roof downspout, floor drain, unsealed manhole cover, storm sewer connections, etc. Compared to inflow sources, infiltration sources are simple; any groundwater intrusion through pipe and manhole defects. Root intrusion was recognized as a major sewer system problem (Sullivan et al. 1977b) that exacerbates infiltration problem. Images of roots growing through pipe joints and cracks are presented in Table 2.1. Gaps in the joints and cracks between pipes and manholes allow ground water to enter the sewer pipes. Depending on the pipe material and age, these faulty sewers can cause a great amount of sewer infiltration.

Barnard et al. (2007) classified I&I into fast, medium, and slow responses. Medium response is defined as "more delayed and attenuated response to rainfall" and this is also referred to as "rapid infiltration." Hodgson & Schultz (1995) used footer drain as an example of the medium response. Nogaj & Hollenback (1981) pointed out that foundation drains and storm sumps are not expected to be highly sensitive to changes in rainfall intensity, which makes these inflow sources classified as medium sources. The RTK method also takes three triangular hydrographs to estimate I&I flow: one for a short-term response, one for an intermediate-term response, and one for a long-term response (Rossman 2004). Thus the inflow sources in Table 2.1 are further divided into the medium and fast responses.

Table 2.1 Possible I&I sources

Infiltration	Inflow	
Slow	Medium	Fast
Defective pipes and manhole walls, Pipe joints, Connections	Sump pumps, Foundation drains, Drains from springs and swampy areas	Roof leaders, Cellar, Yard drains, Patio drains, Area drains, Driveway, Sidewalk, Stairwell drains, Window well drains, Cooling water discharges, Cross connections from storm sewers and combined sewers, Catch basins, Storm sewers, Surface run-off, Street wash water, Drainage, Floor drains, Removed sewer cleanout caps, Leakage from drinking water networks, Manhole covers

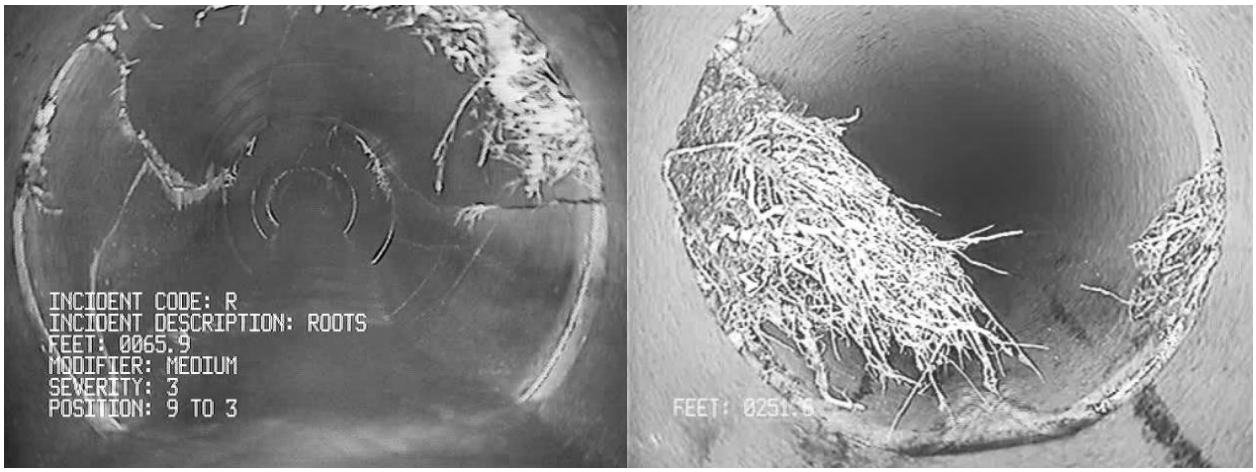

Figure 2.1 Root intrusion through cracks and joints of sewer pipes (Images from Urbana Champaign Sanitary District 2012)

2.2. Methods to Estimate I&I

The amount of I&I ($Q_{I\&I}$) in the measured sewer flow (Q_{sewer}) can be estimated by subtracting the amount of DWF (Q_{DWF});

$$Q_{I\&I} = Q_{sewer} - Q_{DWF}$$

The I&I portion of the flow in a sewer system can be estimated using these methods (De Bénédittis & Bertrand-Krajewski, 2005a, Ertl, 2002, Franz 2007):

1) Statistical method (flow-based method, hydraulic method, quantitative method)
2) Chemical method (pollutant-based method, qualitative method)
3) Drinking water consumption comparison

The statistical method, also called a flow-based, hydraulic, or quantitative method, uses sewer flow measurements during specified conditions or periods (e.g. residual night flow) to obtain domestic wastewater flows. This method is easily applicable since it only requires flow measurements while the other two methods demand extra measurement or analysis on top of flow measurement (Kretschmer et al. 2008). The chemical method, also called a pollutant-based, or qualitative method, uses pollutant concentrations e.g. COD, BOD, ammonia, iron in the sewage discharge and average pollutant discharge per capita (Verbanck et al. 1989, Kracht & Gujer 2005, Bareš 2009). Some physical properties e.g. turbidity, conductivity, and temperature have been also used as I&I indicators with simple dilution relationship (Veldkamp et al. 2002, Aumond & Joannis 2005, Schilperoort 2006, Aumond & Joannis 2008). Instead of using natural pollutants or physical property of DWF, artificial tracer can be used to estimate sewer infiltration

(Verbanck 1993). De Bénédittis & Bertrand- Krajewski (2005b) introduced an infiltration estimation method using oxygen isotopes, ^{18}O, as conservative natural tracers in Lyon, France. The new method was developed based on the difference in oxygen isotope concentration in the ambient groundwater and the drinking water source in the study area. Kracht et al. (2007) also used natural isotopes of water ($^{18}O/^{16}O$ and D/H) to quantify sewer infiltration. Pitterle & Mcginnis-Carter (2010) introduced optical brighteners to identify sewer point sources. Optical brighteners are frequently found in laundry detergent and most household wastewater contains laundry detergent. This substance has been used to track fecal contamination in ambient water but has not been widely applied to I&I estimation except a recent ongoing study by P. Miller & J. Dunker (personal communication, September 26, 2013). The drinking water consumption method uses the number of inhabitants in the study area multiplied by the average value of sewage discharge per capita. Whichever method is selected, sewer monitoring is necessary to obtain I&I hydrograph.

De Bénédittis & Bertrand-Krajewski (2005a) examined 13 different I&I estimation methods, including 11 variants of the statistical (flow-based) method and two variants of the chemical method. Their results showed great variability in the estimated flow volume among the methods. They found that infiltration amounts from the methods vary by as much as 20% of total DWF. To avoid a large uncertainty, at least 8 to 10 days of DWF observation was recommended for the methods that use minimum night flow.

As older sewer systems started aging and experiencing I&I problems in the 1960's and 1970's, many field surveys and inspections were performed and sewer rehabilitation techniques were developed. It was not until 1970s when the most urban communities in the US started to restrict the stormwater flow into sanitary sewers (Gottstein 1976, Barnard et al. 2007). Based on sewer

Table 2.2 Sewer inspection and rehabilitation techniques in 1960's and 1970's

	Authors	Year	Summary of key findings
1	Borland	1956	Experimental study about the relation between sewer infiltration and exfiltration
2	Stacy	1961	Smoke testing to locate leaky sewers
3	Dahlmeyer	1962	Chemical seal technique to stabilize soil and stop sewer infiltration
4	Van Natta	1963	Stiffer requirements in the plumbing ordinances to reduce sewer infiltration
5	Santry	1964	Experimental study about leaky sewer pipe depending on varying depths of submergence and improved pipe joints to minimize infiltration
6	Stepp	1967	Chemical sealing technique to resolve sewer infiltration problem
7	Haugh	1969	Techniques and challenges to coat leaky concrete sewer under damp conditions
8	Public Works	1969	Pictures of root intrusion, broken pipe, and leaky sewer from sewer inspection
9	American Public Works Association	1970	Thorough national study project to understand I&I problems and its impact on sewer systems
10	American Public Works Association	1971	A Manual of Practice composed from American Public Works Association (1970) about prevention and correction of I&I
11	Montgomery County Sanitary Department	1972	The effect of infiltration reduction by joint sealing and closed circuit television techniques
12	Welker and Miller	1974	Detection of illegal connections using smoke test
13	Gutierrez & Wilmut	1975	I&I requirements of the EPA and the feasibility of elimination effort
14	Lutz	1976	Split of I&I hydrograph into infiltration and inflow components
15	Kranik & Johnson	1976	Sewer system evaluation and survey to reduce I&I
16	Maynes	1976	Sewage flow data collection and cost estimate from I&I
17	Elliott et al.	1977	The effectiveness of I&I from private properties
18	Stilley	1977	Required field operations for an I&I analysis
19	Sullivan et al.	1977a	A Manual of Practice for sewer system evaluation, rehabilitation and new construction
20	Public Works	1979	Effectiveness of watertight manhole inserts to remove stormwater inflow through manhole covers

evaluation and cost analysis studies, many cities realized that repairing damaged sewer systems is more economical than expanding the treatment facility (Podolick 1975). The efforts to calculate I&I based on measurements are summarized in Table 2.2**Error! Reference source not found.**. Note that these are all measurement methods, rather than predictive estimation methods presented in chapter 1.

2.3. Space and Time Variability of I&I Process

Each community experiences I&I differently and the major I&I source varies in a particular sewershed. In fact, many different factors affect I&I characteristics: climate, geography, soil characteristics, groundwater table condition, construction material, pipe joint types, pipe age, vegetation, workmanship, construction procedure, and existence of illegal connections. Belhadj et al. (1995) also stressed that RDII is highly temporally and spatially variable depending on the rainfall intensity, groundwater level, and soil moisture.

Seasonal variability is one of the common temporal variabilities in sewer flow. Ertl et al. (2002) discovered a seasonal variation in I&I by analyzing the inflow to a water treatment plant in east Austria. Increased I&I were observed in spring and autumn depending on the groundwater level in the study area. Kretschmer et al. (2008) also analyzed DWF monitoring data with monthly variation in Austria; high in spring and low in summer. Brombach et al. (2002) showed the seasonal variability can be up to 10 times in the high infiltration season compared to the low season. Flooding also raises the local groundwater level and increases I&I (Karpf & Krebs, 2004). This can affect I&I greatly in places with high seasonality in rainfall.

Temporal variability also exists at smaller scales. De Bénédittis & Bertrand-Krajewski (2005b) found strong variations in the hydrograph of infiltration during a day. Two flow peaks were observed in the I&I hydrograph due to the connections of groundwater pumps, and the low DWF depth during nights. Low DWF level in sewer pipes exposes more pipe defects hence increases the infiltration flow during night time as the hydraulic gradient between the wastewater surface level and the groundwater level around the sewer increases.

Antecedent moisture condition (AMC) is an important factor that affects temporal variability of I&I (Czachorski & Van Pelt 2001, Van Pelt & Czachorski 2011, Sadri & Graham 2011). AMC is one source of non-linearity of I&I and Czachorski & Van Pelt (2001) applied a nonlinear system identification method, which is commonly used in aerospace engineering applications for high fidelity modeling of aircraft and space system, to model I&I. Sadri & Graham (2011) suggested a regression method to predict I&I including the AMC for past 10 days. Not many commercial models take account of AMC in I&I estimation. The i3D antecedent moisture (i3D AM) model considers AMC using the system identification technique from aerospace engineering control systems (i3D Technologies, 2010). Investigation about AMC related to infiltration process is covered in the chapter 5 in this thesis.

Inherently I&I has spatial variability, since it is affected by spatially varied parameters such as the age of sewer system, local groundwater condition, etc. Franz (2007) developed a method to optimize infiltration flow measurement locations in a sewer system. To improve the information yield, measurement results from identified measuring locations are paired with other potential measuring points by comparing sub-catchments and classifying reaches. This method is based on the ‘similarity approach’ and multivariate statistical techniques. The similarity approach is based

on the assumption that similar sewer conditions yield similar I&I rates. This optimization method improved the accuracy of I&I estimations by 40%.

References

American Public Works Association. (1970) *Control of infiltration and inflow into sewer systems* (p. 133).

American Public Works Association. (1971) *Prevention and correction of excessive infiltration and inflow into sewer systems: A manual of practice* (p. 125).

Aumond, M., & Joannis, C. (2005) Turbidity monitoring in sewage. *10th International Conference on Urban Drainage*. Copenhagen, Denmark.

Aumond, M., & Joannis, C. (2008) Processing sewage turbidity and conductivity recorded in sewage for assessing sanitary water and infiltration/inflow discharges. *11th International Conference on Urban Drainage* (pp. 1–10). Edinburgh, Scotland, UK.

Barnard, T. E., Whitman, B. E., Hill, C., Mckay, G., Plante, S., & Schmitz, B. A. (2007) *Wastewater collection system modeling and design-CH7* (1st ed., pp. 203–270). Bentley Institute Press.

Bareš, V., Stránský, D., & Sýkora, P. (2009) Sewer infiltration/inflow: long-term monitoring based on diurnal variation of pollutant mass flux. *Water Science and Technology : a Journal of the International Association on Water Pollution Research*, *60*(1), 1–7. doi:10.2166/wst.2009.280

Belhadj, N., Joannis, C., & Raimbault, G. (1995) Modelling of rainfall induced infiltration into separate sewerage. *Water Science & Technology*, *32*(1), 161–168.

Bishop, W. J., Diemer, D. M. & Wallis, M. J. (1987) Regional infiltration/inflow study solves wet weather sewer problems. *Journal of Water Pollution Control Federation* **59**(5), 289–293. Retrieved from http://www.jstor.org/stable/25043247?origin=JSTOR-pdf

Borland, S. (1956) "New data on sewer infiltration-exfiltration ratios." *Public Works* Sep. 1956: 97–98.

Blöschl, G. & Sivapalan, M. (1995) Scale issues in hydrological modelling: A review. *Hydrological Processes* **9**, 251–290.

Brombach, H., Weiss, G., & Lucas, S. (2002) Temporal variation of infiltration inflow in combined sewer systems. *Proceedings of 9th International Conference on Urban Drainage (9ICUD)*, *112*, 125–125. doi:10.1061/40644(2002)125

Czachorski, R. S. & Pelt, T. H. Van. (2001) On the modeling of inflow and infiltration within sanitary collection systems for addressing nonlinearities arising from antecedent moisture conditions. *WEFTEC*, 606.

Dahlmeyer, F. D. (1962) "Chemical seal stops sewer infiltration." *Public Works* Nov. 1962: 91–92.

De Bénédittis, J. & Bertrand-Krajewski, J. L. (2005a) Infiltration in sewer systems: comparison of measurement methods. *Water Science and Technology : a Journal of the International*

Association on Water Pollution Research **52**(3), 219–27. Retrieved from http://www.ncbi.nlm.nih.gov/pubmed/16206862

De Bénédittis, J., & Bertrand-Krajewski, J. L. (2005b) Measurement of infiltration rates in urban sewer systems by use of oxygen isotopes. *Water science and technology: a journal of the International Association on Water Pollution Research*, *52*(3), 229–37. Retrieved from http://www.ncbi.nlm.nih.gov/pubmed/16206863

Elliott, J. C., Hydro, S. K., MAlarich, M. A., & Weaver, W. (1977) "Removing private sources of infiltration and inflow." *Water Environment & Technology* Aug. 1977: 55–60.

EPA. (1985) Infiltration/inflow: I&I analysis and project certification. *Environmental Protection*, 8. Washington, DC.

EPA. (1991) *Sewer system infrastructure analysis and rehabilitation* (p. 92). Cincinnati, OH.

EPA. (1995) Federal Register **60**(234), 62546–62659.

Ertl, T. W., Dlauhy, F., & Haberl, R. (2002) Investigations of the amount of infiltration/inflow into a sewage system. In *Proceedings of the 3rd "Sewer Processes and Networks" International Conference*. Paris, France.

Franz, T. (2007) *Spatial classification methods for efficient infiltration measurements and transfer of measuring results*. Dresden University of Technology, Dresden, Germany.

Gottstein, L. E. (1976) *Sewer system evaluation for infiltration/inflow*. Minneapolis, Minnesota.

Gutierrez, A. F., & Wilmut, C. (1975) “The feasibility of infiltration/inflow elimination.” *Public Works* Apr. 1975: 68–70.

Haugh, H. H. (1969) “Rehabilitation of a concrete sewer under infiltration pressure.” *Public Works* Jul. 1969: 89–90.

Hodgson, J.E., Schultz, N.U., (1995) Sanitary sewage discharges in the city of Edmonton, Alberta, pp. 403-413, in *Seminar Publication: National Conference on Sanitary Sewer Overflows (SSOs)* (p. 588). Washington D.C.

i3D Technologies. (2010) Technical overview: The i3D antecedent moisture model.

Karpf, C., & Krebs, P. (2004) Sewers as drainage systems – quantification of groundwater infiltration. In *Novatech 2004, 6th International conference on sustainable techniques and strategies in urban water managementWater Management* (pp. 969–975). Lyon.

Kracht, O., Gresch, M., & Gujer, W. (2007) A stable isotope approach for the quantification of sewer infiltration. *Environmental Science and Technology technology*, *41*(16), 5839–45. Retrieved from http://www.ncbi.nlm.nih.gov/pubmed/17874795

Kracht, O., & Gujer, W. (2005) Quantification of infiltration into sewers based on time series of pollutant loads. *Water Science and Technology : a Journal of the International Association on Water Pollution Research*, *52*(3), 209–18. Retrieved from http://www.ncbi.nlm.nih.gov/pubmed/16206861

Kretschmer, F., Ertl, T., & Koch, F. (2008) Discharge monitoring and determination of infiltration water in sewer systems. In *11th International Conference on Urban Drainage* (pp. 1–7). Edinburgh, Scotland, UK.

Lutz, J. J. (1976) "Comparing inflow and infiltration." *Water & Sewage Works* May 1976: 68–69.

Maynes, J. S. (1976) Flow data collection for infiltration-inflow analysis. *Journal of Water Pollution Control Federation*, *48*(8), 2055– 2061. Retrieved from http://www.jstor.org/stable/25039977 .

Montgomery County Sanitary Department. (1972) *Ground water infiltration and internal sealing of sanitary sewers* (p. 75). Montgomery County, Ohio.

Nogaj, R. J., & Hollenbeck, A. J. (1981) One technique for estimating inflow with surcharge conditions. *Journal of Water Pollution Control Federation*, *53*(4), 491–496.

Peters, G. L. & Troemper, A. P. (1969) Reduction of hydraulic sewer loading by downspout removal. *Water Pollution Control Federation* **41**(1), 63–81.

Pitterle, B., & Mcginnis-Carter, F. (2010) Optical brightener monitoring in Goleta streams: A summary of monitoring results from August 2009 - November 2009, (January).

Podolick, P. A. (1975) Preparing an infiltration/inflow analysis. *Water & Sewage Works Reference Number*, *1 TAB*, 31–32, 34.

Public Works. (1969) "From the inspector's photo album." *Public Works* Jan. 1969: 73.

Public Works. (1979) “Manhole inserts abate inflow.” *Public Works* Dec. 1979: 47.

Rossman, L. A. (2004) *Storm water management model user’s manual: Version 5.0*. Cincinnati, OH.

Sadri, S. & Graham, E. (2011) Development of an antecedent moisture condition model for prediction of Rainfall-Derived Inflow/Infiltration (RDII). *American Geophysical Union*. San Francisco.

Santry, I. W. J. (1964) Infiltration in sanitary sewers. *Journal of Water Pollution Control Federation*, *36*(10), 1256– 1262. Retrieved from http://www.jstor.org/stable/25035156

Schilperoort, R. P. S., Gruber, G., Flamink, C. M. L., Clemens, F., & Van der Graaf, J. H. J. M. (2006) Temperature and conductivity as control parameters for pollution-based real-time control. *Water Science & Technology*, *54*(11), 257. doi:10.2166/wst.2006.744

Stacy, C. E. (1961) “Locating leaky sewers with smoke.” *Public Works* Nov. 1961: 133.

Stepp, S. G. (1967) “Sealing process resolves infiltration problem.” *Public Works* Jul. 1967: 70–73.

Stilley, S. H. (1977) Simulated field study for I&I analysis. *Public Works*, 50–53.

Sullivan, R. H., Cohn, M. M., Clark, T. J., Thompson, W., & Zaffle, J. (1977a) *Sewer system evaluation, rehabilitation and new construction: A manual of practice* (p. 194). Chicago, IL.

Sullivan, R. H., Gemmell, R. S., Schafer, L. A., & Hurst, W. D. (1977b) *Economic analysis, root control, and backwater flow control as related to infiltration/inflow control* (p. 114). Edison, NJ.

Van Pelt, T. H. & Czachorski, R. S. (2011) The application of system identification to inflow and infiltration modeling and design storm event simulation for sanitary collection systems. *WEFTEC 2011*. Los Angeles, CA.

Van Natta, W. S. (1963) "Fighting infiltration into sewers." *Public Works* Jul. 1963: 158–159.

Veldkamp, R., Henckens, G., Langeveld, J., & Clemens, F. (2002) Field data on time and space scales of transport processes in sewer systems. In E. W. Strecker & W. C. Huver (Eds.), *Urban Drainage 2002* (Vol. 112, pp. 293–293). Portland, Oregon: Asce. doi:10.1061/40644(2002)293

Verbanck, M. A. (1993) A new method for the identification of infiltration waters in sanitary flows. *Water Science & Technology*, *27*(12), 227–230.

Verbanck, M., Vanderborght, J.-P., & Wollast, R. (1989) Major ion content of urban wastewater: Assessment of per capita loading. *Water Pollution Control Federation*, *61*(11/12), 1722–1728.

Welker, F. S., & Miller, D. J. (1974) "Smoke tests detect sources of illegal inflow." *Public Works* Sep. 1974: 90–91.

3. Methodology

In this chapter, it is hypothesized that a space and time tradeoff in a local response and a system response of I&I exists. Roof drain connection, sump pump connection, and leaky sewer lateral are selected as three main I&I sources and physics-based models to derive impulse response functions (IRFs) of the three sources are presented. Based on the assumption that spatial distribution of various I&I sources is negligible in a small sewershed, three main I&I responses are convoluted. The assumption is based on the discussion about space and time scale tradeoff that is presented in section 3.2. The genetic algorithm (GA) that is used to calibrate a system response of I&I is also introduced.

3.1. Introduction

Various efforts have been made to estimate I&I but they are largely empirical. The RTK method, which is one of the most commonly used I&I estimation methods, uses three triangular hydrographs to represent various I&I sources. By adjusting nine parameters to fit to sewer flow monitoring data total I&I is estimated for a sewer system. The parameters determine the peak, time to peak, and duration of the three triangular hydrographs-three parameters for each hydrograph. The RTK method has been widely used because of its simplicity and decent estimation of I&I; however, the RTK method lacks physical meaning of I&I processes.

In this study, a conceptualized model, which better reflects physics of the I&I processes, is introduced. The basic framework of the model falls under the category of the unit hydrograph method, as does the RTK method, but three I&I impulse response functions (IRFs) are derived using physics-based models. Among numerous I&I sources, three most typical sources are selected to represent three IRFs: inflow from roof connections, sump pump connections, and

infiltration through leaky sewer laterals. I&I is originated from mostly private properties (Strand Associate Inc. 2006), not from main sewer system, which makes it difficult to control. For simplicity, a single private residential lot is selected as the model domain.

Roof connections are used in this research to represent all the direct connections into a sanitary sewer system from impervious surfaces (e.g. roof, paved driveways, outdoor stairwells, window wells). Golden (1995) and Peters & Troemper (1969) showed roof connections are one of the most problematic I&I sources. Sump pump connections represent "promoted" percolation flow, which is all the I&I sources that involve mixture of short porous flow and flow through direct connections at the same time. The word "promoted" is used to describe infiltration that is facilitated by introducing engineered soil. Reynolds (1995) indicated that roof drains and sump pumps were suspected to be two major contributors of I&I in the city of South Portland. Longer flow through porous media, or percolation flow, is represented by the infiltration through leaky sewer laterals. Pawlowski et al. (2013) indicated that 98% of I&I volume was originated from downspouts (roof connections) and leaky laterals in the city of Columbus, OH.

The roof connection IRF is developed using the kinematic wave equation (for roof runoff) and level-pool routing, weir, and orifice flow equations (for rain gutter flow). The influence of the flow in the roof downspout and the extended connection to the sewer pipe on the time of concentration is ignored since it is mainly fast vertical flow.

The sump pump connection and the leaky lateral IRFs are developed using the gravity equation imbedded in the MIKE-SHE (DHI Software 2007a, DHI Software 2007b) which is a spatially distributed detailed model. Three different soil properties are selected to represent ambient soil, impervious surface, and highly pervious soil. The equivalent medium approach (Carlier et al.

2007) that uses a single soil layer to imitate a leaky lateral and surrounding backfill is applied to the leaky lateral model.

The IRF from the roof connection shows a high peak and relatively short duration as it represents runoff from an impervious surface. The leaky lateral IRF shows a low peak and long duration since the process involves flow through porous media. The IRF from the sump pump connection falls in between that of the roof connection and the leaky lateral. These three IRFs reflect the physical characteristics of each I&I process instead of expressing I&I using arbitrary triangular unit responses as in the RTK method. Roof connection IRF is dominated by the rainfall hyetograph. The travel time of the flow is short and transformation is negligible. Sump pump flow path through porous media is short and the media is usually disturbed and modified near building foundation. Thus the uncertainty associated with the roof connection IRF and the sump pump IRF is probably small compared to the IRF of infiltration through leaky sewer pipes. RII is distributed throughout the sewer system and affected by wide variety of pipe depths, media properties, compaction of soil, etc. Hence, variability in the IRF of RII is anticipated to be much greater and more significant than for roof connection and sump pump. Therefore, the variability in RII is further examined in this study while the variability in roof connection and sump pump is left for future research.

Following six factors are investigated to examine the variability of RII: antecedent moisture condition (AMC), pedotransfer functions (PTFs), soil hydraulic conductivities, initial conditions (IC), sewer pipe depths, and rainfall characteristics. To understand the effect of AMC on RII hydrograph, a uniform rainfall is added to an actual historical rainfall record at ten random time which results in different AMC conditions for each case. The differences in modeled sewer flow responses between the actual rainfall and the rainfall with the added storm are used to estimate

the infiltration IRF. The effect of soil hydraulic conductivity on RII hydrograph is tested using 14 different conductivity values that are selected from the actual soil data. Seven different PTFs are applied for the same soil data to compare soil hydraulic conductivity values. Ten different simulation periods are tested to investigate the effect of IC on the RII hydrograph. The effect of rainfall characteristics on the RII hydrograph is investigated using various storm durations and shapes. Eleven different sewer pipe depths are tested to see the effect on RII hydrograph. This study is mainly focused on examining how the output – RII hydrograph – changes depending on the change of these six input parameters within anticipated ranges. Any correlation between the six factors is neglected and each factor is investigated one at a time. Details about the investigation are discussed in chapter 5.

3.2. Space and Time Scale of I&I Processes

Figure 3.1 shows the spatial and temporal scales of different urban hydrology components. There is an overall tendency that as the temporal scale increases the spatial scale also increases for a certain hydrological process. This can be interpreted that once the temporal scale becomes large smaller spatial variations become less important. In a sewershed, the response time of a local I&I process relative to the time scale of sewer flow in the entire system determines how important it is to consider the spatial variability of the I&I processes. If the time scale of a local I&I process is much smaller than that of the sewer flow in the system, where the I&I enters the system becomes important. If the time scale of a local I&I process becomes as large as that of the system, then spatial distribution of the local sources becomes not as important. Thus there is a tradeoff between time and space.

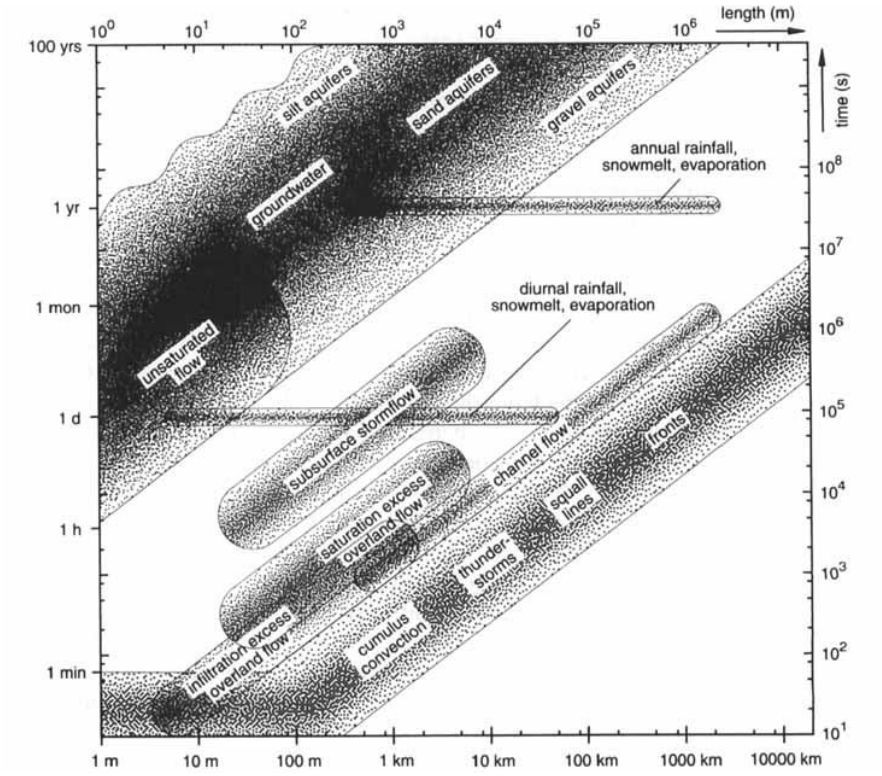

Figure 3.1 Hydrological processes at a range of characteristic space-time scales (Blöschl & Sivapalan 1995)

A reference time scale can be introduced to explain the time and space tradeoff. The reference time is the local event time or the source time (t_s) normalized with a network time or system time (t_*), such as time of concentration (t_c). The local event time or the source time (t_s) is the base time of the local I&I response function, which is defined as the impulse response function (IRF) in this study. Base time is the total time duration of a hydrograph. Time of concentration (t_c) is the time required for water to travel from the most hydraulically remote point in the sewershed to the outlet. The drainage characteristics (e.g length, slope) together with the hydraulic characteristics (e.g. flow paths) determine the time of concentration. Thus criteria like the following can be suggested for the space and time tradeoff between the I&I process and the sewershed flow.

- When $\frac{t_s}{t_*} \ll 1$, spatial distribution of I&I sources becomes more important

- When $\frac{t_s}{t_*} \gg 1$, spatial distribution of I&I sources becomes less important

The ratio between the local time scale and the network time scale can be an important factor for I&I routing in a sewer network. When the ratio is small, spatial distribution of I&I sources in the network may become important. If the ratio is large, it might not be as important. This shows the tradeoff between the temporal scales and spatial distribution of I&I responses.

To understand the spatial variability of I&I sources, characteristics of system responses are investigated in Figure 3.2 and Figure 3.3. Note that the I&I responses that are covered in the later chapters in this thesis are IRF at a lot scale rather than a system scale. The spatial distribution of I&I sources in a system is uncertain because it depends on unknown factors such as pipe age, pipe condition, root intrusion, crack size and location, etc. (Figure 3.2). This means the distribution of the I&I sources in the system can be viewed as random. Thus it is impractical and nearly impossible to distinguish every source in the system. Not only I&I but also DWF enters in many different locations, but the locations of DWF are more predictable as the sewer inlets are built around the DWF sources.

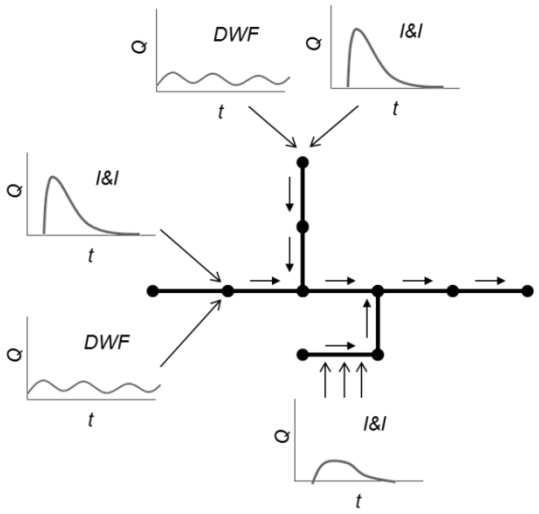

Figure 3.2 Random I&I and DWF input locations in a sewer system

Figure 3.3 shows how the travel time of flow in a sewer network affects fast and slow I&I sources when the entire system response is taken into consideration. The IRF for a lot scale I&I source can be identified and from this the I&I responses for a specified rainfall event can be derived for fast and slow I&I. Both fast and slow I&I enter into the sewer system in three different locations that are marked with an X, triangle, and circle in the figure; from a shorter to a longer path. At the downstream outlet of the sewer network (marked with an upside-down triangle), the system responses for the fast and the slow I&I can be estimated as is shown. The local responses of the three fast I&I are easier to distinguish from each other in the system response while that of the three slow I&I are harder as they overlap to a greater extent. The difference in travel time from the I&I inflow locations to the sewershed outlet among different sources is negligible for slow I&I because the characteristic time (base time) of the IRF is long relative to the travel time. In contrast for fast I&I, when the base time is short relative to the travel time, the locations of the I&I inflow become important. The spatial variability of fast I&I

may need to be considered if the sewershed size is relatively large or the travel time in the system is long compare to the local I&I response time.

Seo & Schmidt (2012) found that the speed and direction of rainstorm movement matters for fast-moving rainstorms in less efficient networks (small Gibbs parameter β). This means spatial variability of rainfall becomes important when the duration of storm is smaller than the duration of network flow (time of concentration of the network); normally this is in large networks. This also applies to I&I processes. If the time of I&I process is shorter than the network travel time of sewer flow, the spatial variability of I&I sources becomes important. Seo et al. (2012) also suggested a theoretical framework to describe stationary rainstorm and moving rainstorms using characteristic time and space scales. The difference in behavior between stationary rainstorms and moving rainstorms was originated by the interdependence between two time scales: storm duration and storm travel time in sewershed. Their work can be extended to I&I into sewer systems and the two time scales can be replaced with: IRF (I&I base time at random locations upstream) and I&I travel time to the outlet.

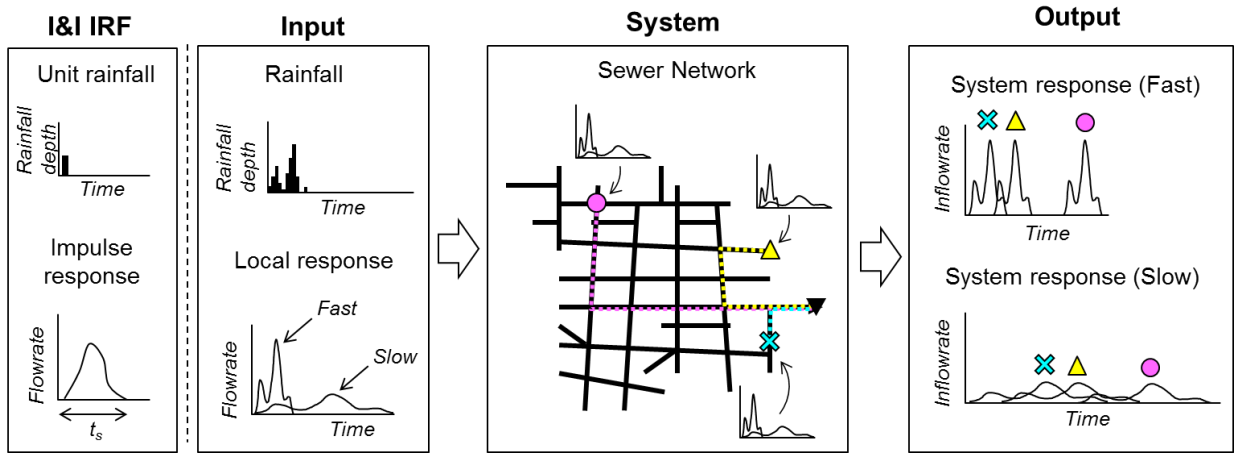

Figure 3.3 Effect of random locations of I&I sources in a sewer network on the fast and slow I&I

Not only the size of a sewershed but also the efficiency of the sewer network can affect the travel time of I&I responses. Figure 3.4 presents two same sized sewer networks with different configurations. Figure 3.4(a) is the least efficient network and Figure 3.4(b) is the most efficient network in terms of drainage. Three random I&I locations are marked as an X, triangle, and circle; from a shorter to a longer distance from the outlet, respectively, and the distance between these locations and the outlet are summarized in Table 3.1. The distance in the least efficient network ranges from 50% to 142% greater than that in the most efficient network. Even though the size of both sewersheds is equal, different sewer network configurations can affect the travel time in the system. This indicates that the configuration of a sewershed may also affect how important it is to consider the spatial variability of I&I sources. There are various factors that affect the travel time in a system other than the network efficiency: pipe slope, flow resistance of pipes, etc. This argument about the temporal scale and network routing can be tested as a future research.

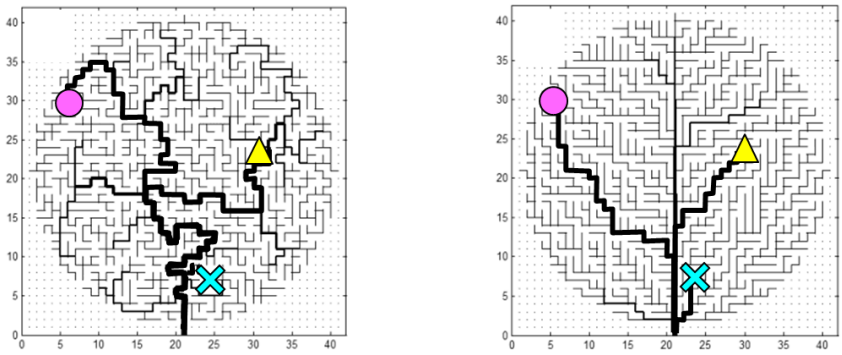

Figure 3.4 Three random I&I locations and the distance to the outlet in the least efficient drainage network (a) and the most efficient network (original source of the networks from Seo 2012)

Table 3.1 Distance of three I&I sources to the outlet

I&I source location (Symbols in Figure 3.4)	Distance to the outlet		Difference in distance (Least – Most)/Most x 100
	Least efficient network Figure 3.4(a)	Most efficient network Figure 3.4(b)	
X	15	10	50%
Triangle	75	31	142%
Circle	83	46	80%

In this section, the relationship between space and time scales of I&I processes was discussed. If the response time of I&I process is shorter than the network travel time, spatial variation of I&I sources becomes important. Conversely, spatial variation of the I&I with relatively slow response time becomes less important. This was explained using a visualized hypothetic example in Figure 3.3. This argument may provide a justification to the assumption that spatial distribution of various I&I sources can be ignored in a small sewershed.

3.3. Modeling of I&I Response Functions

In this section, three representative I&I sources are investigated: roof drain connection, sump pump connection, and leaky sewer lateral. The first two sources are examples of illegal connections to sanitary sewer systems that lead surface water and soil water into sewer pipes. Standard practice is to "drain to light" or drain to a gravity flow – a ditch, a storm sewer, or an overland flow surface, ideally a permeable soil. When the storm sources are connected to sanitary sewer systems extra water is added to wastewater system. Leaky sewer pipes allow soil water or groundwater to intrude to the sanitary sewer system. To model these physical processes, the one-dimensional kinematic wave equation is employed for the roof drain response and one-

dimensional gravity flow equation is used for the sump pump and the leaky sewer lateral responses. To investigate local flow responses, a single residential lot is selected as a model domain. Some model parameters e.g. average surface area of roof, soil hydraulic conductivities, are derived from the available data in the case study area, Hickory Hills, IL. More details about the study area is further described in chapter 4.

3.3.1. Roof Drain Connection

The roof drain model consists of a sloped roof area, flat gutter, and vertical downspout as shown in Figure 3.5. Roof area receives rainfall and leads the flow to the rain gutter. The rain gutter is connected to a downspout(s) to convey flow to a drainage system. These drainage features route the rainfall runoff from the roof away from the house. When the downspout is connected to a sewer system it becomes sewer inflow.

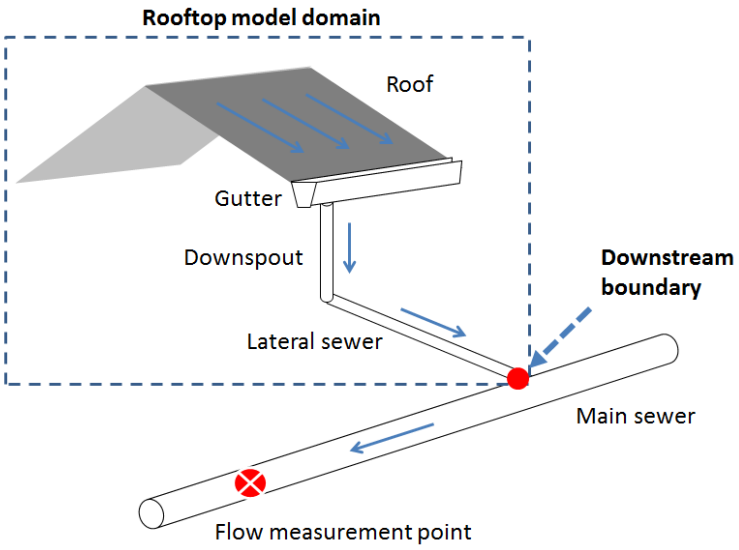

Figure 3.5 Roof connection model domain

The flow from the roof is calculated using the one-dimensional kinematic wave model for rainfall-runoff. Two governing equations describe the rainfall-runoff process when using kinematic wave theory: one-dimensional continuity equation for unit width of sheet flow, and Manning's equation as a momentum equation for one-dimensional steady uniform flow per unit width. The one-dimensional continuity equation is as follows:

$$\frac{\partial h}{\partial t} + \frac{\partial q}{\partial x} = I \tag{1}$$

where h = water depth [L], t = time [T], q = flow rate per unit width [L^2/T], x = distance in down slope (measured from upstream end of plane) [L], I = rainfall intensity [L/T].

Manning's equation can be used as a momentum equation for one-dimensional steady uniform flow per unit width as following.

$$q = \frac{1.49}{n} S_0^{1/2} h^{5/3} \tag{2}$$

where n = Manning's roughness coefficient, S_0 = bottom slope.

In order to have only one dependent variable q, the second equation can be expressed as an equation for h.

$$h = \left(\frac{1.49}{n} S_0^{1/2} \right)^{-3/5} q^{3/5} \tag{3}$$

or

$$h = \alpha q^{\beta} \tag{4}$$

where $\alpha = \left(\frac{1.49}{n} S_0^{1/2} \right)^{-\beta}$, $\beta = 3/5$

by differentiating the equation by *t*,

$$\frac{\partial h}{\partial t} = \alpha\beta q^{\beta-1} \frac{\partial q}{\partial t} \tag{5}$$

This can be substituted to the continuity equation;

$$\alpha\beta q^{\beta-1} \frac{\partial q}{\partial t} + \frac{\partial q}{\partial x} = I \tag{6}$$

or

$$\frac{\partial q}{\partial x} + \alpha\beta q^{\beta-1} \frac{\partial q}{\partial t} = I \tag{7}$$

This is the governing equation that combines continuity equation and momentum equation for kinematic wave model with *q* as only dependent variable.

For a numerical solution, a linear scheme (Chow et al. 1988) was applied in this study. On the *x*-*t* grid with *i* as spatial location index and *j* as temporal location index, each term in the equation can be approximated as;

$$\frac{\partial q}{\partial x} \approx \frac{q_{i+1,j+1} - q_{i,j+1}}{\Delta x} \tag{8}$$

$$\frac{\partial q}{\partial t} \approx \frac{q_{i+1,j+1} - q_{i+1,j}}{\Delta t} \tag{9}$$

$$q \approx \frac{q_{i+1,j} + q_{i,j+1}}{2} \tag{10}$$

$$I \approx \frac{I_{i+1,j+1} + I_{i+1,j}}{2} \tag{11}$$

By substituting these finite-difference approximations in the governing equation, the kinematic wave equation can be derived as following.

$$\frac{q_{i+1,j+1} - q_{i,j+1}}{\Delta x} + \alpha\beta\left(\frac{q_{i+1,j} + q_{i,j+1}}{2}\right)^{\beta-1}\left(\frac{q_{i+1,j+1} - q_{i+1,j}}{\Delta t}\right) = \frac{I_{i+1,j+1} + I_{i+1,j}}{2} \tag{12}$$

By solving the equation for the unknown $q_{i+1,j+1}$, the equation becomes;

$$q_{i+1,j+1} = \frac{\frac{dt}{dx} q_{i,j+1} + \alpha\beta\left(\frac{q_{i+1,j} + q_{i,j+1}}{2}\right)^{\beta-1} q_{i+1,j} + dt\left(\frac{I_{i+1,j+1} + I_{i+1,j}}{2}\right)}{\frac{dt}{dx} + \alpha\beta\left(\frac{q_{i+1,j} + q_{i,j+1}}{2}\right)^{\beta-1}} \tag{13}$$

The gutter is treated as a simple bucket model and the outlet of downspout is treated as a weir or orifice depending on the flow condition. The gutter is modeled using the standard level-pool routing method. Level-pool routing is a lumped flow routing methods that is suitable for a case with horizontal water surface in storage unit. The storage is a function of its water surface elevation. By using the stage-storage relation of the rain gutter and the stage-discharge relation of the downspout this equation can be solved. Stage-discharge relations of the rain gutter-outlet are derived using an orifice and a weir equation.

3.3.2. Sump Pump Connection

Sump pumps involve many different drainage features in a house. They might be connected to foundation drains, window wells, stair wells, etc. The I&I response from a sump pump is slower

than a roof connection, since it involves infiltration through porous media. Compared to sewer infiltration through leaky sewer pipe the flow response is faster since the flow path is shorter (i.e. the order of the foundation depth or less).

To derive the typical response function from a sump pump, the commercial software MIKE SHE (DHI Software, 2007a, 2007b) is employed to model flow to the sump in a single residential lot. MIKE-SHE is a spatially distributed hydrologic model that simulates surface water flow and groundwater flow in three-dimensional gridded form. The one-dimensional gravity flow equation in MIKE SHE is selected as the unsaturated zone equation. The gravity flow equation is a simplified version of the Richards equation, which ignores the pressure head term. The vertical driving force is entirely due to gravity. By selecting the gravity flow module, the dynamics in the unsaturated zone caused by capillarity are ignored. This is typically a valid assumption for coarse soils and drainage trench around a house is usually filled with coarse materials. This is suitable to calculate the recharge rate of groundwater and faster and more stable than Richards equation (Graham & Butts, 2005). The governing equation for Richards equation is presented as following (DHI Software, 2007a, 2007b).

$$h = z + \psi \tag{14}$$

Then the gravity equation becomes

$$h = z \tag{15}$$

where h is hydraulic head [L], z is gravitational head [L], and ψ is pressure head [L].

The vertical gradient of the hydraulic head is the driving force to transport water. Thus, for the Richards equation,

$$\Delta h = \frac{\partial h}{\partial z} \tag{16}$$

and for the gravity equation,

$$\Delta h = \frac{\partial h}{\partial z} = 1 \tag{17}$$

The volumetric flux that is obtained from Darcy's law for the gravity equation is

$$q = -K(\theta)\frac{\partial h}{\partial z} = -K(\theta) \tag{18}$$

where $K(\theta)$ is unsaturated hydraulic conductivity [L^3/T].

For incompressible soil matrix and soil water with constant density, the continuity equation is:

$$\frac{\partial \theta}{\partial t} = -\frac{\partial q}{\partial z} - S(z) \tag{19}$$

where θ is volumetric soil moisture [L^2] and *S* is root extraction sink term [L^2/T]. The sum of root extraction over the entire root zone depth is equal to the total actual evapotranspiration. Direct soil evaporation is computed only in the first node below the surface.

Substituting equation (18) onto equation (19), the following expression is derived.

$$\frac{\partial \theta}{\partial t} = \frac{\partial K(\theta)}{\partial z} - S(z) \tag{20}$$

This can be also expressed using the soil water capacity, $C = \frac{\partial \theta}{\partial \psi}$

$$C\frac{\partial \psi}{\partial t} = \frac{\partial K(\theta)}{\partial z} - S(z) \tag{21}$$

This is called the gravity equation. This equation is selected to calculate the unsaturated zone flow into a sump pump, which is used to derive the typical flow response function or impulse response function (IRF) of a sump pump in this study.

Figure 3.6 shows typical drainage features of home construction. When hydraulic pressure in the perforated footing drain pipe is greater than surroundings, it drains to daylight if gravity drainage is possible (to exterior grades or to a storm sewer). If gravity drainage is not possible, the drain pipe drains to an interior sump. When hydraulic pressure in the sump is greater than surroundings, it drains to impervious area, pervious area, or sewer systems by pumping. The drainage trench around the house consists of backfill below the soil and this vertical feature is reflected in the modeling.

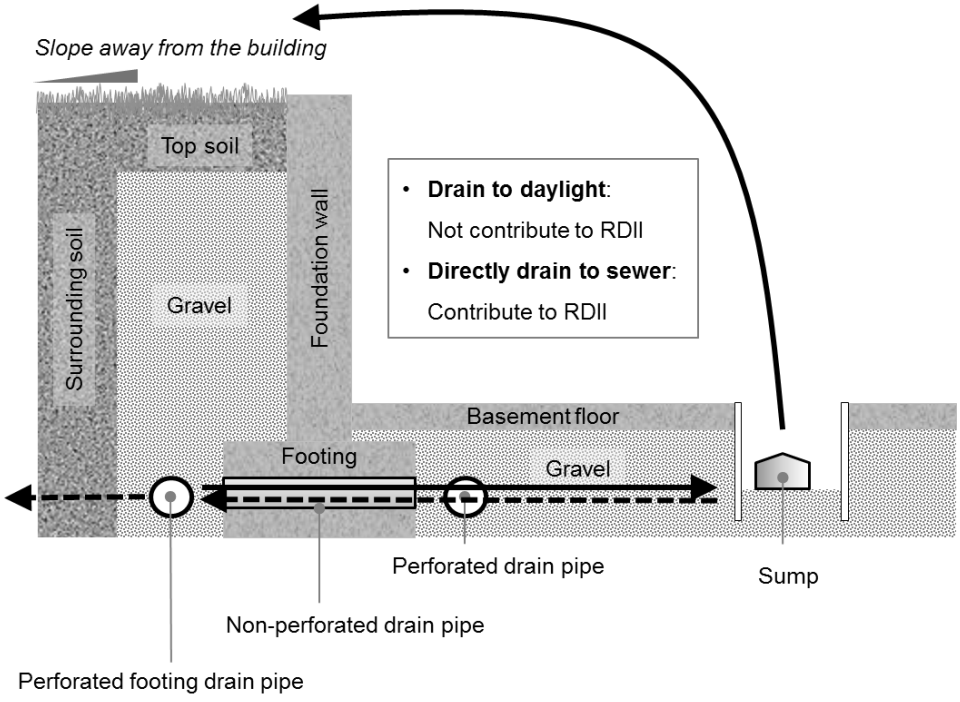

Figure 3.6 Typical foundation drain and sump pump features in a home construction with a sump pump flow in a solid line and a gravity flow in a dashed line; all drain to day light or sewer (modified from Depew 1992)

The drainage trench around the house enables surface water to percolate down to the bottom of the building and it is assumed that this all turns into sump pump. In the model sink cells are placed under the building to mimic sump pump behavior and extract the water from the foundation. Unsaturated zone flow at the foundation level of the drainage trench area is summed and interpreted as total sump pump flow from the house. When the outlet of this sump pump is connected to a sewer system this becomes I&I. Figure 3.7 shows the soil profile definitions that are used for the sump pump modeling. Soil profile 4 indicates backfill below the soil and soil profile 5 indicates backfill below the impervious surface.

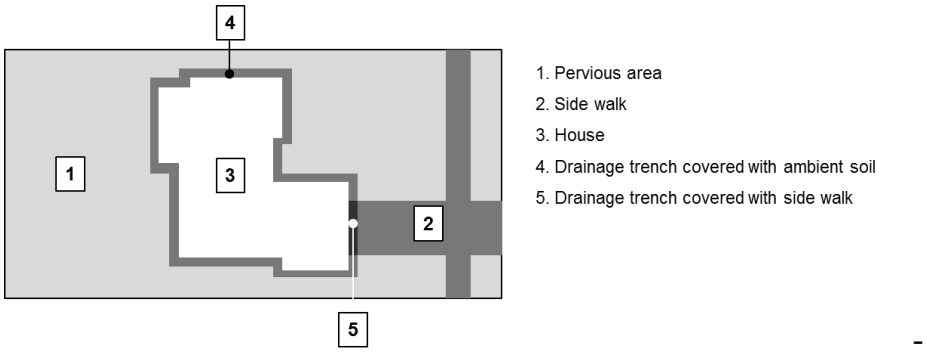

(a)

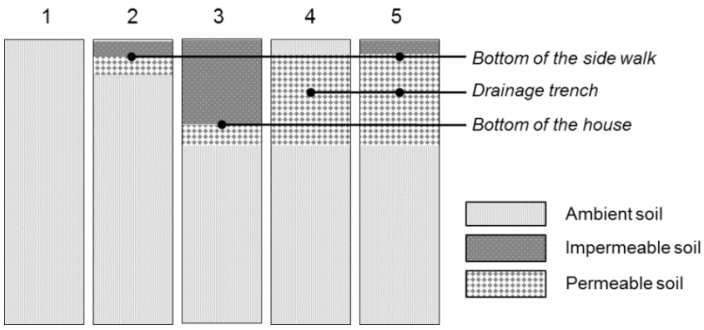

(b)

Figure 3.7 Soil profile definitions of the sump pump modeling (a) plan view (b) vertical view (figures not drawn to scale)

The size of the domain is 50 m lengthwise and 26 m widthwise. The cell size is 0.33 m x 0.33 m thus total 150 × 78 or 11700 cells are created. Vertical cell height is 0.2 m. The vegetation was assumed as uniform grass with Leaf Area Index 5 and Root Depth 100 mm. The width of drainage trench is assumed as 0.33 m and the total number of cells is 149 which leaves around 50 m length of trench. The drainage trench goes down to the base level of the house, 4 m below the surface where the sump is located.

Three soil types are employed in the sump pump model: ambient soil, impermeable soil, and extremely permeable soil. The hydraulic conductivity of the ambient soil is calculated as the average hydraulic conductivity of soil in Hickory Hills, IL which is the area that the model is applied to in chapter 4; $K_{\text{ambient}} = 2.19 \cdot 10^{-7}$ m/sec. The soil data from USDA-NRCS soil data mart are used for the calculation. Hydraulic conductivity of impermeable soil is assumed as $1 \cdot 10^{-12}$ m/sec and $1 \cdot 10^{0}$ m/sec is used for extremely permeable soil. The hydraulic conductivity value of the extremely permeable soil, which represents backfill in the drainage trench is within the range of the hydraulic conductivity for gravels. Based on Chow et al. (1988), the hydraulic conductivity for gravels is from 10^{-1} cm/sec to 10^{2} cm/sec. The Averjanov model (Vogel et al. 2000) is used to simulate a hydraulic conductivity curve that shows the relationship between soil moisture and hydraulic conductivity.

$$K(\theta) = K_s \left(\frac{\theta - \theta_r}{\theta_s - \theta_r} \right)^m \tag{22}$$

where K_S is saturated hydraulic conductivity [L/T], θ_s is saturated water content [L^3L^{-3}], θ_r is residual water content [L^3L^{-3}], and m is an empirical constant. Following values are used for the

sump pump connection model: saturated moisture content θ_s = 0.38, residual moisture content θ_r = 0.01, and empirical constant *m* = 13.

For the MIKE SHE model setting, the Van Genuchten model (Van Genuchten 1980) is used to estimate the retention curve, which is a relationship between moisture content and pressure.

$$\theta(\psi) = \theta_r + \frac{(\theta_s - \theta_r)}{\left[1 + (\alpha\psi)^n\right]^{1-1/n}} \tag{23}$$

where $\theta(\psi)$ is the water retention curve [L^3L^{-3}], ψ is suction pressure [L], α is an empirical constant as the inverse of the air entry suction ($\alpha > 0$) [L^{-1}], and *n* is a measure of the pore-size distribution (*n* > 1). Following values are used for the sump pump connection model: inverse of air entry suction α = 0.067, and pore-size distribution *n* = 1.446.

Bulk density of ambient soil and extremely permeable soil is assumed as 1700 kg/m^3 and that of impermeable soil is assumed as 1600 kg/m^3. Manning's *n* values for overland flow computation for each surface type are 0.013, 0.025, and 0.030 for concrete side walk, asphalt shingle rooftop, and grassed yard, respectively. Evapotranspiration rate is set as 2.76 mm/day, which is based on Grimmond & Oke (1999) for a Chicago area.

3.3.3. Leaky Sewer Lateral

Infiltration is groundwater intrusion into sanitary sewer pipes through cracks and pipe joints. Since sewer infiltration involves long flow paths through the soil layer over the sewer lateral, a slower response is expected than the roof connections and sump pump connections that are described in previous sections. Similar to the sump pump model, the infiltration model is also

developed using MIKE SHE. The equivalent medium approach from Carlier et al. (2007) is adopted to simulate the actual flow into the sewer. This simplified approach provided reasonable results in the flow simulation in agricultural drainage trenches (Carlier et al. 2007). According to the equivalent medium approach, the leaky sewer pipe and surrounding drainage trench area can be modeled as a single soil layer with an equivalent uniform hydraulic conductivity. Hydraulic conductivity of this layer is assumed as 1 m/sec. Soil profile definitions for the leaky sewer pipe model are presented in Figure 3.8; the leaky sewer lateral is represented as the profile 6 (covered by ambient soil) and 7 (covered by side walk) depending on the surface types. Infiltrated flow is estimated as the sum, over the length of the pipe line, of unsaturated flow into the top of the equivalent porous medium representing the leaky pipe line. The same setting with the sump pump model in the chapter 3.1.2 was used for the soil type, soil property, Manning's *n* values, and evapotranspiration rate.

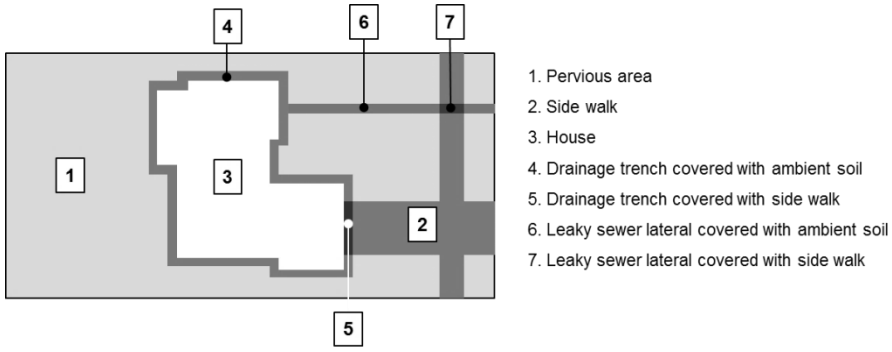

(a)

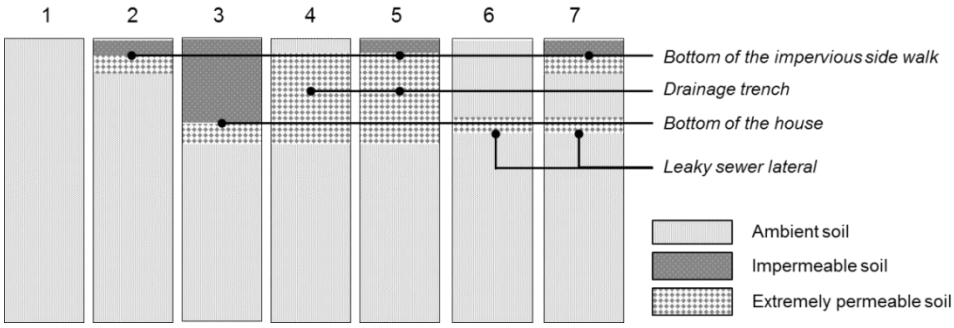

(b)

Figure 3.8 Soil profile definitions of the leaky lateral modeling (a) plan view (b) vertical view (figures not drawn to scale)

3.4. Genetic Algorithm for Model Calibration

3.4.1. Model Calibration

Typical flow hydrographs from the roof connection, sump pump connection, and leaky sewer lateral derived from the methods in section 3.3 can be summed into an overall I&I response of a sewer system when they are assumed as the main sources of I&I. The hydrograph from a roof connection is expected to have a high peak and shorter flow duration that appears earlier in the time axis. The hydrograph from a leaky sewer lateral likely has a low peak and an extended tail that arrives later than the flow response from the roof connection. The sump pump hydrograph fall in between those two responses. These I&I responses as impulse response function (IRF) are conceptually presented in Figure 3.9 for five consecutive impulse rainfall.

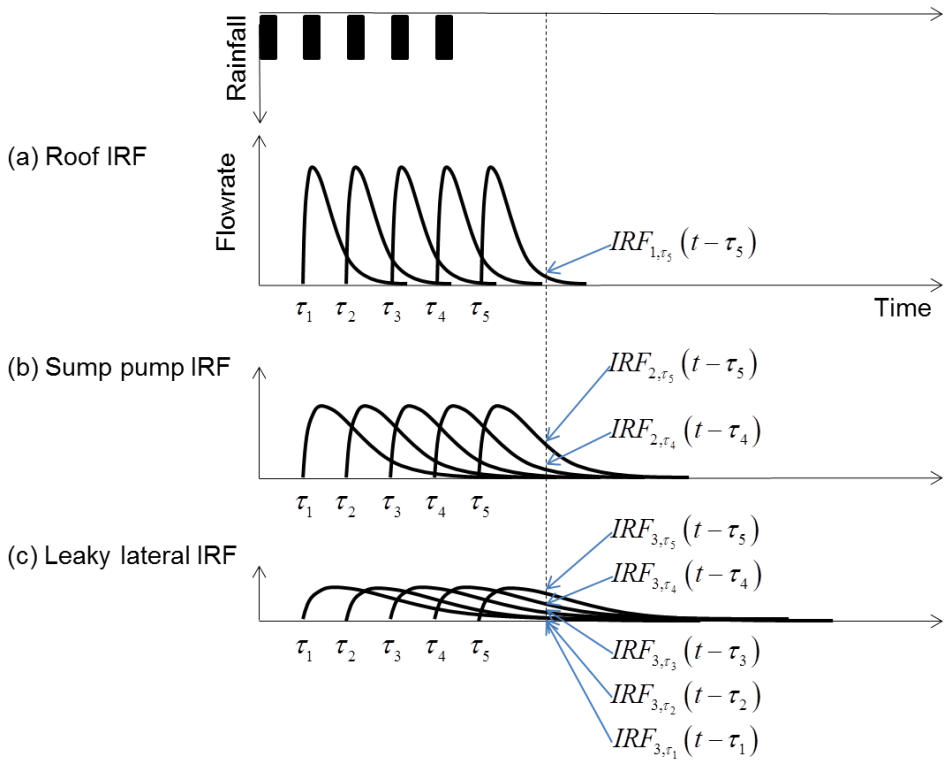

Figure 3.9 Conceptual I&I impulse response functions (IRF) for (a) roof connection, (b) sump pump, and (c) leaky lateral with five consecutive impulse rainfall (refer to equation (2) for index)

These three characteristic response functions represent the impulse response functions of a linear system (Chow et al. 1988). The total I&I, Q can be found by integrating the impulse response function, IRF_i from each model: roof connection, sump pump connection, and leaky sewer lateral model. Then the total I&I flow can be expressed as

$$Q = \text{Convolution}(IRF_i) \quad (1)$$

where i indicates the index for each model component. The convolution of the flow responses would be as following.

$$Q(t) = \sum_{\tau=0}^{t} \left[a \cdot IRF_{1,\tau}(t-\tau) + b \cdot IRF_{2,\tau}(t-\tau) + c \cdot IRF_{3,\tau}(t-\tau) \right] \quad (2)$$

where a, b, c are weighting factors, IRF_i is I&I impulse response functions (IRF) from the roof connection (index = 1), sump pump connection (index = 2), and leaky sewer lateral (index = 3). Since the impulse response function IRF_i is determined using physics-based models as presented in chapter 3.3 only three coefficients: a, b, and c, need to be determined to calculate the I&I. This is a significant advantage compared to the RTK method. In case of the RTK method, a total of nine parameters are required, which are: R; fraction of rainfall volume, T; time to peak, and K; ratio of time of recession to the time to peak, for each I&I source. Typically, increased complexity improves fit but the fit is not a good way to assess predictive ability (Armstrong 2012). Regression-based prediction is most effective when a small number of variables are used.

In this study, dynamic wave model in SWMM is used for the convolution of I&I responses for the IRF and RTK methods. The DWF and I&I input locations on the skeletonized sewer map are depicted in Figure 3.10. RTK method is utilized directly through the RDII input window in SWMM. For the IRF method, three imaginary junctions are created to put the three I&I

responses. The travel time of flow from the DWF input location to the outlet is 27 minutes and that from the I&I input locations is 13 minutes, approximately.

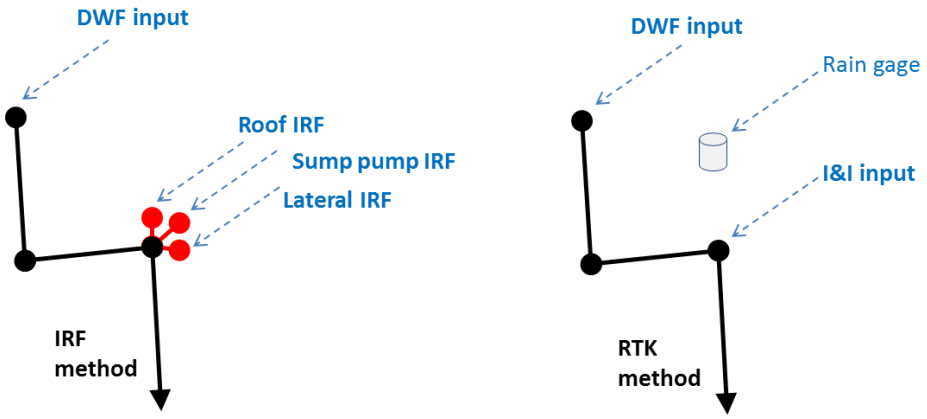

(a) (b)

Figure 3.10 Convolution of I&I responses and DWF using SWMM for (a) IRF method (b) RTK method (not scaled proportionally)

3.4.2. Genetic Algorithm

The total I&I system response that is derived by the convolution of three I&I sources needs to be compared with real data. For the calibration, a genetic algorithm (GA) is utilized in this study. GA is also used for calibrating the flow response using the RTK method to compare both results. GA has been used to optimize RTK parameters in some previous I&I studies (Sargent, 2011).

Genetic algorithm (GA) is an optimization method that resembles the process of natural selection, such as crossover, mutation, and selection. This is one of many evolutionary algorithms (EA). GA has been applied in hydroinformatics field since the algorithm became popular in late 1980s and early 1990s (Minsker 2006). In 2000s the application of GA was widely tested on different hydrologic and hydraulic problems e.g. model calibration,

groundwater monitoring and remediation design, watershed, reservoir, and river management, and water distribution system design. Zimmer et al. (2010) applied GA to real-time combined sewer overflow (CSO) control. In the commercial sector, Innovyze provides GA optimization tools to calibrate the RTK parameters in H2OMap SWMM and InfoSWMM.

The algorithm starts with a random population, which are sets of suitable parameters, or genes, for the problem. These parameter sets are called chromosomes. Then the fitness of the model solutions using these chromosomes is tested for selection. Chromosomes from one population are used to generate a new population and the offsprings in the new population are hoped to be better than the old ones. The new population is created by repeating following steps.

- Selection: Two parent chromosomes are selected on the basis of fitness. The probability of individuals is higher when the fitness of the individual is greater than its competiter's fitness. If the parents have better fitness, there is a greater chance to be selected.

- Crossover: With the user-defined crossover probability, a new offspring is formed by crossover the chromosomes from both parents.

- Mutation: With the user-defined mutation probability, new offspring is mutated at each position in chromosomes. Mutation allows one or more gene values in a chromosome altered from its initial state. This maintains diversity in the solutions that lead to the algorithm searching a wider space for optimal solutions.

- Accepting: New offspring is placed in a new population.

This process is repeated until the solution converges and the error of fitness is minimized. Offsprings with better fitness have more chances to reproduce. Selection and crossover are the

operations that lead GA to converge to a solution with optimal fitness. Mutation is the operation that broadens the search space and hence helps the GA to find a global optimum rather than converge to a local optima and stop.

An example of crossover and mutation of three variables is presented in Figure 3.11 where *a* is the flow coefficient of roof connections, *b* is the flow coefficient of sump pump connections, and *c* is the flow coefficient from leaky laterals. The example shows a single crossover point and the data beyond the point are swapped between two parent chromosomes. In the mutation process, gene *b* of offspring 1 and gene *a* of offspring 2 are mutated.

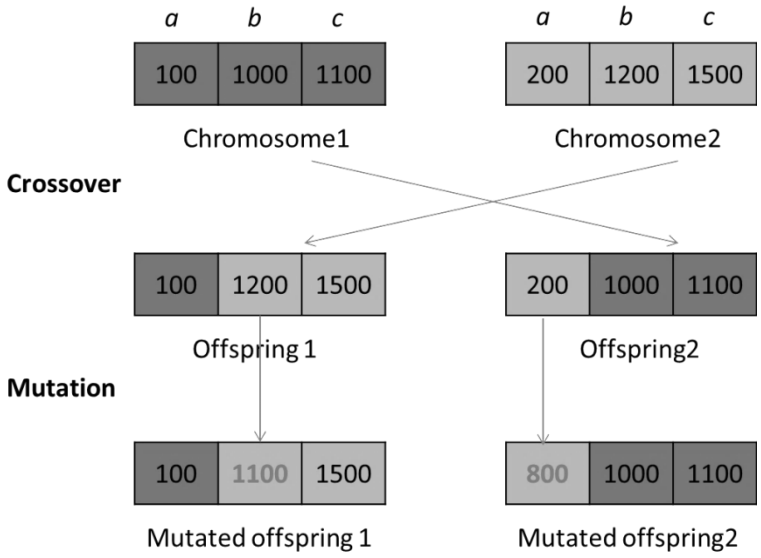

Figure 3.11 An example of crossover and mutation process

The modeler needs to define crossover probability, mutation probability, population size, and number of generations. Crossover probability represents how often crossover will be performed. Using the analogy of biological reproduction, crossover probability indicates a ratio of how many couples in one generation will be picked for mating to generate next generation. Normally

it is good to leave some parts of population survive to next generation and the selection of parents is made based on fitness. When memory is allowed, the best chromosomes are preserved into next generation. Mutation probability is how often parts of chromosome will be mutated. Mutation probability should be small since GA will behave like a random search with high mutation probability. Population size means how many chromosomes are in the population in one generation. With a small population size only small part of search space is explored and one may only find a local solution. With a large population size GA takes longer to run. After some limit, increased population size is found not to be too useful (Minsker 2006).

References

Allitt, R. (2002) Rainfall, runoff and infiltration re-visited. *WaPUG Spring Meeting 2002* (pp. 1–9).

Armstrong, J. S. (2012) Illusions in regression analysis. *International Journal of Forecasting*.

Backmeyer, D. P. (1960) Effects of infiltration. *Water Pollution Control Federation* **32**(5), 539–540.

Bishop, W. J., Diemer, D. M. & Wallis, M. J. (1987) Regional infiltration/inflow study solves wet weather sewer problems. *Journal of Water Pollution Control Federation* **59**(5), 289–293. Retrieved from http://www.jstor.org/stable/25043247?origin=JSTOR-pdf

Buyuktas, D. & Wallender, W. W. (2002) Numerical simulation of water flow and solute transport to tile drains. *Journal of Irrigation and Drainage Engineering* **128**(1), 49–56.

Camp Dresser & McKee (CDM) Inc., F.E. Jordan Associates Inc. & James M. Montgomery Consulting Engineers. (1985) East Bay infiltration/inflow study manual for cost-effectiveness analysis. Oakland, CA.

Carlier, J. P., Kao, C. & Ginzburg, I. (2007) Field-scale modeling of subsurface tile-drained soils using an equivalent-medium approach. *Journal of Hydrology* **341**(1-2), 105–115. doi:10.1016/j.jhydrol.2007.05.006

Carluer, N. & Marsily, G. De. (2004) Assessment and modelling of the influence of man-made networks on the hydrology of a small watershed: implications for fast flow components,

water quality and landscape management. *Journal of Hydrology* **285**(1-4), 76–95. doi:10.1016/j.jhydrol.2003.08.008

Chow, V. Te, Maidment, D. R., & Mays, L. W. (1988) *Applied Hydrology* (pp. 110–115). McGraw-Hill.

Cooke, R. A. & Badiger, S. (2001) Drainage equations for random and irregular tile drainage systems. *Agricultural Water Management* **48**, 207–224.

Crawford, D., Eckley, P. & Pier, E. (1999) Methods for estimating inflow and infiltration into sanitary sewers. *New applications in modeling urban water systems, Volume 7, Conference on Stormwater and Related Water Systems Modeling; Management and Impacts*, 299–315. Toronto: CHI.

De Bénédittis, J. & Bertrand-Krajewski, J. L. (2005) Infiltration in sewer systems: comparison of measurement methods. *Water Science and Technology: a Journal of the International Association on Water Pollution Research* **52**(3), 219–27. Retrieved from http://www.ncbi.nlm.nih.gov/pubmed/16206862

Depew, N. (2007, November 25) Drainage 101, Part I. *Ned Depew House Inspection*. Retrieved March 27, 2014, from http://www.buyershouseinspection.com/HC/HC2.html.

DHI Software. (2007) *MIKE SHE user manual volume 1: user guide* (Vol. 1).

DHI Software. (2007) *MIKE SHE user manual volume 2: reference guide* (Vol. 2).

Ertl, T. W., Dlauhy, F. & Haberl, R. (2002) Investigations of the amount of infiltration / inflow into a sewage system. *Proceedings of the 3rd "Sewer Processes and Networks" International Conference*. Paris, France.

Fipps, G., Skaggs, R. W., & Nieber, J. L. (1986) Drains as a boundary condition in finite elements. *Water Resources Research*, *22*(11), 1613–1621.

Fipps, G., & Skaggs, R. W. (1992) Simple methods for predicting flow to drains. *Journal of Irrigation and Drainage Engineering*, *117*(6), 881–896.

Franz, T. (2007) *Spatial classification methods for efficient infiltration measurements and transfer of measuring results*. Dresden University of Technology, Dresden, Germany.

Golden, J. B. (1995) An introduction to sanitary sewer overflows. In *Seminar publication: National conference on sanitary sewer overflows* (*SSOs*) (pp. 443–450). Washington D.C.: EPA.

Gottstein, L. E. (1976) *Sewer system evaluation for infiltration/inflow*. Minneapolis, Minnesota.

Gustafsson, L. (2000) Alternative drainage schemes for reduction of inflow/infiltration - prediction and follow-up of effects with the aid of an integrated sewer/aquifer model. *1st International Conference on Urban Drainage via Internet* (pp. 21–37).

Innovyze. (2011) InfoWorks CS technical review.

Jardin, N. (2004) Fremdwasser – eine grundsätzliche Problembeschreibung (Extraneous water – a basic description). *Proceedings of 3rd Forum Ruhrverband*. Essen, Germany.

Karpf, C., & Krebs, P. (2004) Sewers as drainage systems – quantification of groundwater infiltration. In *Novatech 2004, 6th International conference on sustainable techniques and strategies in urban water managementWater Management* (pp. 969–975). Lyon.

Kim, S., & Delleur, J. W. (1997) Sensitivity analysis of extended TOPMODEL for agricultural watersheds equipped with tile drains. *Hydrological Processes, 11*, 1243–1261.

Kretschmer, F., Ertl, T., & Koch, F. (2008) Discharge monitoring and determination of infiltration water in sewer systems. In *11th International Conference on Urban Drainage* (pp. 1–7). Edinburgh, Scotland, UK.

Lai, F. D. (2008) Review of sewer design criteria and RDII prediction methods. Washington, DC.

Lindberg, S., Nielsen, J. B., & Carr, R. (1989) An integrated PC-modelling system for hydraulic analysis of drainage systems. *Watercomp '89: The First Australasian Conference on Technical Computing in the Water Industry*. Melbourne, Australia.

Lucas, S. (2003) *Auftreten, Ursachen und Auswirkungen hoher Fremdwasserabflüsse – eine zeitliche und räumliche nalyse (Occurence, causes and effects of high extraneous water flows)*. Universität Karlsruhe.

Minsker, B. (2006) Genetic algorithm. In P. Kumar, J. C. Alameda, P. Bajcsy, M. Folk, & M. Markus (Eds.), *Hydroinformatics: Data integrative approaches in computation, analysis, and modeling* (pp. 437–451). CRC Press.

NCPWI (National Council on Public Works Improvement). (1988) Fragile foundations: a report on America's Public Works, Final report to the president and congress.

NSFC (National Small Flows Clearinghouse). (1999) Infiltration and inflow can be costly for communities. *Pipeline: Small Community Wastewater Issues Explained to the Public*, Vol.10, No.2.

Pawlowski, C. W., Rhea, L., Shuster, W. D., & Barden, G. (2013) Some factors affecting inflow and infiltration from residential sources in a core urban area: A case study in a Columbus OH USA neighborhood. *Journal of Hydraulic Engineering*. doi:10.1061/(ASCE)HY.1943-7900.0000799

Pecher, K. H. (2003) Fremdwasseranfall, Schwankungen und Konsequenzen für die Abwasserbehandlung (Amount of I/I, variations and consequences). *Proceedings of 36th Essener Tagung, Gewässerschutz-Wasser-Abwasser*. Aachen, Germany.

Peters, G. L., & Troemper, A. P. (1969) Reduction of hydraulic sewer loading by downspout removal. *Water Pollution Control Federation*, *41*(1), 63–81.

Petroff, R. G. (1996) An analysis of the root cause of sanitary sewer overflows. In: *Seminar Publication National Conference on Sanitary Sewer Overflows (SSOs): april 24-26, 1995, Washington D.C.*, 8–15. Cincinnati, OH: EPA.

Purkey, D. R., Wallender, W. W., Fogg, G. E. & Sivakumar, B. (2004) Describing near surface, transient flow processes in unconfined aquifers below irrigated lands: Model application in

the Western San Joaquin Valley, California. *Journal of Irrigation and Drainage Engineering* **130**(6), 451–459. doi:10.1061/(ASCE)0733-9437(2004)130

Qiao, F., Lu, H., Derr, H. K., Wang, M., & Chen, M. (2007) A new method of predicting rainfall dependent inflow and infiltration. *Water Environment Federation* (pp. 1883–1890). doi:10.2175/193864707788116040

Reynolds, J. (1995) The roof drain and sump pump removal program: An innovative approach to inflow reduction. In *Seminar publication: National conference on sanitary sewer overflows (SSOs)* (pp. 303–309). Washington D.C.: EPA.

Rossman, L. A. (2010) Storm water management model user's manual version 5.0. Cincinnati, OH.

Sargent, S. W. (2011) How often will sewage spill?: Stochastic analysis & design of a waste-water system with large RDII components. In *Water New Zealand* (pp. 1–28).

Schulz, N., Baur, R., & Krebs, P. (2005) Integrated modelling for the evaluation of infiltration effects. *Water science and technology: a journal of the International Association on Water Pollution Research*, *52*(5), 215–23. Retrieved from http://www.ncbi.nlm.nih.gov/pubmed/16248198

Seo, Y. (2012) *The effect of rainstorm movement on urban drainage network runoff hydrographs*. University of Illinois at Urbana-Champaign.

Seo, Y., & Schmidt, A. R. (2012) The effect of rainstorm movement on urban drainage network runoff hydrographs. *Hydrological Processes*, *26*(25), 3830–3841. doi:10.1002/hyp.8412

Seo, Y., Schmidt, A. R., & Sivapalan, M. (2012) Effect of storm movement on flood peaks: Analysis framework based on characteristic timescales. *Water Resources Research*, *48*(5), n/a–n/a. doi:10.1029/2011WR011761

Sliter, J. T. (1974) Infiltration/inflow guidelines spark controversy. *Journal of Water Pollution Control Federation*, *46*(1), 6–8.

Strand Associates Inc. (2006) *Inflow and Iifiltration from private property*. Cincinnati, OH.

Tarboton, K. C. & Wallender, W. W. (2000) Finite-element grid configurations for drains. *Journal of Irrigation and Drainage Engineering* **126**(4), 243–249.

Vallabhaneni, S., Chan, C. C., & Burgess, E. H. (2007) *Computer tools for sanitary sewer system capacity analysis and planning*. Cincinnati, OH.

Vallabhaneni, S., Lai, F., Chan, C., Burgess, E. H. & Field, R. (2008) SSOAP − A USEPA toolbox for sanitary sewer overflow analysis and control planning. *EWRI 2008 World Environmental & Water Resources Congress, May 13-16, 2008*. Honolulu, HI: American Society of Civil Engineers (ASCE).

Van Genuchten, M. T. (1980) A closed-form equation for predicting the hydraulic conductivity of unsaturated soils. *Soil Science Society of America*, *44*(5), 892–898.

Vogel, T., Van Genuchten, M. T., & Cislerova, M. (2000) Effect of the shape of the soil hydraulic functions near saturation on variably-saturated low predictions. *Advances In Water Resources*, *24*, 133–144.

Weiss, G., Brombach, H. & Haller, B. (2002) Infiltration and inflow in combined sewer systems: long-term analysis. *Water science and technology: a journal of the International Association on Water Pollution Research* **45**(7), 11–9. Retrieved from http://www.ncbi.nlm.nih.gov/pubmed/11989885

Wright, L., Dent, S., Mosley, C., Kadota, P. & Djebbar, Y. (2001) Comparing rainfall dependent inflow and infiltration simulation method. In: *Models and Applications to Urban Water Systems. Monograph 9*, 235–258. Toronto, Ontario, Canada: CHI.

Zimmer, A., Minsker, B., Schmidt, A., & Ostfeld, A. (2010) Evolutionary Algorithm Memory Enhancement for Real-Time CSO Control. In *World Environmental and Water Resources Congress* (pp. 2251–2259). Providence, Rhode Island.

4. I&I Response Functions

4.1. Typical I&I Response Functions

In this section, three I&I response functions of a roof downspout connection, sump pump connection, and leaky lateral are presented using the physics-based models introduced in chapter 3. The impulse response functions (IRF) from three sources show distinguishable differences in response time and peak flowrates. This makes applying Genetic Algorithm (GA) suitable for the IRF integration and the model calibration.

The three IRFs are identified for the study area Hickory Hills, IL where sewer drainage configurations and sewer flow monitoring data are available. Hickory Hills is a city in Cook County, IL with the size of 7.33 km^2 and the population of 14,049 (U.S. Census Bureau 2010). The climate of the city is classified as humid continental (Köppen Dfa) and the average rainfall is approximately 98 cm per year (Hickory Hills (zip 60457), Illinois Climate 2014).

4.1.1. Uniform rainfall

To derive typical I&I responses from the three models, a representative uniform rainfall was introduced. From January 1, 2009 to July 31, 2009, a total of 702 mm of rainfall was recorded in Hickory Hills, IL. Seventeen distinct storm events were identified during this period; hence the average rainfall volume for a single event is 41 mm. The maximum rainfall intensity during the period is 14 mm/hr. Three hours of 14 mm/hr of rainfall produces a total of 42 mm of rainfall volume. Therefore, 3 hour 14 mm/hr uniform rainfall is selected as a representative storm event for the investigation in this section (Figure 4.1). In chapter 5, sensitivity of model for different rainfall distribution is addressed in addition to the 42 mm uniform rainfall.

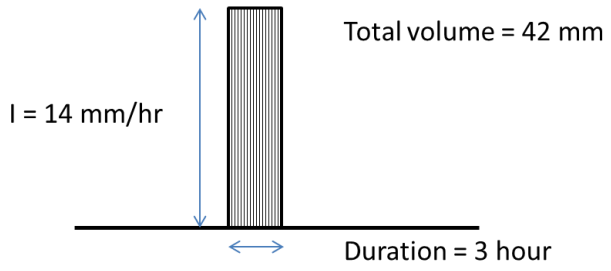

Figure 4.1 Simplified representative rainfall with the maximum rainfall peak 14 mm/hr

For the sump pump model and the leaky lateral model, the uniform rainfall is randomly inserted into the real rainfall time series from June 1, 2009 to July 31, 2009 at ten different times to produce the average flow responses. Time series from January 1, 2009 to July 31, 2009 is used as the control case and the ten random times are presented in Table 4.1. Investigating flow responses to the uniform rainfall at random times also facilitates understanding the effect of antecedent moisture conditions (AMC). In case of the roof connection model, examining the response to the rainfall entered randomly at different times does not affect the I&I response, which means AMC is not an important factor for the roof connection IRF.

Table 4.1 Randomly selected times to insert 42 mm uniform rainfall to define typical I&I responses

	Time of perturbation
1	June 4, 2009 4:00
2	June 11, 2009 0:00
3	June 17, 2009 14:00
4	June 24, 2009 5:00
5	June 25, 2009 20:00
6	July 2, 2009 2:00
7	July 5, 2009 10:00
8	July 10, 2009 15:00
9	July 18, 2009 20:00
10	July 28, 2009 9:00

In Figure 4.2, flow responses to 42 mm uniform rainfall from three sub-models are presented with zoomed-in views of roof runoff and sump pump flow in Figure 4.2 (b). The flowrate values are divided by the corresponding contributing areas so that effective flowrates can be compared. The peak values from each sub-model are 0.0942, 0.0427, and 0.00902 $m^3/day/m^2$ for roof runoff, sump pump, and leaky lateral models, respectively. Total volume of each response is 2.89, 1.54, and 1.63 m^3. These are equivalent to 0.0118, 0.0319, and 0.0842 m (or m^3/m^2) as volume per unit contributing area.

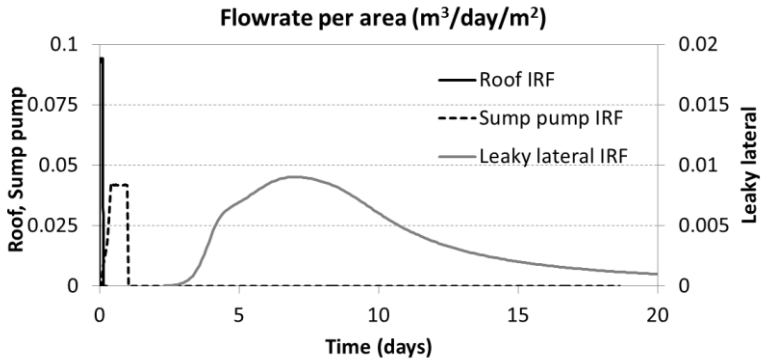

(a)

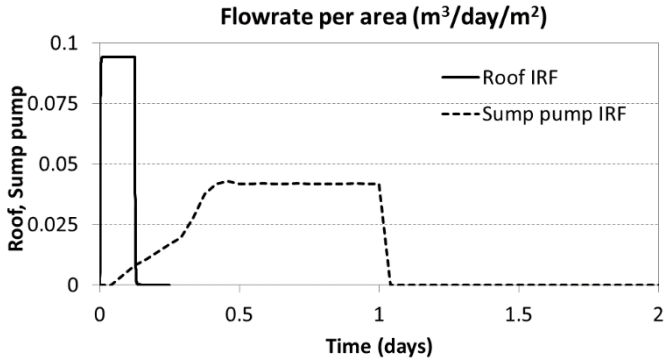

(b)

Figure 4.2 Flow responses from roof connection, sump pump, and leaky lateral models with 42 mm uniform rainfall (a) overall responses, (b) zoomed in view of roof runoff and sump pump flow

Roof runoff has largest peak value among the three flow responses and the flow response closely resembles the rainfall shape. The total response time, which is defined as the time from the start of rainfall until when the IRF hydrograph falls to less than 0.01% of the peak is 3.68 hours and it is in the same order as the rainfall time, which is 3 hours. Response time of sump pump flow to the three-hour rainfall is stretched out to one day while the peak flow rate is about a half of that from roof runoff model. This is because sump pump flow path includes flow through porous media in the drainage trench around the building. Sump pumps are placed to drain excessive water around a building and backfill of drainage trench is composed of more permeable material than ambient soil to promote fast drainage. Thus the flow response time of a sump pump is expected to be shorter than that of a leaky sewer lateral, which involves percolation of water through ambient soil. On top of that, the length of flow path from the surface to a sump pump is normally shorter than that to a sewer lateral. Leaky lateral flow has the smallest peak value and the longest tail. The peak flowrate is about a tenth of that of sump pump flow and the total response time is over eight weeks. Since infiltration process involves flow percolating through ambient soil, the entire response time is greatly extended.

For the IRF model calibration, three IRFs are convoluted using SWMM as depicted in Figure 3.10 based on the assumption that the network routing is negligible. The travel time of flow from the I&I input location to the sewer outlet was around 13 minutes which is shorter than the response time of three IRFs for the uniform rainfall.

4.1.2. Real rainfall

Using the three I&I IRF of the representative unit rainfall, flow responses of three I&I sources—roof drain, sump pump, and leaky lateral—are derived for the real rainfall data from Hickory Hills, IL from April 17, 2009 to July 16, 2009. The total rainfall depth for this period is 372 mm and the peak precipitation rate is 13 mm/hr (Figure 4.3 (a)). The three I&I flow responses are presented in Figure 4.3 (b) with a zoomed-in view for the shorter period, from June 16 to July 3, in Figure 4.3 (c). To compare the net I&I per area, the flow is divided by the effective contributing area of each model: area of roof 246 m^2, area of drainage trench around the building 48 m^2, and area of leaky lateral layer 19 m^2. The effective contributing area assumes that lateral subsurface flow is negligible relative to vertical flow. The flow per unit area is only used for comparison in Figure 4.3; when IRF is used for calibration flow is not scaled per unit area.

In Figure 4.3 (b), the roof response is depicted by a black solid line, the sump pump response as by a black dashed line, and the lateral response as by a grey solid line. The time of roof response peaks match well with that of the rainfall peaks. Similar to the representative uniform rainfall responses, peaks of the sump pump and lateral responses show delays.

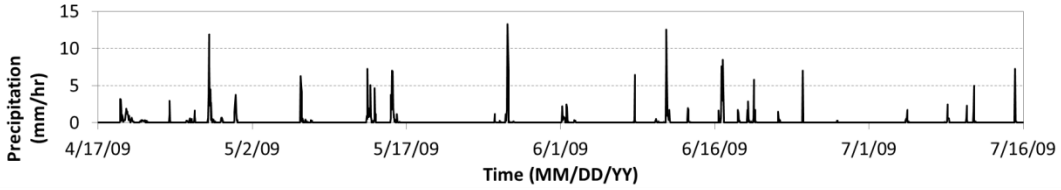

(a)

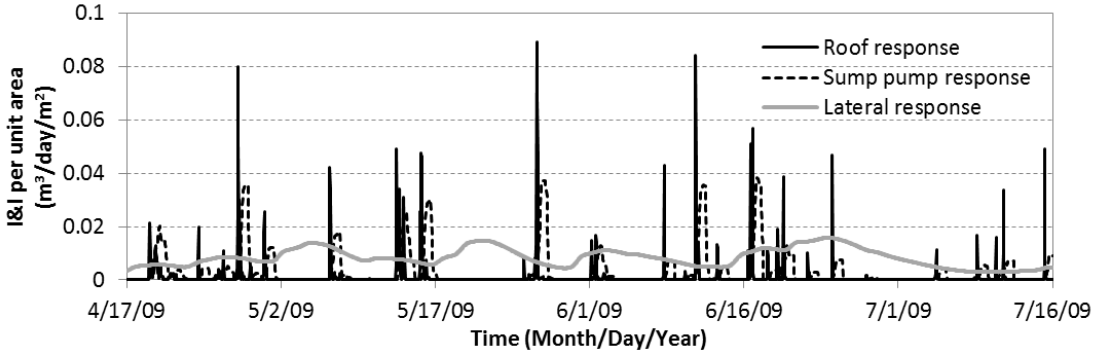

(b)

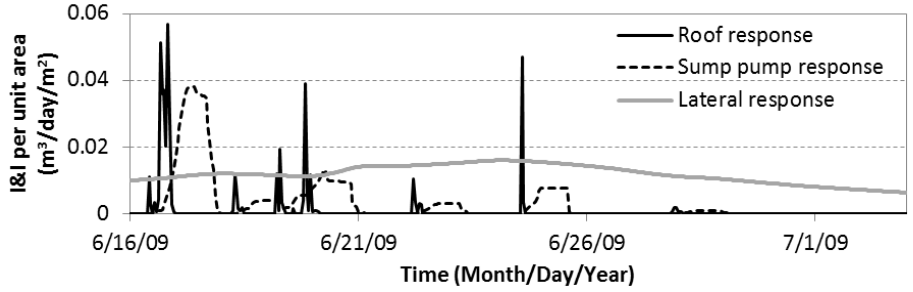

(c)

Figure 4.3 Flow responses from roof drain, sump pump, and leaky lateral models with real rainfall data (a) rainfall, (b) overall flow responses, (c) zoomed in view of the period from June 16, 2009 to July 3, 2009

Figure 4.4 indicates the flow duration curves of the three I&I responses: roof connection, sump pump connection, and leaky lateral, for a three month period from April 17, 2009 to July 16, 2009. The roof connection response depicted in the black solid line shows a steep curve, which means high I&I flows for short periods and this shows a strong evidence that the flow is rain-

caused. The leaky lateral response, which is presented by a grey solid line, shows a flatter curve. This indicates that the infiltration through leaky laterals is sustained longer than the hourly time scale due to the flow through porous media; ambient soil on top of a more permeable layer surrounding the leaky pipe. The sump pump response in the black dashed line falls between the roof connection and the leaky lateral response curves. The sump pump response involves a flow through a porous media like the leaky lateral response but the flow distance in an ambient soil, which has a small hydraulic conductivity, is shorter.

The shapes of the three curves are very different, which provides insight into the very different processes. Roof connection flow duration curve is very steep and indicates that approximately 90% of flow values are nearly zero. Sump pump flow duration curve is also very steep and indicates that approximately 75% of the flows are nearly zero. However, the sump pump curve flattens out at around the exceedance probability 0.05. The model to generate the sump pump IRF considers both the flow into the sump and the capacity of the sump pump and limits the IRF flow to the smaller of these values. The flat flow-duration for the extreme events indicates the storms for which the sump pump capacity limits the flow. The flow duration curve of leaky lateral never hits zero. Peaks never get as high as those from the roof and sump but there is always some flow even though it is small.

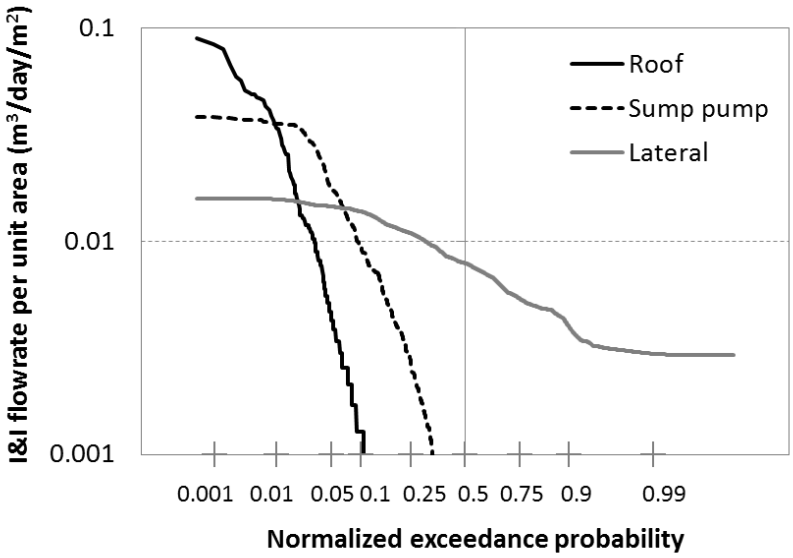

Figure 4.4 Exceedance probability of three I&I responses: Roof connection, sump pump connection, and leaky lateral, per unit area from April 17 to July 16, 2009 (in log scale)

4.2. Model Calibration

4.2.1. Monitoring Data and Dry Weather Flow

The test areas for the model implementation in this study are three neighboring communities in Illinois: Hickory Hills, Palos Hills, and Bridgeview. Sewer flow data were collected by U.S. Geological Survey (USGS) at 17 monitoring locations along the main sewer line that is shown in Figure 4.5. Flow meters were installed and managed by USGS in 2009 and flow recordings are available for the period from April through July. Based on the data quality, site 17 is selected for the model application. Site 17 is located on 104th Street and east of Terry Drive in a manhole at station 41+05 on Metropolitan Water Reclamation District (MWRD)'s interceptor contract CAL 18 F Ext C. This location receives sewer flow from Hickory Hills, Palos Hills, and Bridgeview, IL.

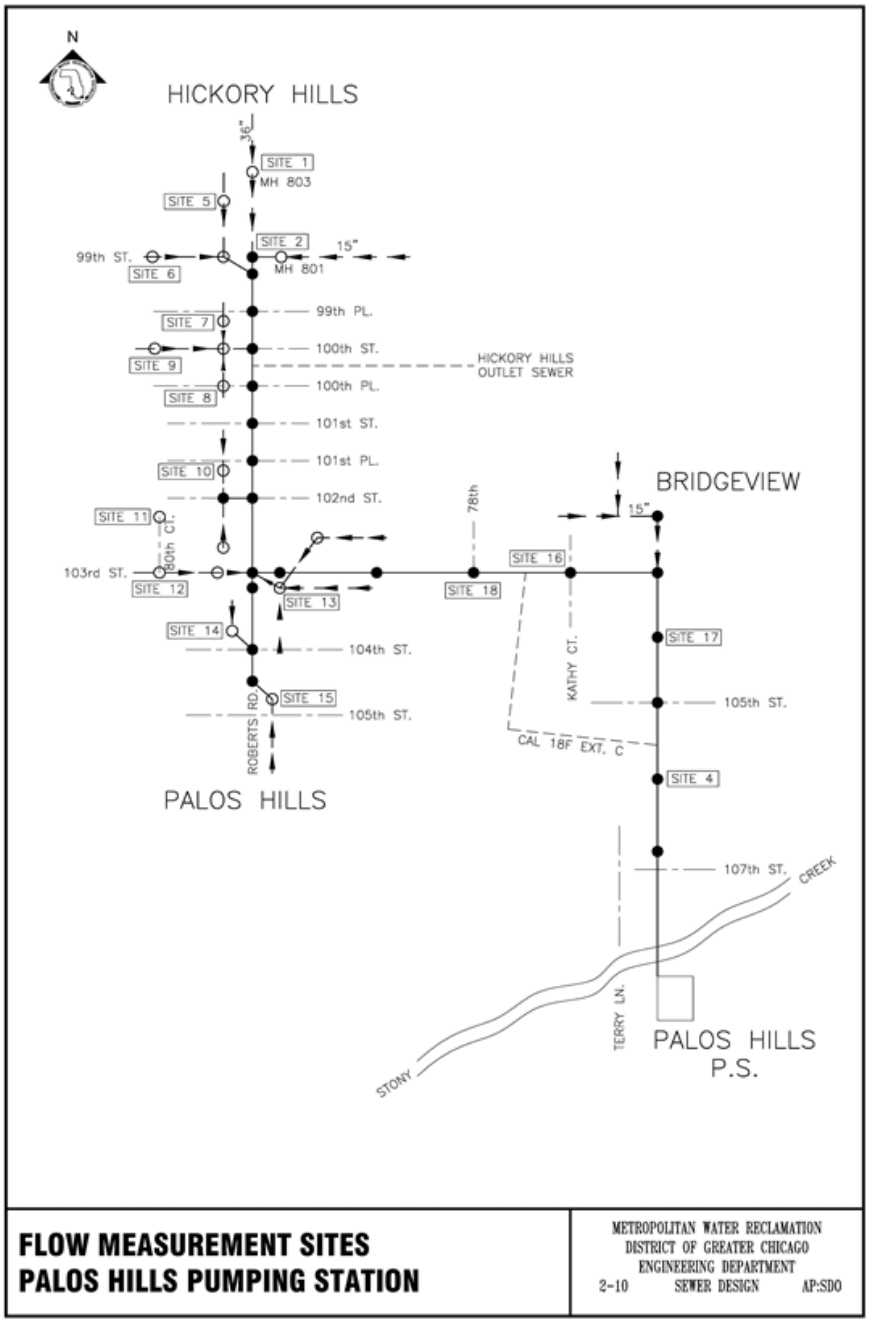

Figure 4.5 Sewage monitoring locations including the test site 17 in the monitoring area Hickory Hills, Palos Hills, and Bridgeview, IL (Black solid line with dots indicates main trunk sewer, arrow line indicates local sewer entry, dashed lines indicate street reference marks)

Rainfall data were obtained from the Illinois State Water Survey (ISWS) by averaging rainfall data from four nearby ISWS rain gages: G11, G12, G16, and G17. The rainfall and flow data from April 17, 2009 to August 3, 2009 are shown in Figure 4.6. The sewer monitoring plot

shows the evidence of I&I in the area since the high flow peaks correspond to the rainfall peaks and the peak flows are attenuated slowly down to the dry weather flow (DWF) after storm events.

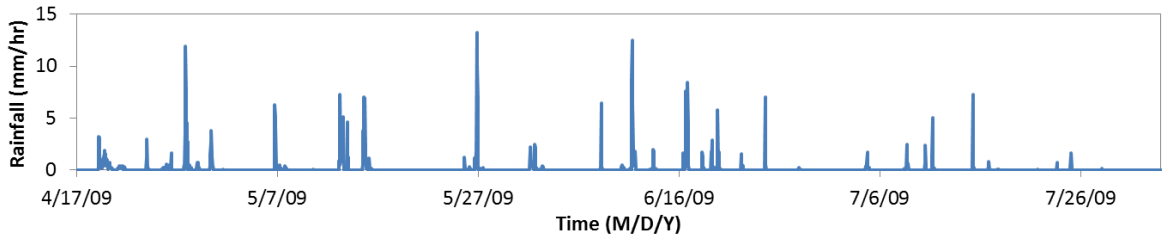

(a)

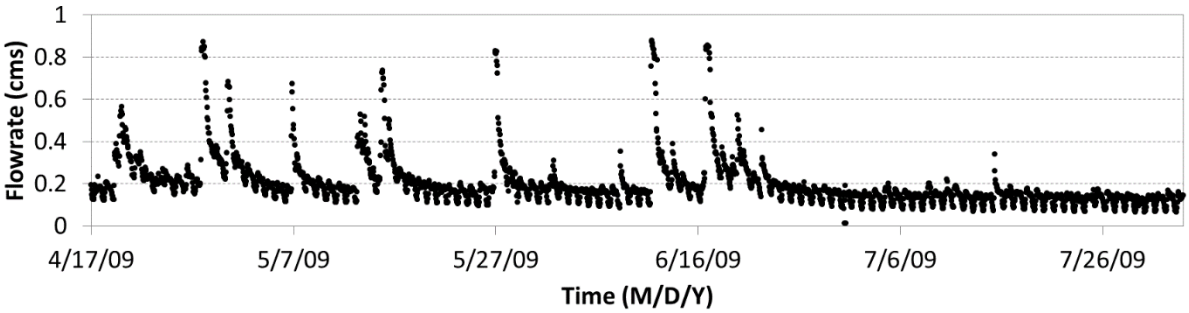

(b)

Figure 4.6 Rainfall and sewer flow data (a) rainfall record from ISWS (b) flow data from USGS sewage monitoring site 17

DWF at the test site is estimated using the DWF estimation component in Special Contributing Area Loading Program (SCALP), which is developed by the United States Army Corps of Engineers (USACE). SCALP is a flow routing model mainly developed for use in the Chicago area. DWF is determined on a per capita basis and distributed in time by coefficients: average DWF loading, monthly pattern, daily pattern, and hourly pattern using following equation (Miller & Schmidt 2010, Epsey et al. 2014).

$$\text{DWF} = \text{average DWF loading} \times \text{monthly pattern} \times \text{daily pattern} \times \text{hourly pattern} \quad (1)$$

These DWF coefficients are estimated using data from a 14-day dry period from July 17, 2009 to July 31, 2009. The 14 days of DWF is averaged and the set of best DWF coefficients is derived by adjusting each value until the best fit to the average DWF was found. Nash-Sutcliffe model efficiency coefficient is used for the fitness.

The monthly pattern is the pattern describing the variability among months within a year. The monthly pattern values are all set to one due to insufficient data to define them. The daily pattern describes the variability among days within a week and the hourly pattern describes the variability among the hours of the day. The average DWF loading is calculated as 0.1246 cms (4.40 cfs) and the DWF patterns are estimated as presented in Table 4.2 and Figure 4.7. The daily pattern shows that DWF is greater during weekends than weekdays. The hourly pattern shows two peaks during a day: in mornings and evenings, and minimum DWF at 4 am. These trends correspond to DWF pattern in residential areas.

Table 4.2 DWF patterns at sewage monitoring site 17

Monthly pattern

Jan	1
Feb	1
Mar	1
Apr	1
May	1
Jun	1
Jul	1
Aug	1
Sep	1
Oct	1
Nov	1
Dec	1

Daily pattern

Sun	1.02
Mon	1
Tue	0.99
Wed	0.95
Thu	0.94
Fri	1.01
Sat	1.10

Hourly pattern

12:00 AM	0.9	12:00 PM	1.17
1:00 AM	0.82	1:00 PM	1.17
2:00 AM	0.7	2:00 PM	1.13
3:00 AM	0.64	3:00 PM	1.1
4:00 AM	0.6	4:00 PM	1.07
5:00 AM	0.63	5:00 PM	1.08
6:00 AM	0.75	6:00 PM	1.1
7:00 AM	0.91	7:00 PM	1.12
8:00 AM	1.06	8:00 PM	1.12
9:00 AM	1.18	9:00 PM	1.15
10:00 AM	1.23	10:00 PM	1.11
11:00 AM	1.22	11:00 PM	1.01

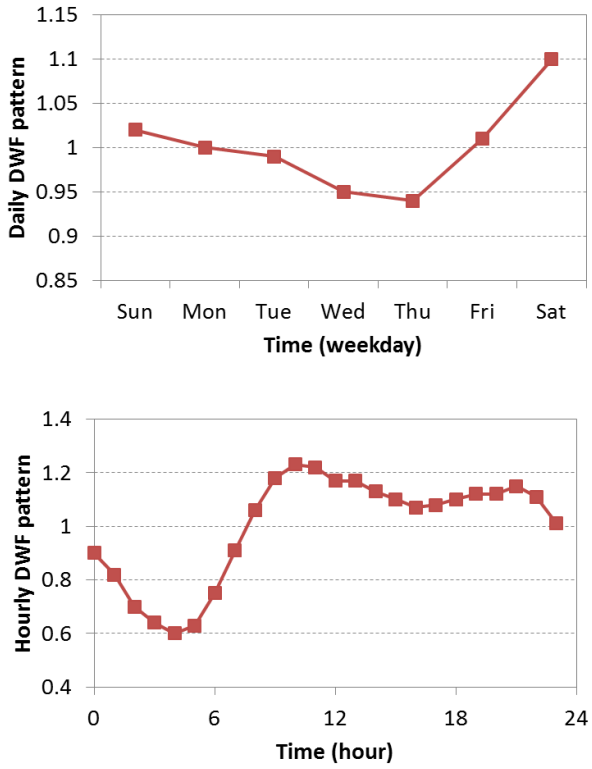

Figure 4.7 Daily and hourly patterns of DWF

4.2.2. Model Calibration using Genetic Algorithm and Comparison with SWMM RTK

The total sewer flow at the test site was calibrated to match the measured flows using a genetic algorithm (GA). The GA is used to optimize the coefficients for the three I&I response functions, which are weights of each IRF. The GA was also used to calibrate total sewer flow at the test site simulated by the SWMM RTK method. The efficiency of both I&I estimation methods is measured using the Nash-Sutcliffe coefficient. Fitting to peak discharges can lead to missing peak arrival time or low flow rates. Fitting to flow volume may result in missing peak and tail values. Thus Nash-Sutcliffe coefficient is selected to fit model result. Nash-Sutcliffe provides a

good fit for overall shape of sewer hydrograph as it is similar to root mean square. The equation of the Nash-Sutcliffe model efficiency coefficient is defined as follows (Nash & Sutcliffe, 1970).

$$E = 1 - \frac{\sum_{t=1}^{T} \left(Q_0^t - Q_m^t \right)^2}{\sum_{t=1}^{T} \left(Q_0^t - \overline{Q_0} \right)^2} \tag{2}$$

where Q_0^t is observed discharge at time *t*, Q_m^t is modeled discharge at time *t*, and $\overline{Q_0}$ is the average of observed discharge. The coefficient ranges from -∞ to 1 and $E = 1$ corresponds to a perfect match between the observed discharge and the modeled discharge.

As larger the Nash-Sutcliffe coefficient better the model fitting, maximizing the coefficient is set as the objective function for the GA optimization. In actual formulation, the objective function is to minimize 1- *E*. Initial guess of the weights of three IRFs are randomly selected.

Among the period of available data, the calibration period is selected from May 9, 2009 to June 7, 2009 and the validation period is from June 9, 2009 to July 8, 2009. The Impulse Response Function (IRF) method has three parameters to calibrate: roof connection scaling factor (R), sump pump connection scaling factor (S), and leaky lateral scaling factor (L). The three I&I response function are derived using the physics-based models. The RTK method has nine parameters to calibrate: R1, R2, R3, T1, T2, T3, K1, K2, and K3.

The GA optimization conditions for both IRF and RTK methods are presented as follows.

- Size of the population = 100
- Maximum number of generations = 300

The probability of crossover and the probability of mutation are also important GA settings. Box plots in Figure 4.8 indicate how IRF parameters (*a*; roof connection coefficient, *b*; sump pump connection coefficient, and *c*; leaky lateral coefficient) and Nash-Sutcliffe coefficients are affected by the probability of crossover and the probability of mutation in the GA setting.

Different values of probability of crossover from 0.8 to 0.99 with 0.01 increments are tested in Figure 4.8 (a). The probability of mutation is 0.06 for all cases. The solutions are unstable in the range of crossover probability between 0.9 and 0.94 and more stable when it is greater than 0.95. Thus 0.95 is selected as the probability of crossover for both IRF and RTK calibration. The probability of mutation is tested from 0.01 to 0.2 as it appears in Figure 4.8 (b). The solutions become unstable as the probability of mutation increases, especially when the probability is greater than 0.11. Thus 0.06 is selected for both IRF and RTK calibration. The calibrated parameter solutions for the IRF and RTK methods are presented in Table 4.4. The optimal solution of the IRF method using the GA is: a = 3359 for roof, b = 22653 for sump pump, and c = 19985 for lateral. These values can be interpreted as I&I volume contribution of each I&I source. Contributing flow volume of each I&I source is derived by multiplying the per-unit-area flow volume of IRFs and the IRF weighting coefficients. Then the contributing I&I volume from the roof, sump pump, and lateral become 9710 m^3, 22653 m^3, and 32543 m^3, respectively, and they are 15%, 35%, and 50% of total estimated I&I flow volume. This simple calculation shows that IRF result can be interpreted as I&I volume contribution of different I&I sources, which shows the most problematic I&I contributor in the system volume-wise. The IRF model application in this study is one realization of a real system and there is lots of uncertainty in the system. However, this result still can provide insights to I&I behavior of the system by providing physical meaning of the solutions.

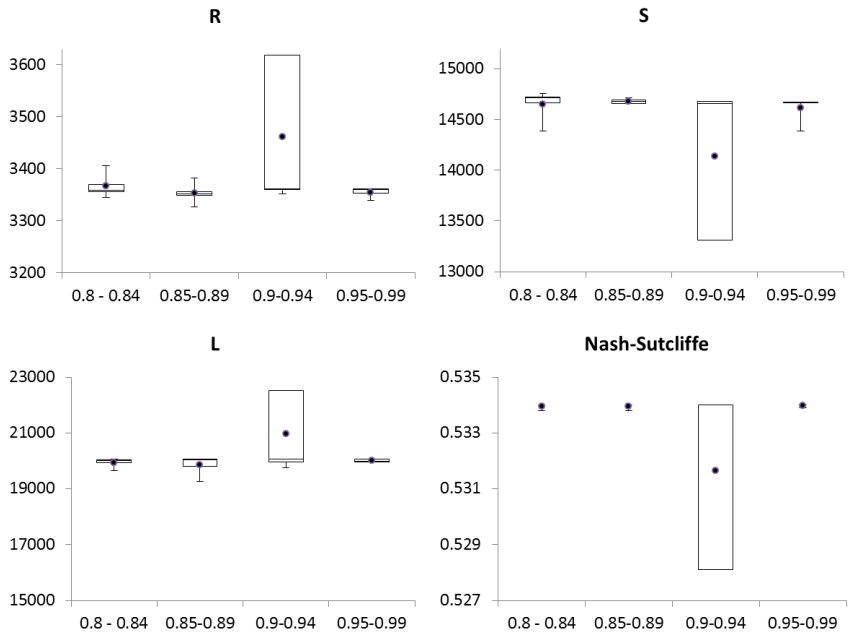

(a)

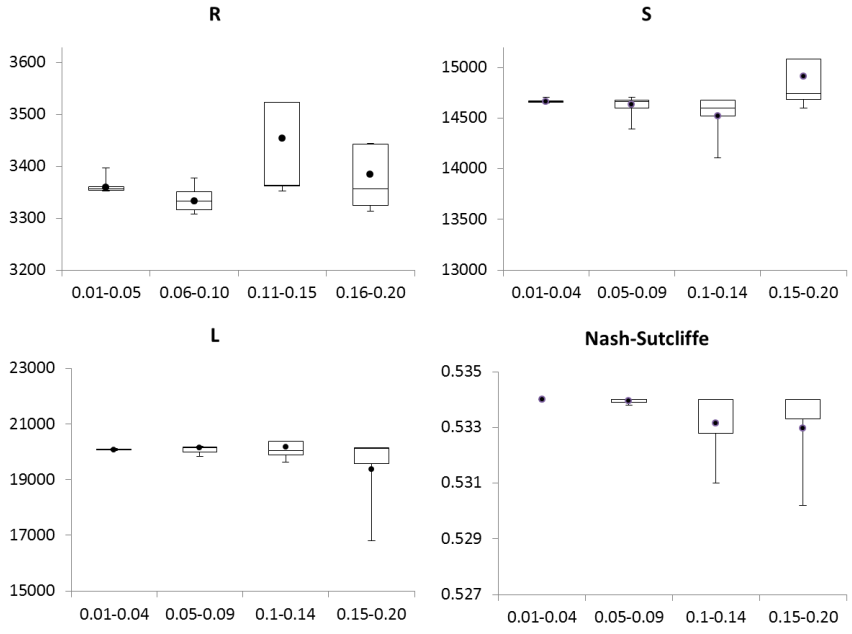

(b)

Figure 4.8 Sensitivity tests on IRF parameters (R; roof connection coefficient, S; sump pump connection coefficient, and L; leaky lateral coefficient) and Nash-Sutcliffe coefficients with (a) different probability of crossover values (with probability of mutation 0.06), and (b) different probability of mutation values (with probability of cross over 0.93)

Table 4.3 Contributing flow volume of three I&I sources using the IRF volume and the weighting coefficients

	Roof	Sump	Lateral
Effective contributing area (m^2)	245.56	48.44	19.33
Flow volume under IRF (m^3)	2.89	1.54	1.63
Flow volume per unit area (m)	0.0118	0.0319	0.0842
IRF weighting coefficients	3359	14663	19985
Total contributing volume (m^3)	9701	22653	32543
Contributing volume / total I&I volume (%)	15	35	50

The Nash-Sutcliffe model efficiency coefficient of the IRF solution is 0.534 in the calibration period and 0.5599 in the validation period (Table 4.4). The Nash-Sutcliffe coefficient of the best RTK solution is 0.8481 in the calibration period and 0.7951 in the validation period. Overall model efficiency is higher in the RTK method since the method calibrates nine parameters rather than three. However, in the validation period, model efficiency is increased for the IRF solution but decreased for the RTK solution. This may imply the pitfall of the RTK method that the method is not consistent and may not be very robust.

Note that the IRF solutions are a unique solution even though the initial population is randomly selected. In contrast, RTK method results in different solutions every time the model runs. Examples of different RTK solutions are presented in Table 4.5 from 30 random runs and they are arranged from the best fit to the worst fit to the monitoring data in the calibration period. The Nash-Sutcliffe coefficient of the best case is 0.8481 and that of the worst case is 0.6808. For the GA optimization, certain ranges of parameter values need to be assigned and the boundary values are also presented in Table 4.5. The solutions are highly dependent on the given ranges and the given boundary values are often found in the solutions.

RTK method has many local optimal solutions, which indicates that nine coefficients are not independent. Thus the starting points or constraints of the parameters cause other parameters to adjust to obtain a local optimum that behaves similarly for calibration data. Box plots of the nine RTK parameters from the 30 model runs in Table 4.5 are presented in Figure 4.9 and three triangular hydrographs from the parameters are shown in Figure 4.10. Greater variability is observed in RTK parameters for the second and third triangular hydrographs, especially the third one. This is because the model tries to adjust these parameters depending on the preceding constraints.

Different RTK local solutions can result in the same model fitness. For example, case 15 and 16 in Table 4.5 show almost identical model fitness with Nash-Sutcliffe coefficients 0.7968 and 0.7937, respectively. However, T3 and K3 values are very different between those cases. Three triangular hydrographs are constructed using the calibrated parameters for the two cases and presented in Figure 4.11. Even with very similar R1 values (0.0242 and 0.0243), difference in T1 and K1 values result in a big difference in the peak of the first hydrograph with rhombus markers. The peak of the first hydrograph in case 15 is 0.046 and that in case 16 is 0.091. Duration of the third hydrographs with triangle markers are 27 hours and 209 hours for case 15 and 16, respectively. It is clearly shown that three hydrographs compensate each other and are correlated. Change in one hydrograph affects other two hydrographs to simply achieve the best fitness. Even with the difference between the triangular hydrographs, two cases simulated monitoring data with very similar model fitness. This indicates the problem of the RTK method that physical processes are not reflected in the modeling.

Because RTK method has nine parameters to adjust and they interact to each other, calibration tends to be curve fitting rather than finding more physically based independent parameters. The

IRF approach tends to be more robust because three parameters adjust three IRF that represent processes based on physics. Each IRF shape is defined independently using physics-based models and the parameters weight the contribution from each of the three IRF. In contrast, the RTK approach includes weighting parameters of each of the three hydrographs and two parameters for each of the three hydrographs to adjust the shape of the hydrograph. Hence, the calibration of the RTK method adjusts both the weights and the hydrograph shapes to obtain a best fit to calibration data. Thus the RTK method is more likely to provide poor simulation of response for conditions outside the calibration range.

Table 4.4 IRF-GA and RKT-GA results with Nash-Sutcliffe coefficients for the calibration period (May 9, 2009 to June 7, 2009) and validation period (June 9, 2009 to July 8, 2009)

Method	Estimated parameters	Nash-Sutcliffe coefficient	
		Calibration	Validation
IRF	Roof connection scaling factor, a = 3359 Sump pump connection scaling factor, b = 14663 Leakey sewer lateral scaling factor, c = 19985	0.534	0.5599
RTK	R1 = 0.02, T1 = 0.338, K1 = 2 R2 = 0.0478, T2 = 1, K2 = 10 R3 = 0.123, T3 = 8.5493, K3 = 14.6686	0.8481	0.7951

Table 4.5 Parameter boundary values and solutions of 30 random RTK-GA runs along with Nash-Sutcliffe coefficients for the calibration period (May 9, 2009 to June 7, 2009)

	R1	R2	R3	T1	T2	T3	K1	K2	K3	Nash-Sutcliffe
Upper boundary	0.2	0.2	0.2	1	10	80	2	10	30	
Lower boundary	0	0	0	0.1	1	1	1	1	1	
1	0.02	0.0478	0.123	0.338	1	8.55	2	10	14.67	0.8481
2	0.019	0.0479	0.1177	1	1	7.2	1	10	16.97	0.8477
3	0.0193	0.0462	0.1167	0.1	1.11	5.11	1	10	24.26	0.8453
4	0.0154	0.0517	0.1222	0.1	1	4.38	1	10	30	0.8424
5	0.0237	0.0439	0.1125	0.1	1	7.35	1	10	15.93	0.8381
6	0.0232	0.0583	0.0972	0.727	1.38	18.71	1.005	10	4.92	0.8328
7	0.0219	0.0551	0.0868	0.165	1.97	13.49	1.186	5.73	7.77	0.8264
8	0.0221	0.0715	0.089	0.1	1.8	31.15	1	10	3.08	0.8239
9	0.0239	0.0677	0.0889	0.1	2.34	22.92	2	7.26	5.66	0.8215
10	0.0232	0.0404	0.1303	0.544	1.84	5.38	1.241	7.09	30	0.8185
11	0.0245	0.076	0.0924	0.1	2.2	46.37	2	1	1.93	0.8111
12	0.0271	0.0698	0.1022	0.1	2.71	28.5	1.217	7.78	4.37	0.8101
13	0.0233	0.0789	0.0851	0.1	2.11	59.78	1	10	1.15	0.8024
14	0.0173	0.1256	0.0321	0.1	7.96	1.15	1	8.43	4.76	0.8001
15	0.0242	0.0412	0.125	0.237	1.94	13.47	1.231	5.21	14.51	0.7968
16	0.0243	0.075	0.0761	0.53	2.04	43.58	1	10	1	0.7937
17	0.0217	0.0916	0.0838	0.457	2.91	45.07	1	7.46	2.33	0.7881
18	0.0242	0.0671	0.0821	0.119	2.74	8.3	1	4.08	21.94	0.7763
19	0.026	0.0799	0.0527	1	2.38	56.03	1	8.32	1	0.7741
20	0.0292	0.0475	0.0927	1	5.15	5.64	1.53	4.68	21.40	0.7423
21	0.0307	0.0505	0.0774	0.99	3.82	47.55	1	2.50	1.24	0.7406
22	0.0168	0.0832	0.0729	1	7.48	1	1	10	25.80	0.734
23	0.0169	0.0606	0.0528	0.192	2.73	8.72	1.41	3.45	10.57	0.7337
24	0.0129	0.0771	0.1001	0.581	3.19	31.35	1.54	7.48	6.73	0.7322
25	0.0358	0.0946	0.0675	1	3.52	80	2	10	1	0.731
26	0.0279	0.0765	0.0814	1	5.04	79.08	1.4	5.01	1	0.7305
27	0.0065	0.0762	0.1083	0.1	1	5.82	1	9.17	30	0.7271
28	0.0231	0.038	0.0663	0.345	10	1	1.48	7.22	30	0.7134
29	0.0333	0.0859	0.0311	0.504	3.36	21.97	1.12	9.95	11.86	0.6995
30	0.025	0.066	0.0753	0.1	6.23	42.93	1.23	1	1	0.6808
Max	0.0358	0.1256	0.1303	1	10	80	2	10	30	0.6808
Min	0.0065	0.038	0.0311	0.1	1	1	1	1	1	0.8481

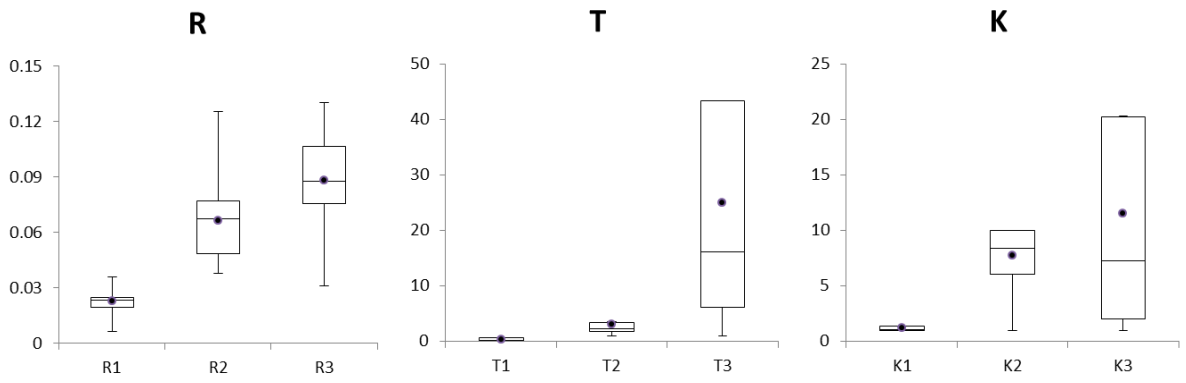

Figure 4.9 Box plots of RTK solutions in Table 4.5

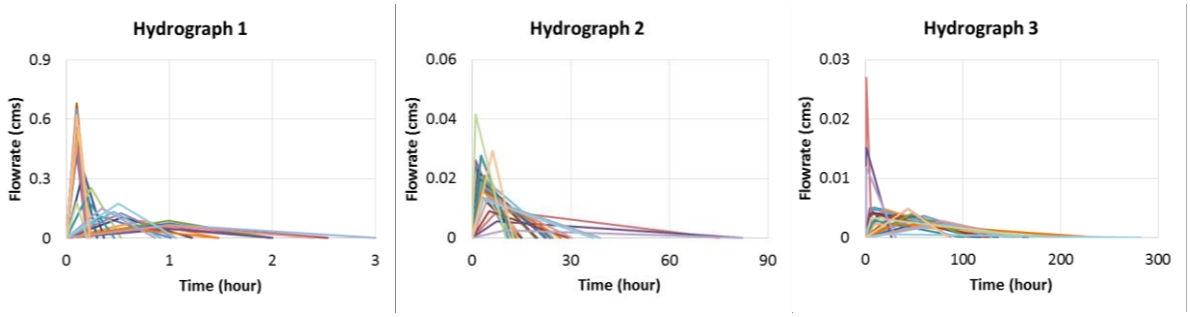

Figure 4.10 Three RTK triangular hydrographs from 30 different model runs (flowrate for 1 cm of rain over the unit area 1 km^2)

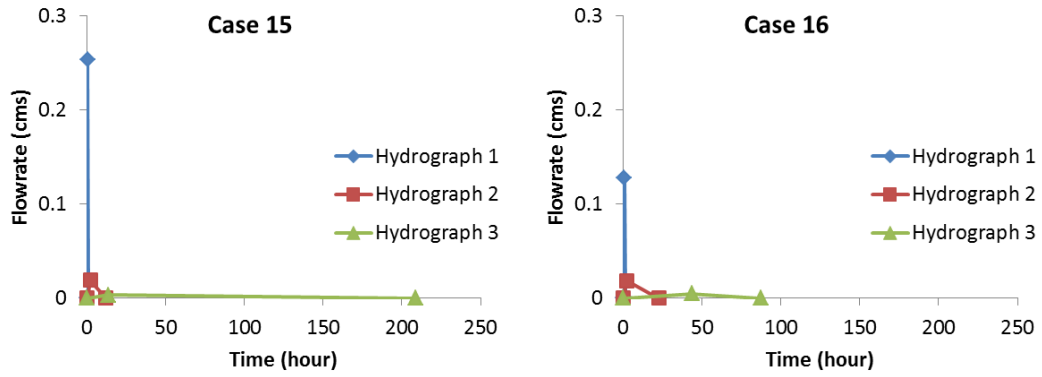

Figure 4.11 Case 15 and case 16 of RTK parameter solutions in Table 4.5 that result in similar Nash-Sutcliffe model fitness coefficients: 0.797 and 0.794, respectively (flowrate for 1 cm of rain over the unit area 1 km^2)

Figure 4.12 shows the IRF solution and the best case of the RTK solutions along with the monitoring data. Both methods predict the monitoring data fairly well in both calibration period and validation period. In June 24, both methods predict flow peaks but the peak is not observed. The flow peak might have happened in such a short time period and the flow monitor might have failed to capture the peak. Overall, RTK method is more efficient in predicting the flow than the IRF method especially at the falling limbs of the peaks where IRF underestimates the flow.

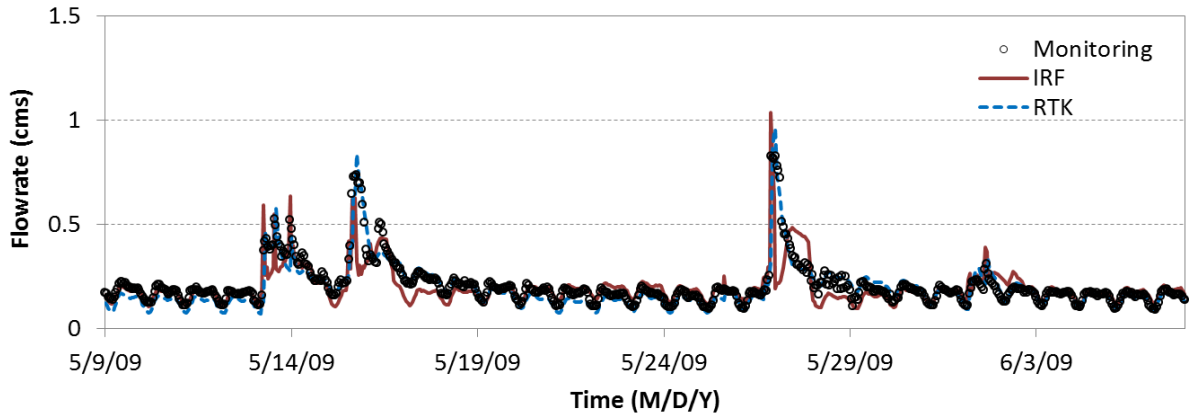

(a)

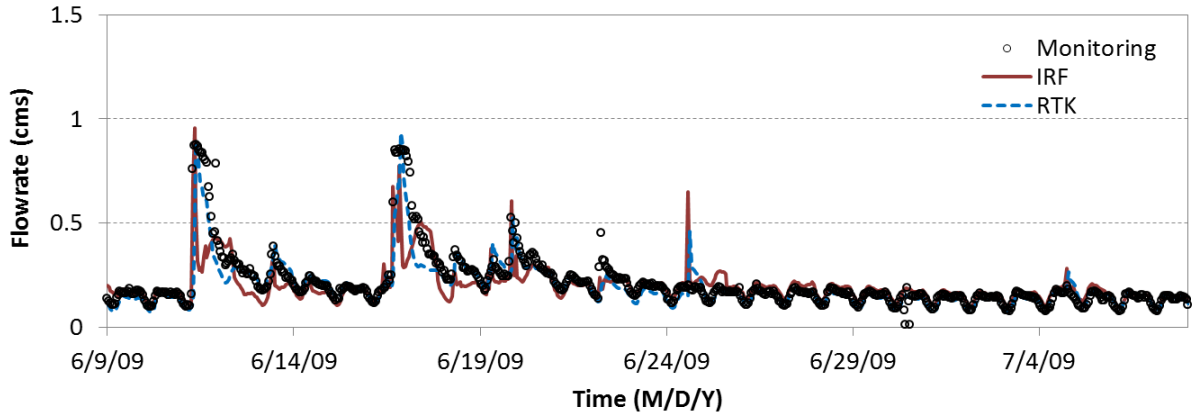

(b)

Figure 4.12 IRF-GA and RTK-GA results in the (a) calibration period (May 9, 2009 to June 7, 2009) and the (b) validation period (June 9, 2009 to July 8, 2009)

Figure 4.13 show roughly five distinguishable storm events that start at: May 13, May 15, May 27, June 11, and June 11, 2009 in four windows. The volume and the peak flow values for the estimated DWF, observed sewer flow, IRF model result, and RTK model result are summarized in Table 4.6. Flowrate 0.3 cms is selected to define the beginning and the end of each storm. The observed sewer flow, IRF results, and RTK results are compared to the estimated DWF using the following equation.

$$\text{Compare to DWF} = \frac{(\text{Observed sewer flow})}{(\text{Estimated DWF})} \tag{3}$$

The observed sewer flow is three to four times of DWF in volume and three to six times in peaks during the storms. Considering the monitoring location is sanitary only, a great deal of I&I exists in the area.

The IRF result and RTK result are compared to the observed sewer flow using the following equation.

$$\text{Compare to monitoring} = \frac{(\text{(IRF) or (RTK)}) - (\text{Observed sewer flow})}{(\text{Observed sewer flow})} \times 100 \tag{4}$$

Both models underestimate the flow volume; IRF method underestimates flow volume by 9% to 28% and RTK method underestimates flow volume by 4% to 26% compare to monitoring volume. In terms of flow peaks, RTK method overestimates peak flowrate from 1% to 16%. IRF method overestimates peak flowrate for May 13, May 27, and June 11 storms by 19%, 25%, and 9%, respectively. IRF method underestimates peak flowrate for May 15, and June 16 by 15% and 8%, respectively.

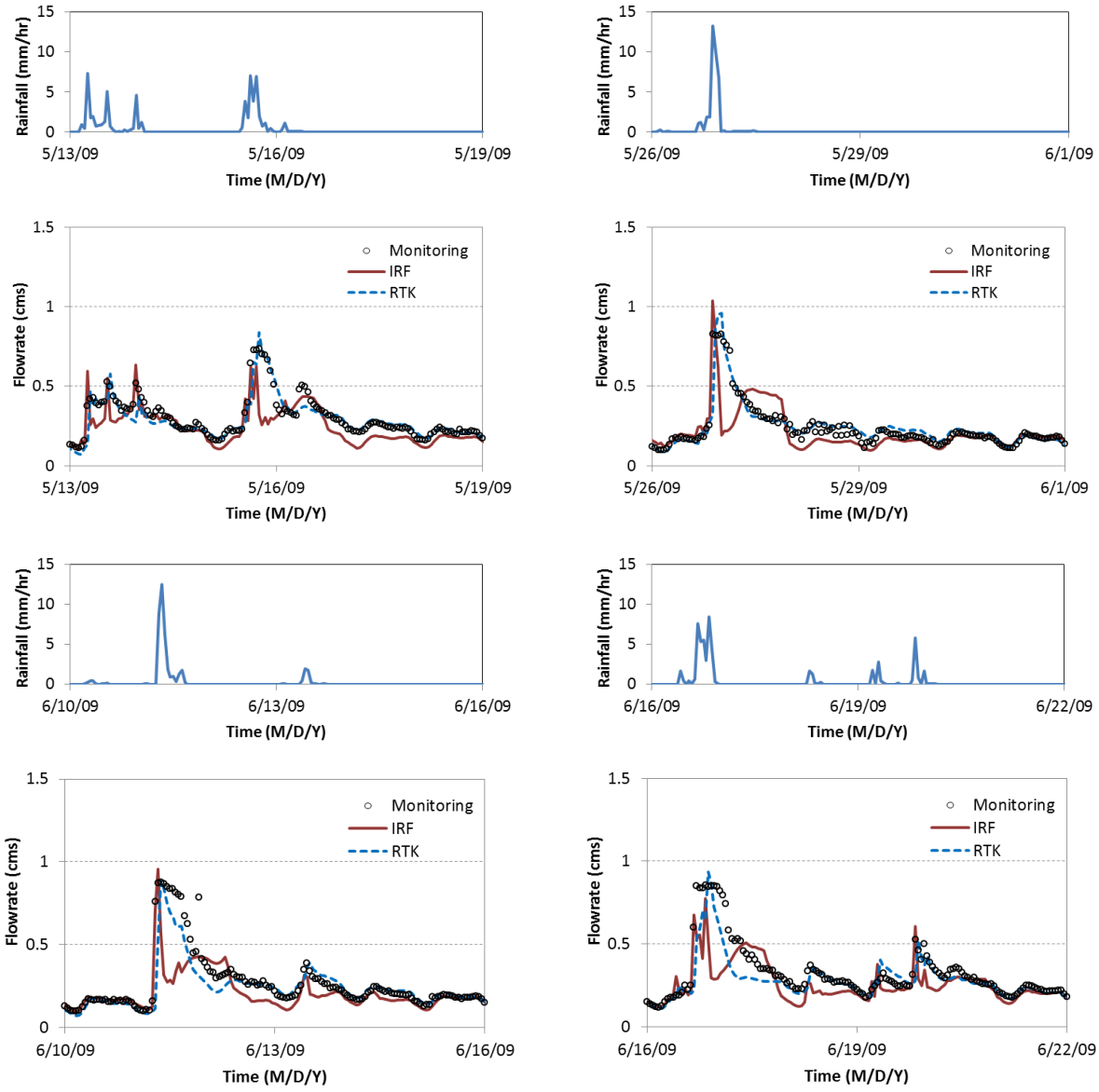

Figure 4.13 Comparison of the best cases of IRF and RTK solutions for four different periods

Table 4.6 Volume and peak of the estimated DWF, observed sewer flow, IRF result, and RTK result for five storm events (Flowrate over 0.3 cms is used as the criteria to separate storms and following formula is used to compare. (Compare to DWF) = (Observed sewer flow)/(Estimated DWF), (Compare to monitoring) = ((IRF or RTK)-(Observed sewer flow))/(Observed sewer flow)*100, Negative values are in italic.)

Storm	Estimated DWF		Observed sewer flow		IRF		RTK	
	Volume [10^3 m^3]	Peak [cms]	Volume [10^3 m^3]	Peak [cms]	Volume [10^3 m^3]	Peak [cms]	Volume [10^3 m^3]	Peak [cms]
			Compare to DWF		Compare to Monitoring			
May 13, 2009	12.23	0.15	40.49	0.53	34.74	0.63	35.49	0.58
			3.31	3.53	*-14.20*	18.87	*-12.35*	9.43
May 15, 2009	15.16	0.17	51.03	0.74	40.80	0.63	48.80	0.84
			3.37	4.35	*-20.05*	*-14.86*	*-4.37*	13.51
May 27, 2009	10.77	0.15	43.36	0.83	39.47	1.04	40.77	0.96
			4.03	5.53	*-8.97*	25.30	*-5.97*	15.66
June 11, 2009	13.75	0.15	60.35	0.88	43.28	0.96	44.94	0.89
			4.39	5.87	*-28.29*	9.09	*-25.53*	1.14
June 16, 2009	19.08	0.15	77.63	0.85	56.56	0.78	59.69	0.93
			4.07	5.67	*-27.14*	*-8.24*	*-23.11*	9.41

Residual plots of the IRF and the best RTK solutions for the calibration period and the validation period are presented in Figure 4.14. Residuals are the difference between the observed value of the dependent variable and the predicted value. Each data point has one residual and is defined with the following equation.

Residual = Observed value – Predicted value (5)

Residuals are plotted against the observed value in the *x* axis. There are clusters of points at low flowrate, which represent tails in the hydrographs. In Figure 4.14 (a), IRF underestimates the peaks as most of the residuals are in the positive side. These points are from the storms in May 15, 2009 and May 27, 2009. This trend is also observed in the validation period and the outliers are from the storms in June 11, 2009 and June 16, 2009 (Figure 4.14 (b)). In validation period, RTK also underestimated peaks as most of high flow points are in the positive side. This means the best RTK solution for the calibration period loses the efficiency in the validation period. This explains the decrease of Nash-Sutcliffe coefficient of RTK method in the validation period as presented in Table 4.5 and supports that RTK method is more of a curve fitting method with limited physical meaning. On the other hand, underestimation of peaks indicates the shortcoming of using Nash-Sutcliffe coefficient for the GA conversion criteria and a different technique such as optimization function could be tested in future research.

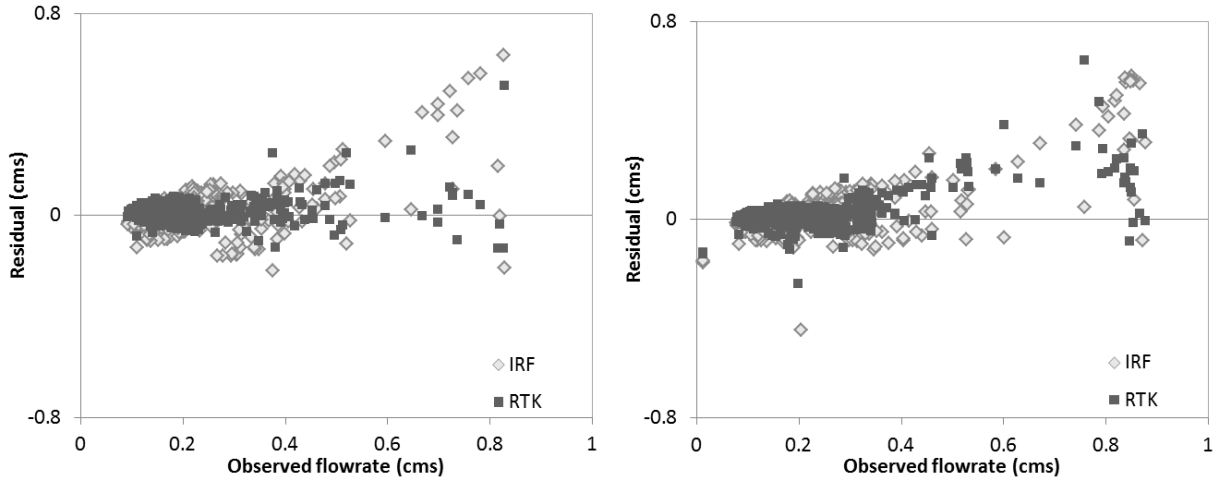

Figure 4.14 Residual plots of IRF and RTK methods for (a) calibration period and (b) validation period

In this section, the IRF method was applied to a Chicago area and compared with the RTK method. Even though the RTK method showed better prediction of the flow as a pure empirical curve fitting method, the IRF method showed more robust solution with physical meanings. RTK method is completely arbitrary and the strong correlation between the RTK parameters simply allows them to offset one another to achieve a better fit.

4.2.3. Modified Nash-Sutcliffe coefficient

The IRF method showed smaller Nash-Sutcliffe model fitting coefficient which means the RTK method performs better at predicting flows. Even though the IRF method is based on a physics-based approach, the result can be discouraging for one to use. However, Nash-Sutcliffe coefficient is only one way of measuring a model fitness. The I&I flow data is consist of mainly low flows by nature and peak flows may not be represented as well.

Figure 4.14 (a) shows that flow peaks are underestimated when the IRF method was used. Data points are concentrated in lower flow range as 88% of them are smaller than 0.3 cms. The characteristic of the data set makes Nash-Sutcliffe method put more weight on lower flowrates. By putting more weights on peak flow data, the Nash-Sutcliffe value can be greatly improved.

One example of the modified model efficiency is to apply bigger weights on larger flow ranges. For example, weighting factor one can be applied to low flows, two can be applied to medium flows, and three can be applied to peak flow values. The original Nash-Sutcliffe formulation can be modified as following.

$$E_j = 1 - \frac{\sum_{t=1}^{T} W_{t,j}\left(Q_0^t - Q_m^t\right)^2}{\sum_{t=1}^{T} W_{t,j}\left(Q_0^t - \overline{Q_0}\right)^2} \quad (6)$$

where j is an weighting factor (j = 1, 2, and 3).

In this way smaller runoff values are deemphasized and larger peaks are more pronounced. Table 4.7 clearly shows that the modified model fitting method results in improved fitting coefficients. Nash-Sutcliffe coefficient using regular formulation is 0.534 and that using the weighted formulation is 0.8992 in the calibration period. Thus forcing to fit peaks more than low flows improved the model fitness.

Table 4.7 Improved model fitness using a weighted Nash-Sutcliffe method in the IRF-GA and RKT-GA for the calibration period (May 9, 2009 to June 7, 2009) and validation period (June 9, 2009 to July 8, 2009) (R = Roof connection scaling factor, S = Sump pump connection scaling factor, L = Leakey sewer lateral scaling factor)

Method	Estimated parameters	Nash-Sutcliffe coefficient	
		Calibration	Validation
Regular Nash-Sutcliffe	R = 3359 S = 14663 L = 19985	0.534	0.5599
Weighted Nash-Sutcliffe (1 for 80 percentile, 2 for between 80 and 90 percentile, 3 for above 90 percentile)	R = 3359 S = 14663 L = 19985	0.8992	0.8660

References

Espey Jr., W. H., Clemmens, B., & Halverson, B. (2014) *Lake Michigan Diversion Committee: Findings of the seventh technical committee for review of diversion flow measurements and accounting procedures* (p. 124). Chicago, IL.

Hickory Hills (zip 60457), Illinois Climate. (2014, June). Retrieved January 6, 2016, from http://www.bestplaces.net/climate/zip-code/illinois/hickory_hills/60457.

Miller, K., & Schmidt, A. R. (2010) *Hydraulic modeling of the Calumet interceptor network, Tunnel and Reservoir plan, Report No.10*. Urbana, IL.

Nash, J. E., & Sutcliffe, J. V. (1970) River flow forecasting through conceptual models, Part I - a discussion of principles. *Journal of Hydrology*, *10*, 282–290.

U.S. Census Bureau, Profile of General Population and Housing characteristics: 2010 Demographic Profile Data (DP-1): Hickory Hills city, Illinois, American Factfinder. Retrieved January 6, 2016 from http://factfinder.census.gov/faces/tableservices/jsf/pages/productview.xhtml?src=bkmk.

5. Uncertainty in Rainfall Induced Infiltration

5.1. Introduction

This study suggests a lumped model of I&I using scaling factors of three I&I hydrographs that are derived from physics-based models. Thus error is expected to be introduced in the modeling. In this chapter, possible uncertainties in rainfall induced infiltration (RII) through a leaky pipe are examined. Uncertainty resulting from the following six factors is independently examined: antecedent moisture condition (AMC), pedotransfer functions (PTFs), soil hydraulic conductivities, sewer pipe depths, initial conditions (IC), and rainfall characteristics.

Uncertainty in unsaturated flow modeling can be divided into two kinds: intrinsic uncertainty and information uncertainty (Dettinger & Wilson 1981). Tung & Yen (2005) referred to these two kinds of uncertainty as natural variability and knowledge deficiency (Figure 1). The six factors under the uncertainty investigation involve uncertainties from both natural variability and knowledge deficiency. In Table1, uncertainty sources related to the six factors of interest are summarized. Since the impact of all the uncertainty sources is either difficult or impractical to measure, the uncertainty investigation is performed only for limited sources as described in the following paragraphs.

Antecedent moisture condition (AMC) includes the uncertainty related to climatic, hydrologic, and geologic natural variability as well as data deficiency. In this study, the effect of variable AMC between storms on infiltration hydrograph is investigated thus the interest is only focused on short term climatic variability.

Pedotransfer functions (PTFs) are closely connected with the uncertainty in soil hydraulic conductivity. PTFs are empirical models that are developed to reduce the uncertainty in estimating hydraulic conductivity by using directly measurable soil properties (e.g. soil composition). However, directly measurable soil properties also involve uncertainties: geologic variability and knowledge deficiency in data. There are various PTFs to choose from and different PTFs give different solutions, which also results in model uncertainty. More easily measurable soil property values are also limited. Thus the error is from natural variability, insufficient data, and different PTF models. In this study, seven different PTFs are tested using the same soil properties in the test area and the hydraulic conductivity values that are derived from the PTFs are compared to each other.

The soil hydraulic conductivity is used as a model parameter in this study and the uncertainty is originated from geologic variability (e.g. non-uniform ground condition), knowledge deficiency in model parameter and data (e.g. limited data availability), and measurement error. The impact of different hydraulic conductivity values on the infiltration hydrograph is examined.

Sewer pipe depths affect the infiltration hydrograph and involve uncertainty mainly from knowledge deficiency, data measurement errors, inadequate sampling, and error caused by handling and transcription mistakes. The effect of different sewer pipe depths on the RII hydrograph is investigated.

The infiltration model has a start-up period where the solution has not converged to equilibrium. The duration required for the start-up period depends on the initial condition (IC). However, the solution eventually converges to a stable behavior no matter what the ICs are. This implies that this is a boundary-value problem. The infiltration model does not converge until the effect of the

boundary condition dissipates. Ten different simulation periods are tested to investigate the effect of IC on the infiltration hydrograph and to estimate the average start-up period.

Different rainfall characteristics affect the infiltration response and both natural variability, especially climatic variability, and data deficiency cause the uncertainty. To understand the impact of rainfall characteristics on the RII hydrograph, various storm durations and shapes are applied in the modeling.

This study suggests a lumped I&I model using representative IRFs that are applied across sewershed with scaling parameters. The lumped model introduces error but it is impossible to physically model every flow path into the sewer system. For example, depths of all sewer pipes in the sewershed are different. Hydraulic conductivity values vary from lateral locations and depth. Thus this chapter is prepared to investigate uncertainty introduced by the variability of the modeling factors. Each factor is examined independently and changes in IRF to uniform rainfall or unsaturated flow response to actual rainfall are evaluated by changing model inputs.

To see how AMC affects IRF, IRFs for a uniform rainfall following different AMCs is evaluated. For comparison of different PTFs, seven different PTFs are simply applied to the same soil data to determine the estimated hydraulic conductivity resulting from different PTF. For hydraulic conductivity, unsaturated flow response to the real rainfall is compared with different hydraulic conductivity values that cover the range of measured hydraulic conductivity and calculated ones from the PTFs. Different sewer depths are tested for the infiltration model with real rainfall and the unsaturated flow responses are compared. The infiltration model start-up periods vary for different simulation periods. Thus the start-up periods for nine different simulation periods, and the average start-up period are calculated. For rainfall characteristics,

different rainfall shapes and durations are used for model input and the changes in the infiltration IRF are investigated.

All these possible errors caused by the uncertainty factors in the infiltration modeling could have an effect on the model calibration. For physical simulation models, these calibration data are not readily available (Melching et al. 1987) so various data values are tested to understand how much impact would have made on the infiltration response.

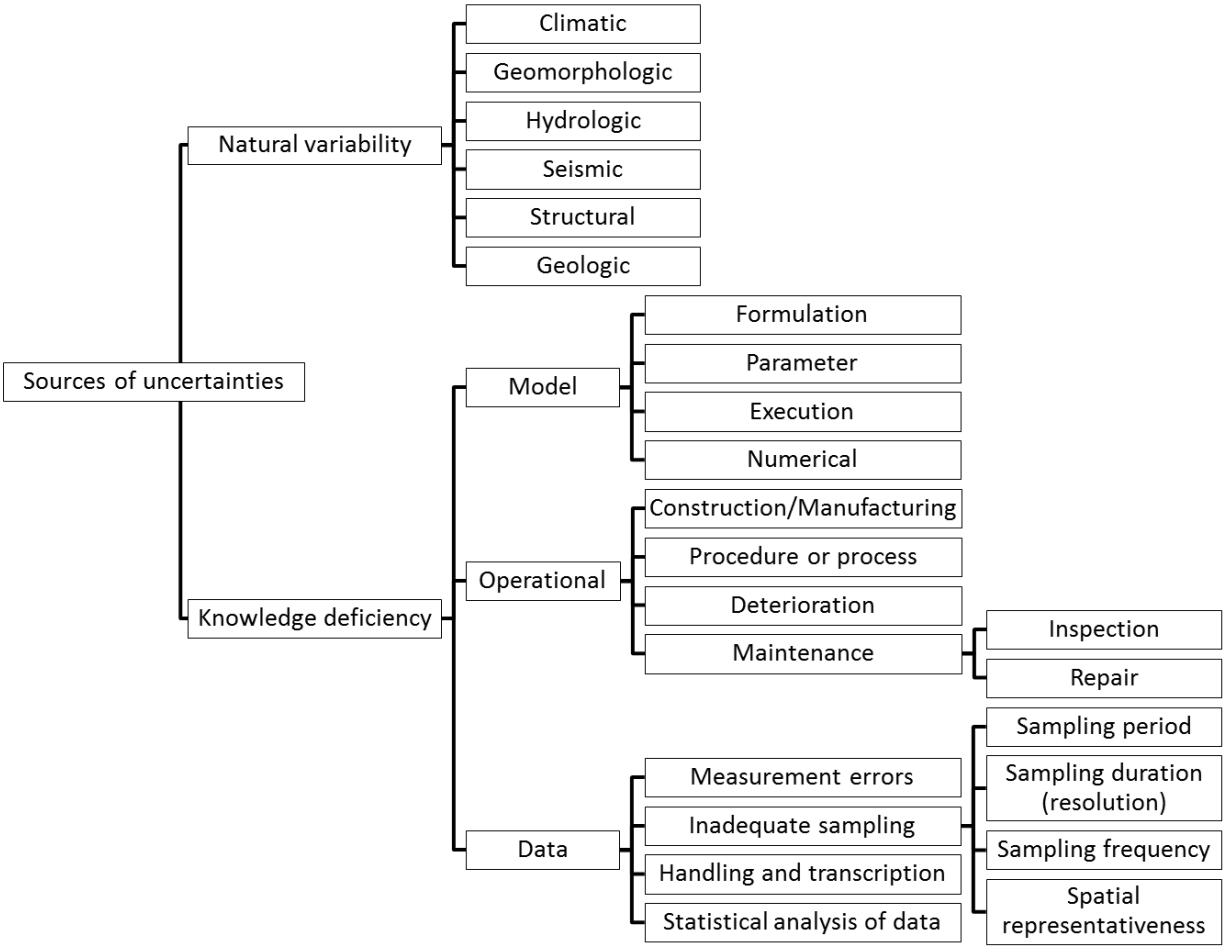

Figure 5.1 Sources of uncertainties (modified from Figure 1.1 in Tung & Yen (2005))

Table 5.1 Uncertainty involved in six factors of interest

Factors of interest	Sources of uncertainty
Antecedent moisture condition (AMC)	• Natural variability (Climatic, Hydrologic, Geologic) • Knowledge deficiency (Data)
Pedotransfer functions (PTFs)	• Natural variability (Geologic) • Knowledge deficiency (Model, Data)
Soil hydraulic conductivity	• Natural variability (Geologic) • Knowledge deficiency (Model parameter, Data)
Sewer pipe depths	• Knowledge deficiency (Operational construction, Maintenance, Data measurement errors, inadequate sampling, handling and transcription)
Initial condition (IC)	• Natural variability (Climatic, Hydrologic, Geologic) • Knowledge deficiency (Model parameter)
Rainfall characteristics	• Natural variability (Climatic) • Knowledge deficiency (Data)

Previous studies of uncertainty in sewer infiltration were focused on separating the sewer flow hydrograph into different flow components. Bénédittis & Bertrand-Krajewski (2005a) presented uncertainties in various infiltration estimation methods and found a strong variability between them. The study found that the methods based on the night flow or pollutant concentration tend to overestimate infiltration. In the night flow method, the sewer flow during the night is considered as an estimated infiltration flow. The largest uncertainty in daily infiltration values during March 2003 in an experimental site (Ecully catchment) was up to 50% depending on the estimation methods. Bénédittis & Bertrand-Krajewski (2005b) suggested that the oxygen isotope method is reliable to estimate infiltration and measuring additional hydrogen isotopes decreases uncertainty. Sampling during night periods was also suggested as a way to decrease uncertainty. Kracht et al (2007) performed comprehensive uncertainty analysis on a stable isotope approach. The study revealed larger variation of isotopes in groundwater than drinking water. To assess the combined measurement uncertainty of infiltration estimation, Monte Carlo simulation scheme was used in the paper. Bareš et al. (2009) performed uncertainty analysis on the infiltration

estimation using pollutant load and continuous water quality and quantity monitoring. The analysis found that chemical oxygen demand (COD) is preferred as a natural tracer over total suspended solid (TSS). Starting time during a day and sampling interval also affected uncertainty; larger uncertainty was observed for longer sampling interval. Franz (2007) applied modified multivariate statistical technique to optimize sewer measuring points and the new method reduced up to 40% of uncertainty related to measurements. These study efforts only have provided insights on uncertainty in measurements of flows or substances in wastewater. These studies also focused on groundwater infiltration to sewer systems rather than RII.

Pawlowski et al. (2013) found that storm intensity and AMC affects the contribution of different I&I sources to the total rainfall derived infiltration and inflow volume. Contribution of I&I from downspout connections increased with high intensity storms under dry AMC and the flow contribution from faulty sewer lateral increased with low intensity storms under wet AMC. By investigating the impact of the six variables in RII, this study will provide better understanding about sewer infiltration modeling.

5.2. Uncertainty Factors

5.2.1. Antecedent Moisture Condition

The effect of AMC on RII is evaluated by adding a perturbation into the rainfall record and comparing with the control case, which is the result without the perturbation. The perturbation is the uniform 3-hour, 42-mm rainfall presented in section 4.1.2 and this is added at ten different random times in the rainfall record. The list of random times is presented in Table 1 of chapter 4 and the changed hyetographs are presented in Figure 5.2. The IRFs of the perturbation are

compared to evaluate the effect of AMC as each case contains different preceding rainfall conditions.

The 3-hour 42 mm rainfall, or representative rainfall, is added as a rainfall perturbation and the flow response for the perturbation is derived by subtracting the response from the rainfall without the perturbation. The schematic of the procedure is presented in Figure 5.3 using the July 28th, 2009 case. By averaging these perturbation responses from ten test cases, the IRF of the leaky lateral is derived in section 4.1.1.

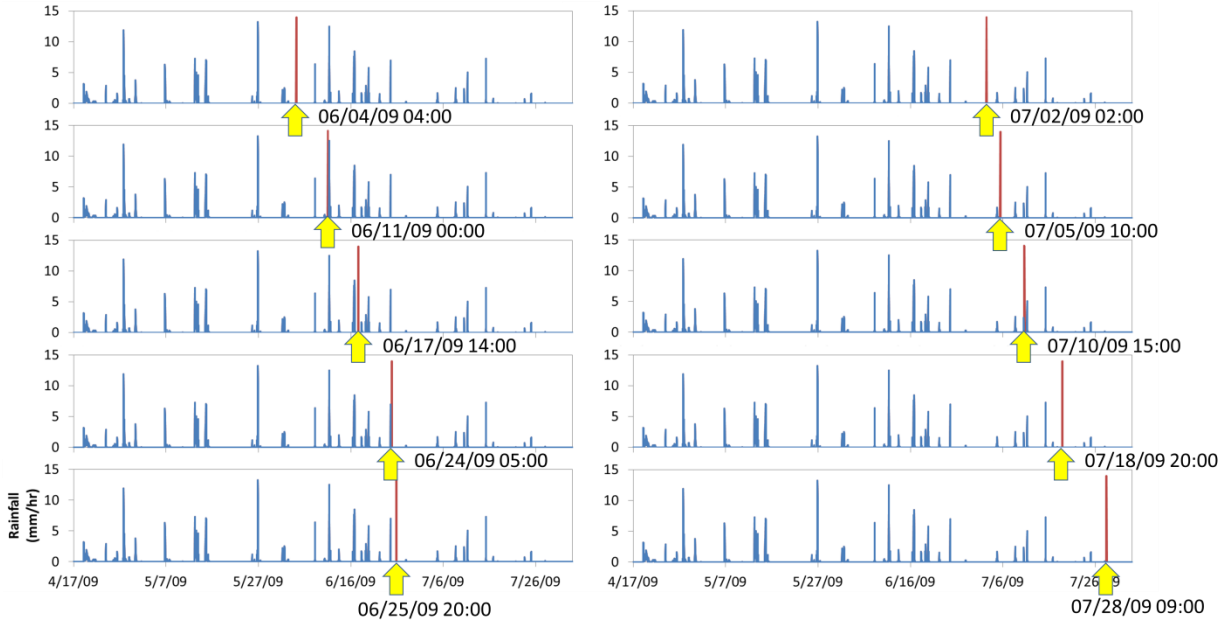

Figure 5.2 Changed hyetographs with the addition of 3-hr 42-mm uniform rainfall at ten random times listed in Table 1 of chapter 4

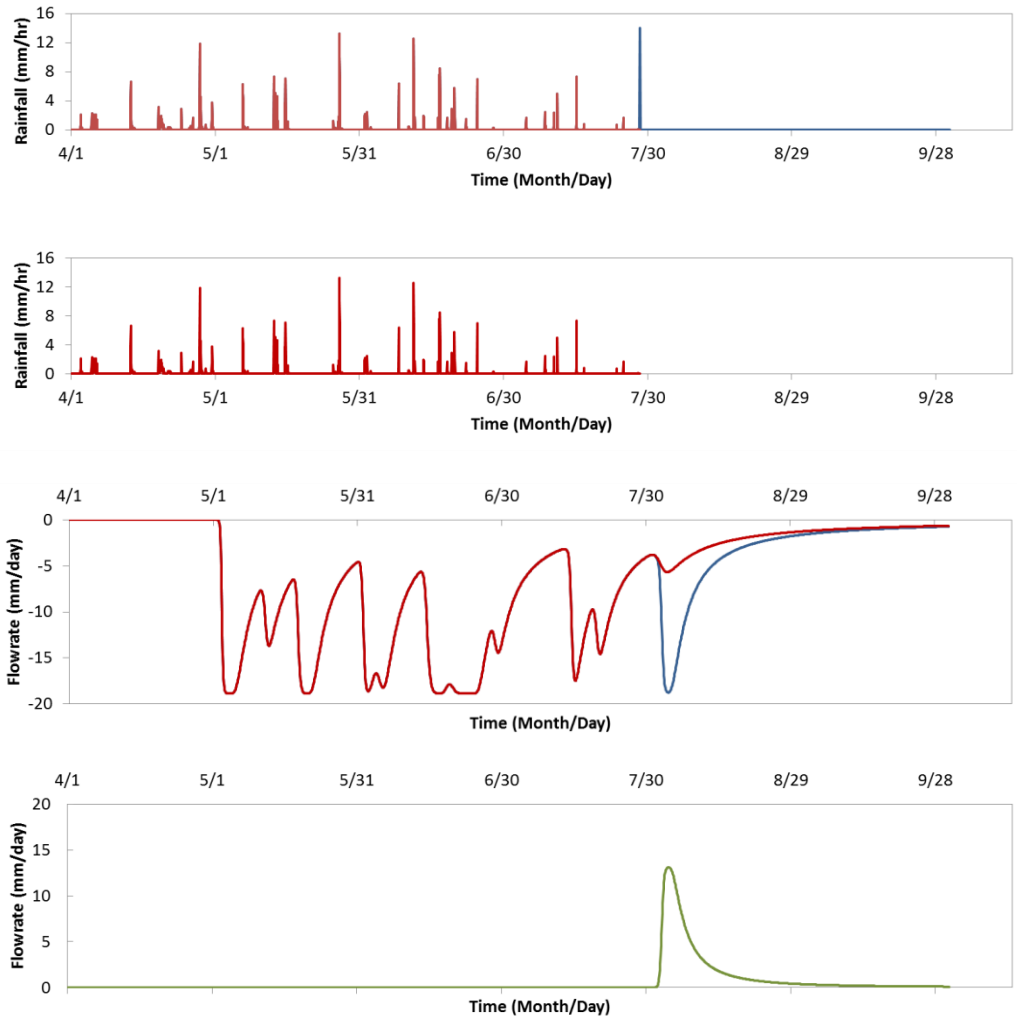

Figure 5.3 Infiltration response for the rainfall perturbation derived by subtracting the response from the rainfall without the perturbation using the July 28th, 2009 case (average of this response for ten different cases become leaky lateral IRF)

5.2.2. Pedotransfer Functions

Soil hydraulic conductivity can be measured directly using a specialized device but direct measurement is costly and time consuming. A hydraulic conductivity value from a direct measurement gives a local estimate of a property with a large spatial variability. To estimate the actual hydraulic conductivity would require many measurements to define this spatial variability. Pedotransfer functions (PTFs) are indirect methods to estimate the hydraulic conductivity using

more easily measured soil properties (e.g. texture class, geometric mean particle size, organic carbon content, bulk density, or effective porosity). Since the hydraulic conductivity values for different soil types that are provided by NRCS Soil Data Mart also contain uncertainty, estimating the hydraulic conductivity with other available physical soil data might be beneficial. In this study, total seven different PTFs that were presented by Rasoulzadeh (2011) are tested for the given soil data and each PTF is explained below.

Brakensiek et al. (1984) presented following form of PTF.

$$K_s = 24 \cdot \exp(x) \text{ [cm/d] or} \tag{3}$$

$$K_s = 2.778 \cdot 10^{-6} \cdot \exp(x) \text{ [m/s]} \tag{4}$$

where

$$\begin{aligned} x = {} & 19.52348(\theta_s) - 8.96847 - 0.028212(Clay) + 1.8107 \cdot 10^{-4}(Sand^2) - 9.4125 \cdot 10^{-3}(Clay^2) \\ & - 8.395215(\theta_s^2) + 0.077718(Sand)(\theta_s) - 0.00298(Sand^2)(\theta_s^2) - 0.019492(Clay^2)(\theta_s^2) \\ & + 1.73 \cdot 10^{-5}(Sand^2)(Clay) + 0.02733(Clay^2)(\theta_s) + 0.001434(Sand^2)(\theta_s) \\ & - 3.5 \cdot 10^{-6}(Clay^2)(Sand) \end{aligned}$$

K_s = saturated hydraulic conductivity, θ_s =saturated water content, *Clay* = clay content (%), and *Sand* = sand content (%).

Cosby et al. (1984) suggested a PTF only using sand and clay contents as following.

$$K_s = 60.96 \cdot 10^{\{-0.6 + 0.0126(Sand) - 0.0064(Clay)\}} \text{ [cm/d] or} \tag{5}$$

$$K_s = 7.05556 \cdot 10^{\{-6.6 + 0.0126(Sand) - 0.0064(Clay)\}} \text{ [m/s]} \tag{6}$$

Campbell (1985) introduced a PTF using particle size distribution.

$$K_s = 339\left(\frac{1.3}{BD}\right)^{1.3b} \exp\left(-6.9\left(m_{clay}\right) - 3.7\left(m_{silt}\right)\right) \text{ [cm/d] or} \tag{7}$$

$$K_s = 3.9236\cdot 10^{-5}\left(\frac{1.3}{BD}\right)^{1.3b} \exp\left(-6.9\left(m_{clay}\right) - 3.7\left(m_{silt}\right)\right) \text{ [m/s]} \tag{8}$$

where BD = bulk density (g/cm^3), b = empirical parameter of Campbell's soil water retention function $b = d_g^{-0.5} + 0.2\sigma_g$, d_g = geometric mean particle diameter (mm) $d_g = \exp\sum_{i=1}^{3} m_i \ln d_i$, σ_g = standard deviation of mean particle diameter $\sigma_g = \exp\left[\sum_{i=1}^{3} m_i \left(\ln d_i\right)^2 - \left(\sum_{i=1}^{3} m_i \left(\ln d_i\right)\right)^2\right]$, m_i = mass fraction of textural class i ($m_1 = m_{\text{clay}}$, $m_2 = m_{\text{silt}}$, $m_3 = m_{\text{sand}}$) (%), and d_i = arithmetic mean diameter of class i (normal values: d_{clay} = 0.001 mm, d_{silt} = 0.026 mm, d_{sand} = 1.025 mm).

Saxton et al. (1986) suggested a shorter formulation of the variable x in the PTF from Brakensiek et al. (1984) which presented in equation (3) and (4).

$$x = 12.012 - 7.55\cdot 10^{-2}\left(Sand\right) + \frac{\left(-3.895 + 3.671\cdot 10^{-2}\left(Sand\right) - 0.1103\left(Clay\right) + 8.7546\cdot 10^{-4}\left(Clay^2\right)\right)}{\theta_s} \tag{9}$$

Saturated water content θ_s can be estimated using the following equation (Tietje & Hennings, 1996).

$$\theta_s = 0.332 - 7.251\cdot 10^{-4}\left(Sand\right) + 0.1276\log_{10}\left(Clay\right) \tag{10}$$

Following PTF from Vereecken et al. (1990) includes organic matter content.

$$K_s = \exp\begin{pmatrix} 20.62 - 0.96\ln(Clay) - 0.66\ln(Sand) \\ -0.46\ln(Om) - 8.43(BD) \end{pmatrix} \text{ [cm/d] or} \quad (11)$$

$$K_s = 1.1574 \cdot 10^{-7} \exp\begin{pmatrix} 20.62 - 0.96\ln(Clay) - 0.66\ln(Sand) \\ -0.46\ln(Om) - 0.00843(BD) \end{pmatrix} \text{ [m/s]} \quad (12)$$

where *Clay* = clay content (%), *Sand* = sand content (%), *Om* = organic matter content (%), and *BD* = bulk density in g/cm^3.

Wösten et al. (1997) suggested following PTF with the distinction of topsoil property.

$$K_s = 1.15741 \cdot 10^{-7} \exp(x) \text{ [m/s]} \quad (13)$$

where

$$x = 7.755 + 0.0352(Silt) + 0.93(Topsoil) - 0.967(BD^2) - 0.000484(Clay^2)$$
$$-0.000322(Silt^2) + \frac{0.001}{(Silt)} - \frac{0.0748}{(Om)} - 0.643\ln(Silt) - 0.01398(BD)(Clay)$$
$$-0.1673(BD)(Om) + 0.02986(Topsoil)(Clay) - 0.03305(Topsoil)(Silt)$$

BD = bulk density in g/cm^3, *Sand* = sand content (%), *Clay* = clay content (%), *Silt* = silt content (%), *Topsoil* = topsoil parameter (0 = subsoil, 1 = topsoil), *Om* = organic matter content (%), θ_s = saturated water content.

Ferrer-Julià et al. (2004) suggested a PTF which only contains sand content.

$$K_s = 0.92e^{(0.0491(Sand))} \text{ [mm/h] or} \quad (14)$$

$$K_s = 2.556 \cdot 10^{-7} e^{(0.0491(Sand))} \text{ [m/s]} \quad (15)$$

5.2.3. Soil Hydraulic Conductivities

Hydraulic conductivity is often considered as one of the most difficult factors to estimate in unsaturated flow modeling (El-Kadi 1987, Baroni et al. 2010). Three different soil properties are used to represent ambient soil, impermeable soil, and extremely permeable soil in the model. The impermeable soil represents impervious surface areas (e.g. sidewalks, and buildings). The extremely permeable soil characterizes the leaky sewer pipe. The hydraulic conductivity for both soil layers are assumed as 10^{-12} m/s and 10^{-2} m/s, respectively. Various hydraulic conductivity values for the ambient soil are presented in Table 5.2 for testing. The actual soil data are obtained from NRCS Soil Data Mart for a sample area, Hickory Hills, IL, and the testing values in Table 5.2 are determined based on the data distribution. The area-weighted average value of hydraulic conductivity in the area is $2.19 \cdot 10^{-7}$ m/s and 16 cases with different hydraulic conductivity values are tested. Note that case 15 and 16 are based on the hydraulic conductivity

Table 5.2 Hydraulic conductivity values for the test

	Cumulative area % smaller	K_s (m/s)
1	5	$4.61 \cdot 10^{-8}$
2	10	$5.07 \cdot 10^{-8}$
3	20	$5.98 \cdot 10^{-8}$
4	25 (30)	$6.53 \cdot 10^{-8}$
5	40	$6.70 \cdot 10^{-8}$
6	50	$7.17 \cdot 10^{-8}$
7	60	$7.60 \cdot 10^{-8}$
8	70	$1.06 \cdot 10^{-7}$
9	Area weighted average	$2.19 \cdot 10^{-7}$
10	75	$3.14 \cdot 10^{-7}$
11	80	$6.19 \cdot 10^{-7}$
12	85	$6.32 \cdot 10^{-7}$
13	90	$6.44 \cdot 10^{-7}$
14	95	$6.57 \cdot 10^{-7}$
15	Additional case (1st quartile of PTF results)	$1.28 \cdot 10^{-6}$
16	Additional case (3rd quartile of PTF results)	$1.80 \cdot 10^{-6}$

values derived from the application result of different PTFs that is presented in the later section 5.3.2 in this chapter.

5.2.4. Sewer Pipe Depths

The sewer pipe depth determines the length of unsaturated flow paths. To estimate the sewer depth in the study area, the digitized sewer map for Hickory Hills, IL is analyzed. Figure 5.4 is the illustration of sewer junctions in the area and available data points are highlighted. The total number of junctions in the area is 1089 and 713 have both invert and ground elevations available, which is 65% of the entire junctions.

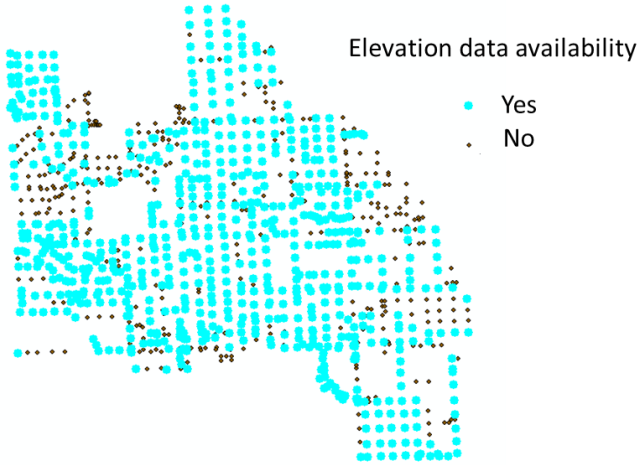

Figure 5.4 Sewer junctions in Hickory Hills, IL with elevation data availability

A junction depth is defined as the difference between the ground elevation and the junction invert elevation. The frequency plot of the junction depths is presented in Figure 5.5.The average sewer depth is 2.62 m, median depth is 2.42 m, and the most frequent depth is 2.44 m. Thus the sewer lateral depth for the representative case is assumed as 2.5 m for convenience. To evaluate

the impact of different sewer depths on an infiltration hydrograph, total 16 different sewer depths are tested (Table 5.3).

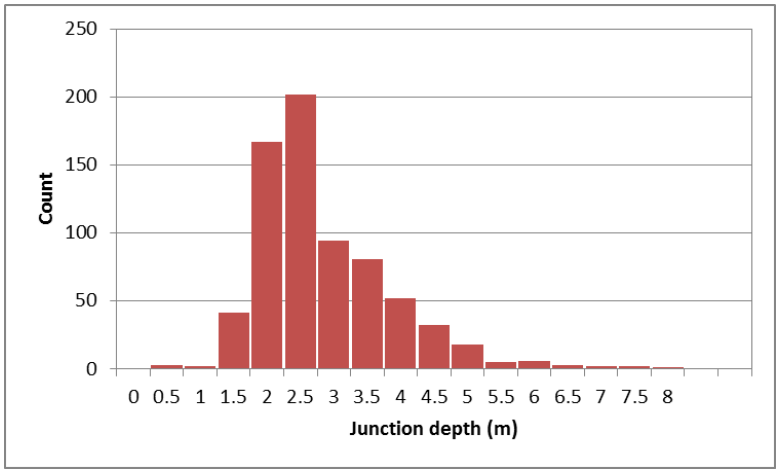

Figure 5.5 Sewer junction depths distribution in Hickory Hills, IL

Table 5.3 Tested sewer depths

Test cases	Sewer pipe depth
1	1.5 m
2	2 m
3	2.1 m
4	2.2 m
5	2.3 m
6	2.4 m
7 (representative case)	2.5 m
8	2.6 m
9	2.7 m
10	2.8 m
11	2.9 m
12	3 m
13	3.5 m
14	4 m
15	4.5 m
16	5 m

5.2.5. Initial Condition

To investigate the effect of IC on the RII hydrograph and to determine the average model start-up period, nine different simulation periods are randomly selected as test cases (Table 5.4). RII responses from the nine test cases are compared with the response from the control case, which includes the whole simulation period from January 1, 2009 to July 30, 2009. Test cases are selected within the control period with different starting time and the control case starts early enough that the boundary value effect is dissipated by the time the flow response is compared to the test cases.

Table 5.4 Test cases with different simulation start times to investigate the initial condition (IC)

Test cases	Sewer pipe depth
1	1.5 m
2	2 m
3	2.1 m
4	2.2 m
5	2.3 m
6	2.4 m
7 (representative case)	2.5 m
8	2.6 m
9	2.7 m
10	2.8 m

5.2.6. Rainfall Characteristics

To investigate the impact of different rainfall durations and rainfall shapes, total nine various rainfall cases are tested (Figure 5.6). The test cases are variations of the control rainfall, which is the uniform rainfall with 3 hour duration and 42 mm volume. Five different rainfall durations: 1-hour, 6-hours, 12-hour, 24-hour, and 48-hours, and three different triangular hyetographs: forward skewed, centered, and backward skewed, are tested with the same rainfall volume. These perturbations are arbitrarily included in real rainfall record and the RII hydrographs are compared after subtracting the original hydrograph without the perturbations (Figure 5.7).

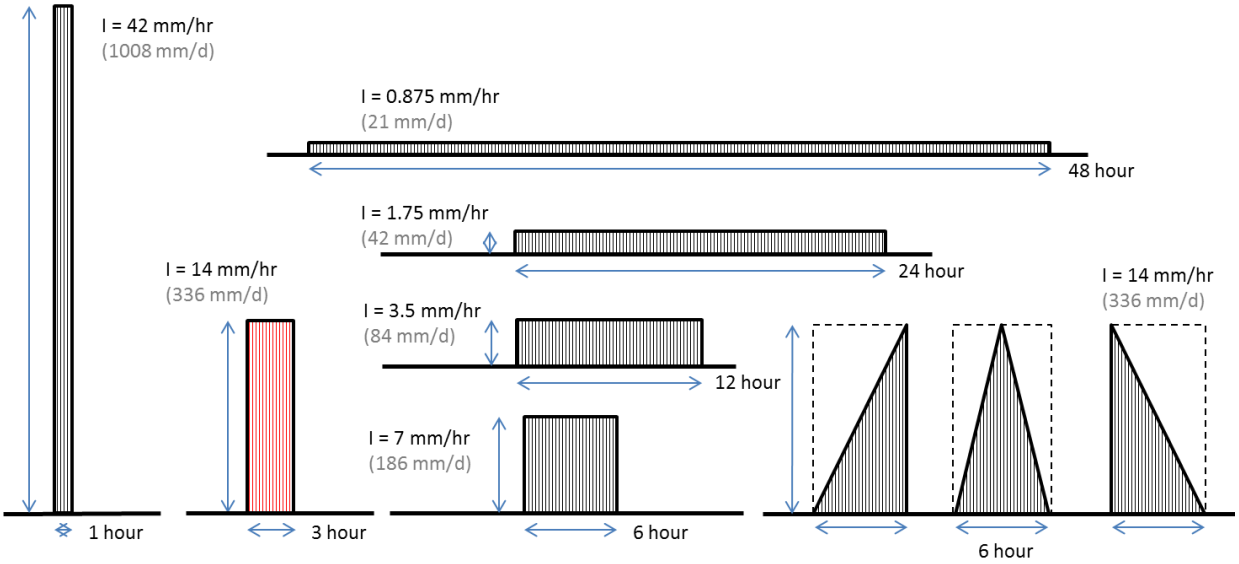

Figure 5.6 Tested rainfall durations and shapes (representative case with 3-hour 42-mm rainfall)

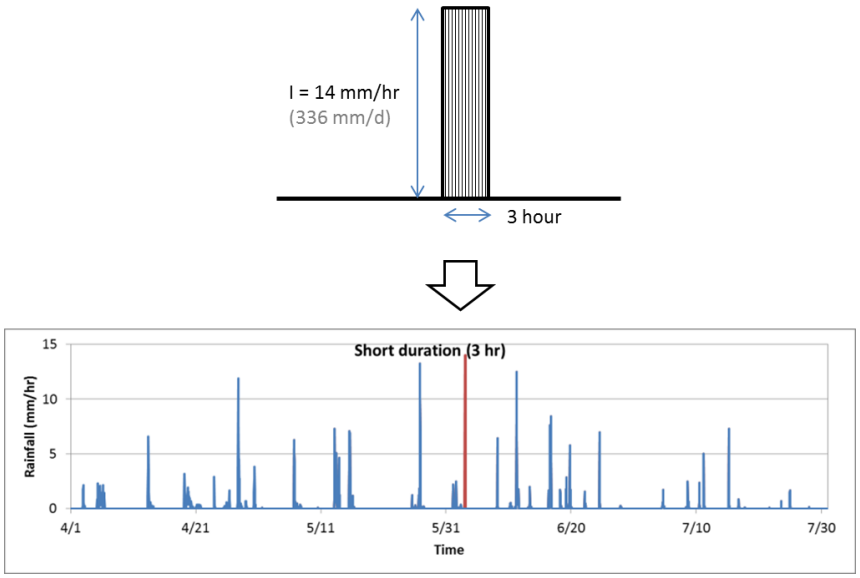

Figure 5.7 Arbitrary inclusion of the rainfall perturbation using the representative case

5.3. Results and Discussion

5.3.1. Antecedent Moisture Condition

The RII flow responses at the leaky sewer lateral with the uniform rainfall at different times are presented in Figure 5.8. The overall average infiltration response of all the cases is presented with black solid lines throughout the plots. Figure 5.8 (a), (b), and (c) show three distinguishable infiltration flow response shapes. The three shapes are named forward, centered, and backward responses based on the way that the peaks are skewed. Figure 5.8 (a) illustrates the forward infiltration responses with the average forward response shown with a dashed line. The forward response shows higher peak that precedes the peak of the overall average response (shown by the solid line). Figure 5.8 (b) shows the centered infiltration responses with the average shown by dashed line. This matches well with the overall average response. Figure 5.8 (c) illustrates the backward infiltration responses with the average backward response shown by a dashed line. The backward response also has a higher peak that follows the peak of the overall average in time. In Figure 5.8 (d), the cumulative depths of rainfall in the *N* days preceding the storm events being examined are shown, with the number of days, *N*, given on the *x*-axis. The three curves shown illustrate the cumulative rainfall preceding the event for average forward, centered, and backward events. Difference in cumulative rainfall depths for the three cases is clear until 29 days. Forward response is the result of drier antecedent conditions and backward response is due to wetter antecedent condition. Centered response falls in between them. A rainfall event in drier periods (cumulative rainfall for 29 days ≈ 20 mm) brings the forward response in the infiltration. Rainfall in wetter periods (cumulative rainfall for 29 days ≈ 60 mm) results in backward response. The ones in between (20 mm < cumulative rainfall for 29 days < 60 mm) cause centered response, which matches with the overall average infiltration response. In terms of the

infiltration volume, the forward responses have larger volume (47 mm) compared to the centered response (45 mm) and the backward responses (44 mm). This might be caused by the fact that unsaturated soil layer has greater capacity to absorb and drain water from the surface to the leaky pipe when it is in drier condition. Dry soil promotes water to percolate down into the soil while wet soil induces more surface runoff. Infiltration rate is generally high when the soil is dry as dry soils have pore and cracks that allow water to pass faster (USDA-NRCS, 2001, 2012). However, as sewer I&I is expected to increase during wet weather, greater RII through a defective sewer following dry preceding moisture condition can be counterintuitive. The relationship between soil moisture condition and RII through a leaky sewer pipe has not been thoroughly investigated and further research is needed to understand the physics of this behavior.

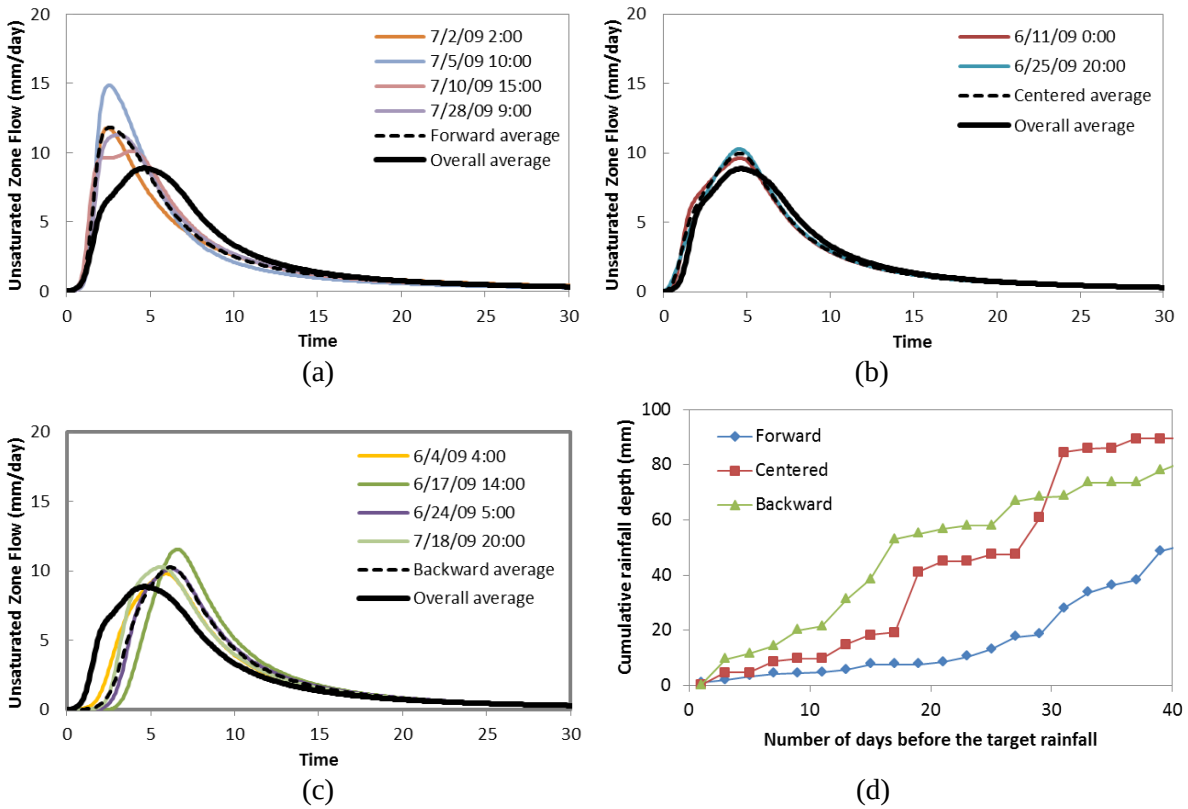

Figure 5.8 Infiltration flow response with three distinguishable AMCs (a) forward response with average infiltration volume 47 mm, (b) centered response with average infiltration volume 45 mm, (c) backward response with average infiltration volume 44 mm, (d) average cumulative rainfall depths for forward, centered, and backward cases

5.3.2. Pedotransfer Functions

The calculated hydraulic conductivity values for each soil type using different pedotransfer functions (PTFs) are presented in Figure 5.9 and Table 5.5 with the average values. Thin solid lines represent single types of soil and the range of hydraulic conductivity values is from 10^{-8} to 10^{-5} m/s. The soil type with the code 49A shows high K_s values for all the PTFs in the figure but the area that this soil type covers is a fraction of the entire area (0.45%). The area weighted average is smaller than the arithmetic mean value throughout the PTFs. The average hydraulic conductivity value which is calculated directly from the data is $2.19 \cdot 10^{-7}$ m/s. Compare to this, average hydraulic conductivity values using PTFs are overestimated. As the last column of Table 5.5 indicates, overall hydraulic conductivity value using PTFs is 4.75 times larger than the values directly calculated from the data. To take into account larger hydraulic conductivity values from the PTF application, larger test cases: 1st quartile and 3rd quartile of area weighted K_s, are added for hydraulic conductivity test in Table 5.2.

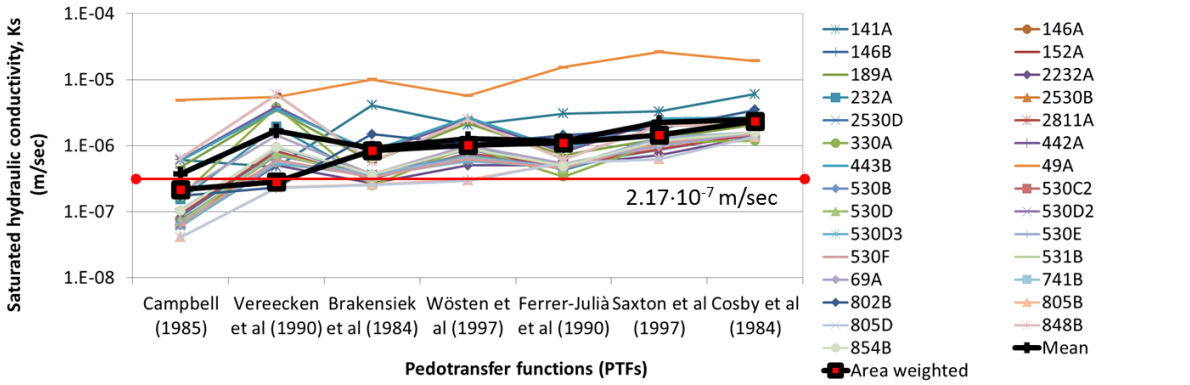

Figure 5.9 Hydraulic conductivity values of different soil types in Hickory Hills, IL using different PTFs along with average hydraulic conductivity; a thin solid line indicates one soil type, the thick solid line with black cross markers indicates the arithmetic mean and thick solid line with square markers indicates the area weighted mean)

Table 5.5 Average hydraulic conductivity values (arithmetic mean and area weighted mean) estimated by different PTFs and the comparison of the area weighted mean to the average hydraulic conductivity from the data

	Methods	Estimated K_s (m/s)	Estimated area weighted K_s (m/s)	Area weighted K_s compare to the data-based K_s (= $2.19 \cdot 10^{-7}$ m/s)
1	Campbell (1985)	$3.71 \cdot 10^{-7}$	$2.15 \cdot 10^{-7}$	.99
2	Brakensiek et al (1984)	$9.12 \cdot 10^{-7}$	$8.38 \cdot 10^{-7}$	3.86
3	Ferrer-Julià et al (1990)	$1.18 \cdot 10^{-6}$	$1.10 \cdot 10^{-6}$	5.07
4	Wösten et al (1997)	$1.26 \cdot 10^{-6}$	$1.02 \cdot 10^{-6}$	4.70
5	Vereecken et al (1990)	$1.69 \cdot 10^{-6}$	$2.85 \cdot 10^{-7}$	1.31
6	Saxton et al (1997)	$2.26 \cdot 10^{-6}$	$1.45 \cdot 10^{-6}$	6.68
7	Cosby et al (1984)	$2.49 \cdot 10^{-6}$	$2.33 \cdot 10^{-6}$	10.74
Average across PTFs		$1.45 \cdot 10^{-6}$	$1.03 \cdot 10^{-6}$	4.75
1st quartile			$1.28 \cdot 10^{-6}$	
3rd quartile			$1.80 \cdot 10^{-6}$	

5.3.3. Soil Hydraulic Conductivities

Figure 5.10 presents input and results of different soil hydraulic conductivity test. A larger hydraulic conductivity of the soil results in higher infiltration into the leaky sewer pipe (Figure 5.10 (b)). As Figure 5.10 (c) indicates, the larger the hydraulic conductivity the larger the infiltration peak. Not only the magnitude of flow peaks but also the onset of flow responses differs in time. Small hydraulic conductivity requires a longer period of time for infiltration to take place. In Figure 5.10 (b), if hydraulic conductivity is smaller than $7.60 \cdot 10^{-8}$ m/s, infiltration hydrograph fails to capture the rainfall trend and constant infiltration is observed. The relationship between hydraulic conductivity and time delay of hydrographs is presented in Figure 5.10(d). The larger hydraulic conductivity the slower flow and the longer elapsed time to the onset of flow response.

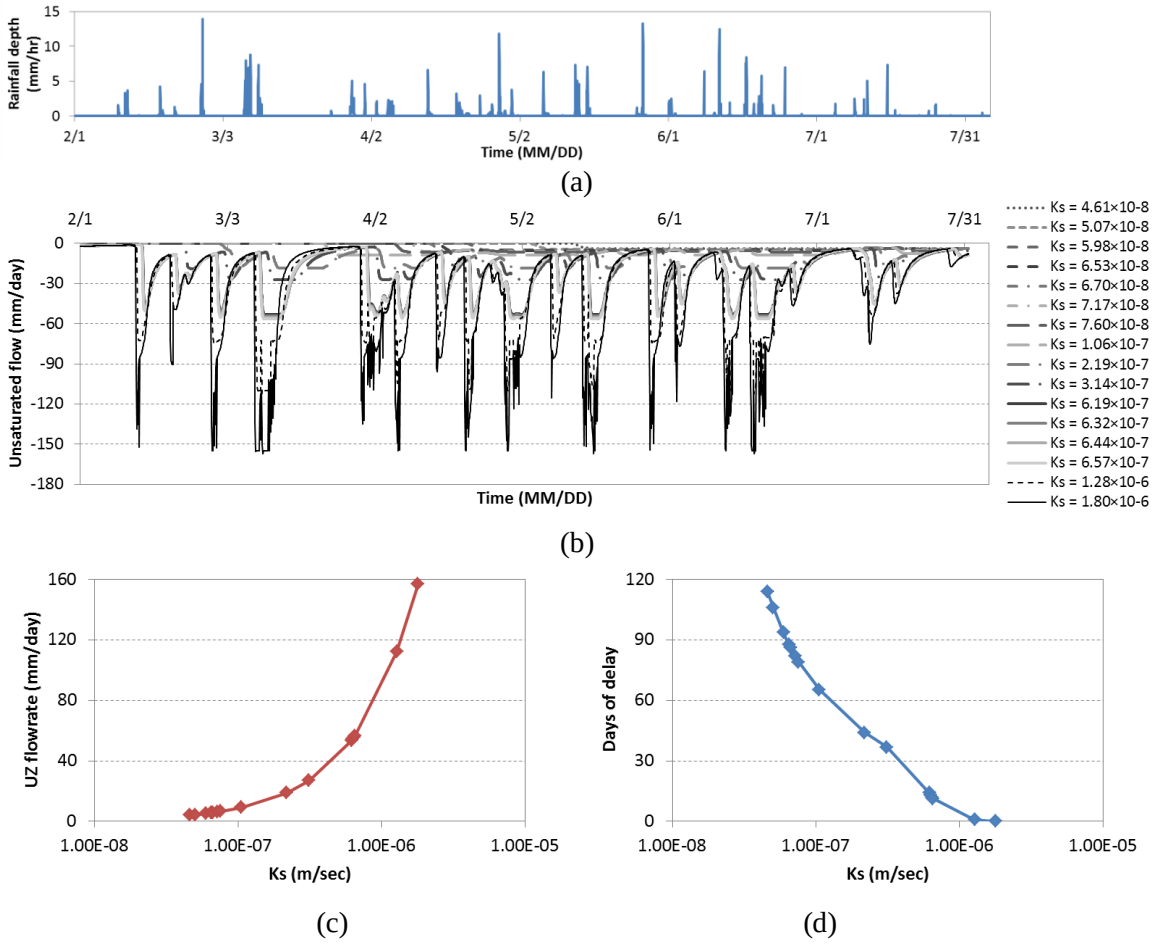

Figure 5.10 Model input and results of different soil hydraulic conductivity tests (a) rainfall input, (b) infiltration rate at the leaky lateral with different hydraulic conductivity values as unsaturated flow, (c) maximum peak values, and (d) elapsed time to the onset of flow response compare to the largest K_s case (K_s = 1.80·10^{-6} m/s)

5.3.4. Sewer Pipe Depths

Figure 5.11 (a) presents infiltration responses with different sewer pipe depths. Different points on the response curves of the test cases are further investigated in terms of flow peak (Figure 5.11 (b)) and time (Figure 5.11 (c)). For the flow peak and time investigation, test cases with sewer depths between 2 m and 3 m are only selected. Each flow response starts at the black square markers on Figure 5.11 (a) and this is affected by the ICs of each simulation as investigated in the section 5.3.4. Larger sewer depth increases the distance that unsaturated flow

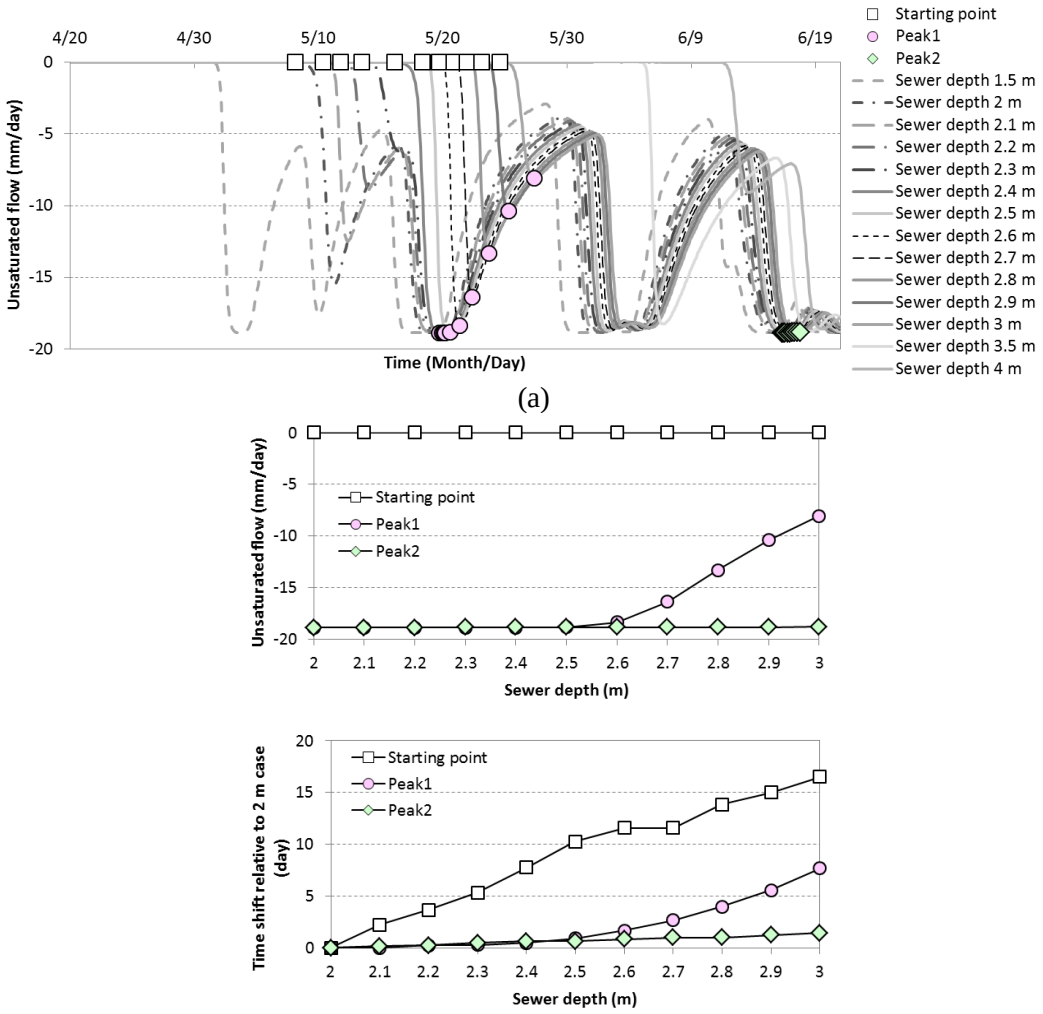

Figure 5.11 Infiltration hydrographs with different sewer pipe depths; peak investigation (a) Infiltration hydrographs, (b) Peak magnitudes, (c) Peak time (Square markers indicate the beginning of each infiltration response, circle markers indicate peak 1, and rhombus markers indicate peak 2)

takes and delays the starting time of flow response. Because of the delay, flow responses of the sewer depth 4.5 m and 5 m cases do not even appear in the modeling window. This time delay causes the flow hydrographs to fail to capture some effects of earlier rainfall events. However, infiltration hydrographs collapse close to each other once the ICs are met. To compare an early peak and a late peak, two flow peaks are selected and named as peak 1 (marked by circle

markers) and peak 2 (marked by rhombus markers) in Figure 5.11. Peak 1 is still under the effect of IC so the magnitude and time change greatly depending on the sewer depths. Compare to peak 1, a little difference is found in peak 2 in terms of the peak magnitude and the time. This is because the solution comes to the equilibrium with time. Thus different sewer depths does not affect peak flow rate greatly once the effect of IC dissipates.

Not only peak values in the infiltration curves but also tail values in the receding limbs are investigated in Figure 5.12. The term "tail" is used for the lowest points of receding limbs here. To compare an early tail and a late tail, two flow tails are selected and named tail 1 (marked by circle markers) and tail 2 (marked by rhombus markers) in Figure 5.12. As Figure 5.12 (b) and Figure 5.12 (c) indicate, the infiltration hydrographs shift consistently at tail points as the slope of the graphs appear constant. In Figure 5.12 (b), the slope of the tail 1 curve is $1.27 \cdot 10^{-3}$ /day and that of the tail 2 curve is $1.24 \cdot 10^{-3}$ /day. This means that one meter of sewer depth change causes changes in infiltration rate by $1.27 \cdot 10^{-3}$ mm/day and $1.24 \cdot 10^{-3}$ mm/day in tail values for the first and the second receding limbs respectively. A larger sewer pipe depth results in longer time of a tail to reach the pipe. The slope of time curves in Figure 5.12 (c) is 2.67 day/m and 2.83 day/m for tail 1 and tail 2 groups respectively. This implies that one meter change in sewer depth causes average 2.67 day and 2.84 day of time delay of the tail points in the first and the second receding limbs respectively. These values have to be perceived with a caution since they may change depending on interevent time of rainfall data and soil hydraulic conductivity values.

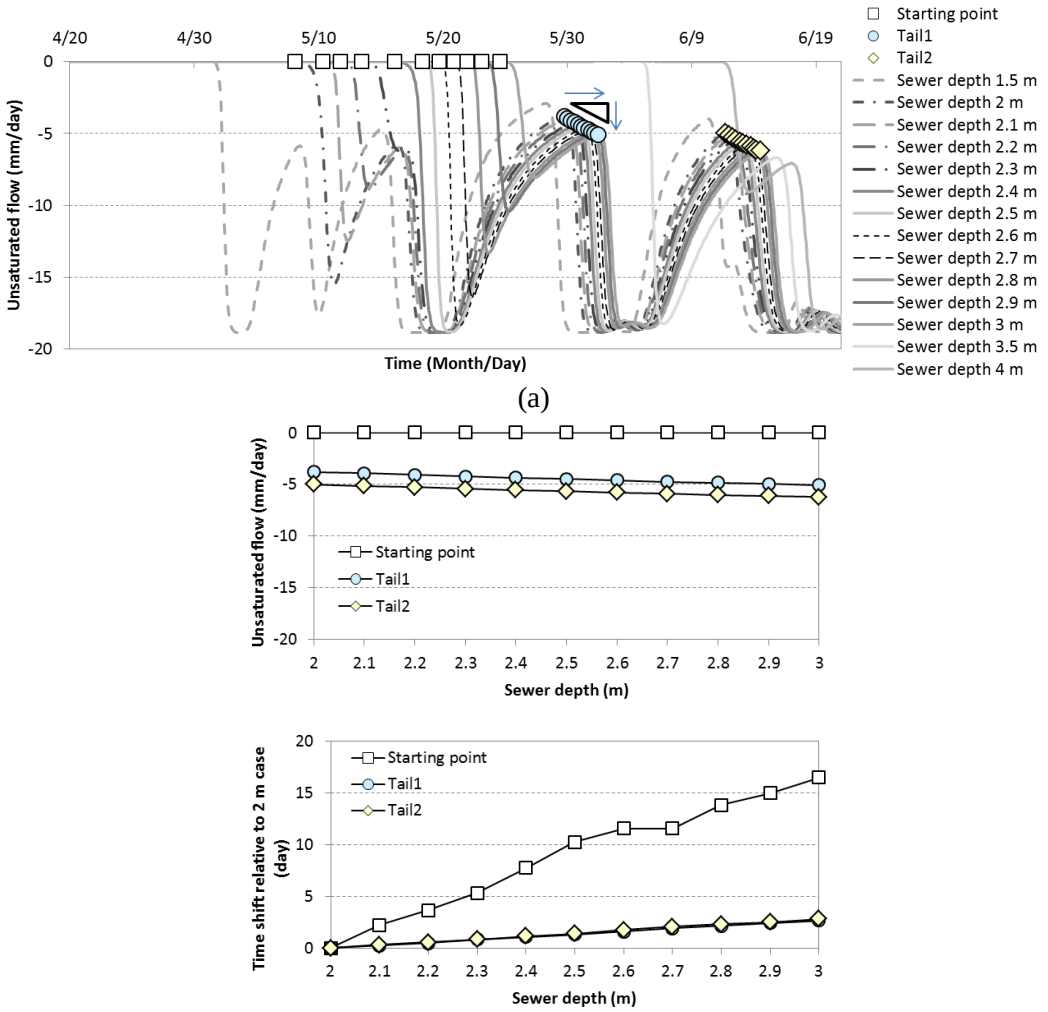

Figure 5.12 Infiltration hydrographs with different sewer pipe depths; tail investigation (a) Infiltration hydrographs, (b) Tail magnitude, (c) Delay time (Square markers indicate the beginning of each infiltration response, circle markers indicate tail 1, and rhombus markers indicate tail2)

5.3.5. Initial Condition

The percent errors in infiltration rate for the nine test cases with different simulation starting times are presented in Figure 5.14 (a). The flow response from the longer simulation period, from January 1, 2009 to July 31, 2009, is assumed as the true infiltration behavior (depicted in Figure 5.13 with the red solid line) and each flow response from shorter simulation periods is

compared to this true value to calculate the error. An example of the test case that converges on Marcy 3, 2009 is illustrated in Figure 5.13 with the blue solid line. The definition of percent error is presented as

$$\text{Percent error} = \frac{\text{Error}}{\text{True or theoretical value}} \times 100 \tag{18}$$

where Error is the difference between experimental value and true value (Error = Experimental value – True or theoretical value).

Most of the error curves show sudden change from -100% to near 0% at different times. This transition from -100% to 0% is observed no later than 20 days of simulation for all the cases. The median and average errors are presented in Figure 5.14 (b) along with the maximum, minimum, 1st quartile, and 3rd quartile values. Difference between the median and average curves in the figure indicates a skewed distribution of the data. Overall the average percent error decreases with time and most of the error is dissipated after 20 days. This result is when the sewer pipe depth is 2.5 m and different sewer depth will result in change of the length of the warm-up period.

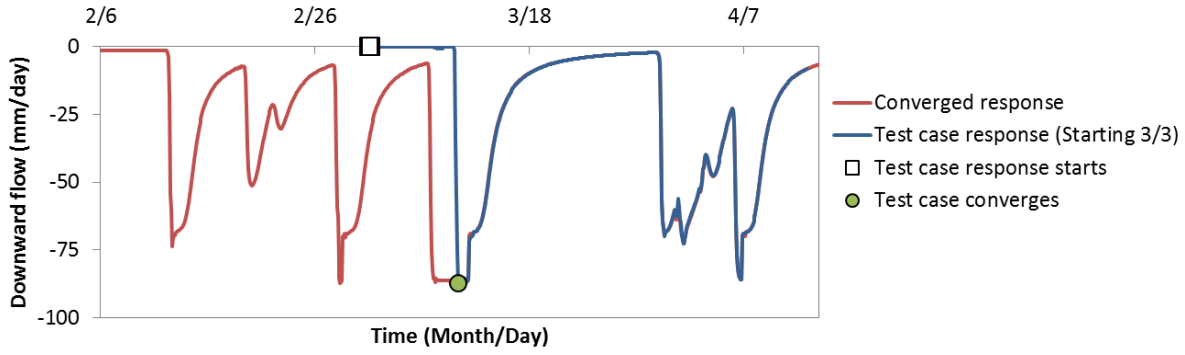

Figure 5.13 Comparison of infiltration response for the converged case and the test case of March 3rd, 2009

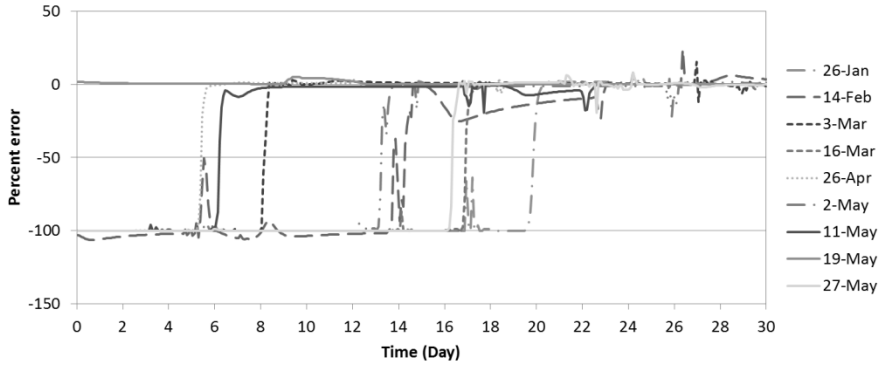

(a)

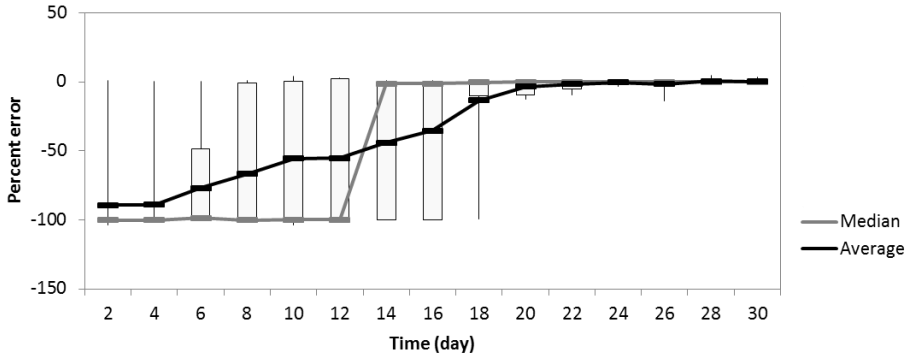

(b)

Figure 5.14 Percent error in infiltration rate of the nine test cases with different starting times (a) Individual error curves, (b) Median and average along with the maximum, minimum, 1st quartile, and 3rd quartile values

5.3.6. Rainfall Characteristics

Figure 5.15 shows the RII hydrographs at the leaky sewer pipe using different rainfall durations (Figure 5.15 (a)) and shapes (Figure 5.15 (b)). In Figure 5.15 (a), total flow duration and flow peaks show no major difference among different rainfall durations: 1-hour, 3-hour, 6-hours, 12-hours, 24-hours, and 48-hour. Near the peaks, some fluctuations are observed but overall difference is negligible. In Figure 5.15 (b), forward, centered, and backward rainfall shapes also do not show significant difference in the infiltration hydrographs. Thus, neither rainfall durations nor rainfall shapes affect infiltration response to a great extent. The change in peak discharge from changes in rainfall duration and shape was smaller than 4% and the change in volume was

smaller than 5% of the representative rainfall case. This might be due to the time scale difference between rainfall and infiltration processes. The time scale of rainfall is from hours to days but that of the sewer infiltration process is from weeks to months. Therefore, changes in the rainfall duration and shapes do not propagate to the infiltration process with a great impact.

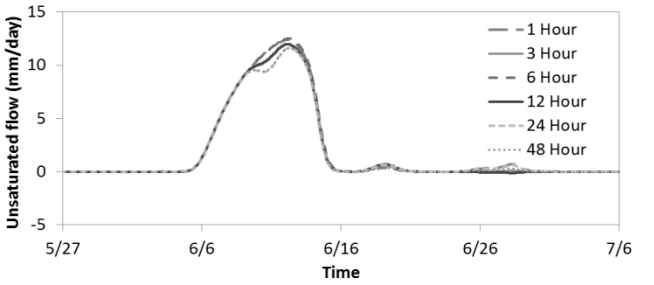

(a)

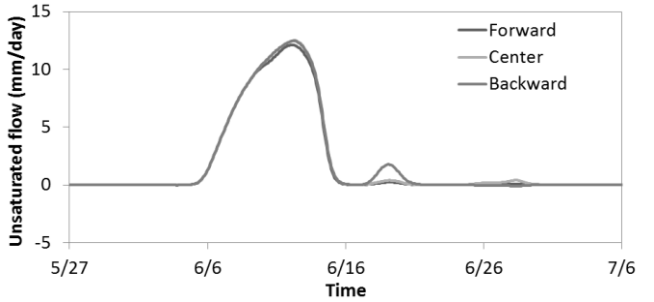

(b)

Figure 5.15 Flow responses from different rainfall durations and shapes

5.4. Summary

In this study, possible uncertainty factors in rainfall induced infiltration (RII) modeling were examined using a detailed physics-based model. Following six factors were tested to understand the possible uncertainty: antecedent moisture condition (AMC), pedotransfer functions (PTFs), soil hydraulic conductivities, sewer pipe depths, initial conditions (IC), and rainfall characteristics. Different PTFs affected the average hydraulic conductivity of soil and the difference was up to one order of magnitude. This implies that much attention should be paid to the estimation of hydraulic conductivity of the soil in the infiltration modeling. Regarding AMC,

an infiltration peak arrived earlier in a hydrograph and total infiltration volume increased during dry periods. In contrast, the onset of the peak occurred later and the total infiltration volume decreased during wet periods. The overall results showed that the most sensitive factor among them was the soil hydraulic conductivity and this soil property defined the maximum infiltration rate. Different sewer depths brought different model start-up periods. A larger sewer depth required longer start-up period since it increased the distance of flow paths. In terms of IC, roughly 20 days of start-up period were required to guarantee the error gets dissipated and the flow response finally reflects the rainfall effect. Different rainfall durations and shapes did not affect the infiltration hydrographs as much as other factors. This is because the time scale of rainfall is much shorter than the infiltration process. These findings bring insights to the sewer infiltration modeling and better understanding of the uncertainty underlies the sewer infiltration process.

References

Bareš, V., Stránský, D., & Sýkora, P. (2009) Sewer infiltration/inflow: long-term monitoring based on diurnal variation of pollutant mass flux. *Water Science and Technology : A Journal of the International Association on Water Pollution Research*, *60*(1), 1–7. doi:10.2166/wst.2009.280

Baroni, G., Facchi, A., Gandolfi, C., Ortuani, B., Horeschi, D., & Dam, J. C. van. (2010) Uncertainty in the determination of soil hydraulic parameters and its influence on the performance of two hydrological models of different complexity. *Hydrology and Earth System Science*, *14*, 251–270.

Brakensiek, D. L., Rawls, W. J., & Stephenson, G. R. (1984) *Modifying SCS hydrologic soil groups and curve numbers for rangeland soils. ASAE Paper No. PNR-84-203*. St. Joseph, MI.

Campbell, G. S. (1985) *Soil Physics With Basic: Transport Models for Soil-Plant Systems* (p. 149). New York: Elsevier.

Cosby, B. J., Hornberger, G. M., Clapp, R. B., & Ginn, T. R. (1984) A Statistical Exploration of the Relationships of Soil Moisture Characteristics to the Physical Properties of Soils. *Water Resources Research*, *20*(6), 682. doi:10.1029/WR020i006p00682

De Bénédittis, J., & Bertrand-Krajewski, J. L. (2005a) Infiltration in sewer systems: comparison of measurement methods. *Water Science and Technology : A Journal of the International*

Association on Water Pollution Research, *52*(3), 219–27. Retrieved from http://www.ncbi.nlm.nih.gov/pubmed/16206862

De Bénédittis, J., & Bertrand-Krajewski, J. L. (2005b) Measurement of infiltration rates in urban sewer systems by use of oxygen isotopes. *Water Science and Technology: A Journal of the International Association on Water Pollution Research*, *52*(3), 229–37. Retrieved from http://www.ncbi.nlm.nih.gov/pubmed/16206863

Dettinger, M. D., & Wilson, J. L. (1981) First order analysis of uncertainty in numerical models of groundwater flow Part 1. Mathematical development. *Water Resources Research*, *17*(1), 149–161.

DHI Software. (2007a) MIKE SHE user manual volume 1: user guide, Vol. 1.

DHI Software. (2007b) MIKE SHE user manual volume 2: reference guide, Vol. 2.

El-Kadi, A. I. (1987) Variability of infiltration under uncertainty in unsaturated zone parameters. *Journal of Hydrology*, *90*(1-2), 61–80. doi:10.1016/0022-1694(87)90173-9

Ferrer-Julià, M., Estrela Monreal, T., Sánchez del Corral Jiménez, A., & García Meléndez, E. (2004) Constructing a saturated hydraulic conductivity map of Spain using pedotransfer functions and spatial prediction. *Geoderma*, *123*(3-4), 257–277. doi:10.1016/j.geoderma.2004.02.011

Franz, T. (2007) *Spatial classification methods for efficient infiltration measurements and transfer of measuring results*. Dresden University of Technology, Dresden, Germany.

Kracht, O., Gresch, M., & Gujer, W. (2007) A stable isotope approach for the quantification of sewer infiltration. *Environmental Science and Technology technology*, *41*(16), 5839–45. Retrieved from http://www.ncbi.nlm.nih.gov/pubmed/17874795

Melching, C. S., Yen, B. C., & Wenzel Jr., H. G. (1987) *WRC Research Report No. 208, Incorporation of uncertainties in real-time catchment flood forecasting* (p. 194). Urbana, IL.

USDA-NRCS. (2001) Soil quality information sheet: Rangeland soil quality — Infiltration.

USDA-NRCS. (2012) Soil infiltration: Soil quality kit - Guides for educators.

NRCS Soil Data Mart http://soildatamart.nrcs.usda.gov/

Pawlowski, C. W., Rhea, L., Shuster, W. D., & Barden, G. (2013) Some factors affecting inflow and infiltration from residential sources in a core urban area: A case study in a Columbus OH USA neighborhood. *Journal of Hydraulic Engineering*. doi:10.1061/(ASCE)HY.1943-7900.0000799

Rasoulzadeh, A. (2011) Estimating hydraulic conductivity using pedotransfer functions. In L. Elango (Ed.), *Hydraulic Conductivity - Issues, Determination and Applications* (pp. 145–164). InTech.

Saxton, K.E., Rawls, W.J., Romberger, J.S., and Papendick, R.I. (1986) Estimating generalized soil water characteristics from texture. *Soil Science Society of America Journal* 50: 1301-1036.

Tietje, O. & Hennings, V. (1996) Accuracy of the saturated hydraulic conductivity prediction by pedo-transfer functions compared to the variability within FAO textural classes. *Geoderma* **69**(1-2), 71–84. doi:10.1016/0016-7061(95)00050-X

Tung, Y., & Yen, B. (2005) Uncertainties in hydrosystems engineering and management. In Hydrosystems engineering uncertainty analysis (pp. 1–12). McGraw-Hill.

Vereecken, H., Maes, J., and Feyen, J. (1990) Estimating unsaturated hydraulic conductivity from easily measured soil properties. *Soil Science* 149: 1-12.

Wösten, J.H.M. (1997) Pedotransfer functions to evaluate soil quality. In:Gegorich, E.G., Carter, M.R. (Eds.), Soil Quality for Crop Production and Ecosystem Health. Developments in Soils Science, vol. 25, Elsesevier, Amesterdam 221-245.

Wösten, J.H.M., Lilly, A., Nemes, A., and Le Bas, C. (1999) Development and use of a database of hydraulic properties of European soils. *Geoderma* 90: 169-185.

Summary and Conclusions

This study was conducted to investigate detailed I&I physical processes for three major sources of I&I into urban sewer systems: roof downspout, sump pump, and leaky lateral. The I&I response for the representative uniform rainfall from each of the three sources is referred to as impulse response function (IRF). The IRF of a roof downspout connection was modeled using the one-dimensional kinematic wave equation and the level-pool routing equation. The roof dimension was estimated using the average roof configuration in the community of Hickory Hills, IL. The flow response from the roof connection had the largest peak flow and shortest time to peak among the IRF from the three sources. IRF of a sump pump connection was modeled using the gravity flow equation provided by the commercial software MIKE SHE. The flow from the sump pump showed a smaller peak, a longer time to peak, and a longer flow duration compared to the flow from the roof connection. IRF of the leaky sewer lateral was also simulated using the detailed hydrologic model, MIKE SHE. The flow response showed the smallest peak and the longest flow duration among the three I&I sources. For 3-hour uniform rainfall, the order of total response time, which is defined as the time from the start of rainfall until when the IRF hydrograph falls to less than 0.01% of the peak, for roof, sump pump, and the leaky lateral were 10^0 hours, 10^1 hours, and 10^2 hours, respectively.

The three I&I models or the IRF method was applied to estimate I&I in a Chicago area where rainfall and sewage monitoring data are available. The IRF represents the inflow to the system from a typical roof, sump pump, or leaky lateral. Since the number and location of each of these sources is unknown, the model is calibrated by applying a weighting factor to each of the IRF and adjusting these three weights to obtain the best fit to a time series of observed sewer flows

representing a range of precipitation events. The model was calibrated using genetic algorithm (GA) technique and it predicted the I&I fairly well with the Nash-Sutcliffe coefficients around 0.55. For comparison, one of the most widely used I&I estimation methods, RTK method was also tested with GA calibration and it showed better prediction with the Nash-Sutcliffe coefficients around 0.80. Even though the RTK method better predicted the I&I in the test case, the model showed numerous local optima rather than converging to a unique solution. In the validation period, the fitness was improved with the IRF method but decreased with the RTK method. The IRF method was based on the physical understanding of I&I processes, which makes the model more robust.

The relationship between space and time scales of I&I processes was also investigated. It was concluded that depending on the relative time scale of I&I processes and the network travel time, the importance of spatial variability of I&I sources changes. If the time scale of an I&I response is shorter than the network travel time, spatial variation of the I&I source becomes important. Conversely, if the time scale of the I&I response is longer than the network travel time, spatial variation of the I&I source becomes less important. This discussion provided a justification to the assumption that the network routing of the three I&I responses can be ignored as the time scale of the three I&I responses were longer than the network travel time in this study.

Infiltration through a leaky lateral was further examined using six different uncertainty factors: antecedent moisture condition (AMC), pedotransfer functions (PTFs), soil hydraulic conductivities, sewer pipe depths, initial conditions (IC), and rainfall characteristics. The infiltration IRF was affected by all these factors. AMC affected the arrival time of the infiltration peak and the flow volume. Dry AMC resulted in forward skewed peaks and large infiltration volume. Wet AMC resulted in backward skewed peaks and small infiltration volume. This is

because dry soil allows water to pass through the soil faster while wet soil induces more surface runoff. Relative dryness and wetness is determined by the cumulative rainfall of 29 days preceding the event.

Soil hydraulic conductivity is the most influential factor affecting the uncertainty of the infiltration IRF. Hydraulic conductivity can be estimated based on hydraulic conductivity data for soils in the area or based on PTFs that use other, more available data to approximate the hydraulic conductivity. Hydraulic conductivities determined from soil data for the test watershed varied from the order of 10^{-8} and 10^{-7} m/s. Hydraulic conductivity based on seven different PTFs generally overestimated hydraulic conductivity compared to reported values, with PTF-calculated hydraulic conductivities ranges from the order of 10^{-7} and 10^{-6} m/s. Based on the soil statistics, a total of 16 different hydraulic conductivity values were tested based on the soil data from the Hickory Hills, IL and the result of different PTF models. The infiltration response of the largest hydraulic conductivity case showed more than 100 times greater flow peaks than that of the smallest case. Thus the infiltration IRF is highly influenced by the hydraulic conductivity of the soil.

Relative to the soil hydraulic conductivity, rest of the uncertainty factors have less impact on the infiltration response. Sewer pipe depths affected the length of start-up period to reach the IC. Larger the sewer pipe depths longer the start-up period. In terms of IC, when 2.5 m was selected for the sewer pipe depth, average 20 days of simulation was required to converge. . Different rainfall duration and shapes did not make a big change in the IRF of sewer infiltration through leaky pipe. The change in peak discharge from changes in rainfall duration and shape was smaller than 4% and the change in volume was smaller than 5% of the representative rainfall

case. The reason why changes in rainfall characteristics have a little impact on the IRF is because of the scale difference between rainfall events and infiltration process.

For several decades, various I&I estimation methods have been developed and applied to urban areas. However, along with the effort to correctly estimate I&I, basic understanding about the detailed I&I process should be also sought. This study provides fundamental understanding about three of the major I&I processes and also understanding about the uncertainty in predicting the infiltration process. This study also successfully shows the potential of a detailed hydrologic modeling approach to investigate small scale infiltration process.

Future Research and Suggestions

The I&I models presented in this document can be used to provide IRF for representative I&I sources. Estimation of the total I&I of an urban catchment can be accomplished by the convolution of the IRFs where each IRF is multiplied by a weighting factor determined by calibration to observed data. Since each IRF is derived for the three major I&I sources: roof downspout, sump pump, and leaky lateral; the flow contribution of each source can be identified based on the weights. This enables identifying the most problematic I&I source in the sewershed, which helps reducing the cost of sewer maintenance and rehabilitation.

Each model has a room for refinement to test different model settings and locations. In the infiltration modeling part of this study, as an example, an equivalent medium approach was selected to approximate the leaky lateral area, including the drainage trench. This is a simplified representation of the system and more detailed modeling could be performed to examine questions such as what impact lining or repairing the sewer would have on infiltration to the system. Then the model results can be compared depending on the level of details.

In this study, IRFs were developed for three specific I&I sources: roof downspout, sump pump, and leaky lateral, for a specific study area Hickory Hills, IL. However, most problematic I&I sources differ in different communities and IRFs can be developed for other I&I sources as well depending on the local issues.

Depending on the relative time scale difference between the I&I local response and the sewershed response, spatial distribution of the I&I sources may not be important. If the I&I local response time is significantly shorter than the sewershed response time, network routing of the

local response becomes important. In this case use of a single weighting factor as was done in this research may not adequately represent the sewershed response to the rainfall-derived I&I. Further research is needed to examine the tradeoff between I&I and sewershed response times and spatial distribution of I&I to determine when the assumptions made in this research are appropriate. This research about the time and space scale tradeoff can be tested using methods such as Monte-Carlo simulation.

The detailed physical modeling of the infiltration process in this study can be also suitable to evaluate storm water best management practices (BMPs) in an urban area. Many urban communities have been introducing various sustainable storm water management practices. Many of these practices attempt to reduce stormwater runoff volumes by maximizing the percolation of stormwater to the underlying soil. While many studies have attempted to quantify the reduction in surface runoff from various BMPs, no study to date has examine the potential increase in I&I to sewer systems that may result from these practices. Detailed physical modeling using the tools implemented in this research can provide a tool to understand the behavior and impact of the BMPs on I&I to the existing sewer system.

For the detailed hydrologic modeling, monitoring different hydrologic and hydraulic properties in the field is suggested. The data will help validating these models and possibly provide more research opportunities. The challenge limiting improved understanding of I&I to sewers is the limits of current instrumentation to quantify I&I at a scale that allows detailed understanding. A recent USGS study that coupled state-of the art acoustic flow meters and sampling for fluorescence from optical brighteners monitored flows in 1.52 m diameter pipe and the acoustic flow meter could go as small as 91.44 cm diameter pipe with minimum of 15.24 cm of water above the instrument. New instruments such as fiber optic distributed temperature sensing could

be used to quantify the spatial distribution of inflows to sewer systems, providing unprecedented insight into the I&I characteristics of sewers.